NASA

Technical Memorandum **79660**

(NASA-TM-79660) ENERGETIC PARTICLES IN SOLAR FLARES. CHAPTER 4 IN THE PROCEEDINGS OF THE 2ND SKYLAB WORKSHOP ON SOLAR FLARES (NASA) 120 p HC A06/MF A01 CSCL 03B

N79-13984

Unclas
G3/92 40945

Energetic Particles In Solar Flares Chapter 4 In The Proceedings of the Second Skylab Workshop on Solar Flares

R. Ramaty, S. A. Colgate, G. A. Dulk, P. Hoyng, J. W. Knight, R. P. Lin, D. B. Melrose, C. Paizis, F. Orrall, P. R. Shapiro, D. F. Smith, and M. Van Hollebeke

OCTOBER 1978

National Aeronautics and Space Administration

Goddard Space Flight Center
Greenbelt, Maryland 20771

ENERGETIC PARTICLES IN SOLAR FLARES

CHAPTER 4 in the

Proceedings of the Second Skylab
Workshop on Solar Flares
Boulder, Colorado, 1976-1977

by

R. Ramaty - Goddard Space Flight Center, Greenbelt, Maryland, USA
S. A. Colgate - Los Alamos Scientific Laboratory, Los Alamos, New Mexico, USA
G. A. Dulk - Dept. of Astrogeophysics, University of Colorado, Boulder, Colorado, USA
P. Hoyng - Space Research Laboratory, The Astronomical Institute at Utrecht, The Netherlands
J. W. Knight - Institute for Plasma Research, Stanford University, Stanford, California, USA
R. P. Lin - Space Science Laboratory, University of California, Berkeley, California, USA
D. B. Melrose - Australian National University, Canberra, Australia
C. Paizis - Goddard Space Flight Center, Greenbelt, Maryland, USA
F. Orrall - Institute of Astronomy, University of Hawaii, Honolulu, Hawaii, USA
P. R. Shapiro - Center of Astrophysics, Harvard University, Cambridge, Massachusetts, USA
D. F. Smith - High Altitude Observatory, Boulder, Colorado, USA
M. Von Hollebeke - Goddard Space Flight Center, Greenbelt, Maryland, USA

TABLE OF CONTENTS

4.1 INTRODUCTION

Energetic solar particles, broadly defined as particles of energies greater than about 10 keV, are a very important constituent of solar flares. Energetic particle production seems to be intimately related to the flare mechanism itself, and, moreover, the interactions of the energetic particles with the solar atmosphere appear to be responsible for a great variety of flare phenomena.

The most direct observational evidence for the acceleration of particles at the Sun consists of radio emission produced by fast electrons interacting with the solar plasma and magnetic fields (Wild et al. 1963), X-ray emission from the bremsstrahlung of energetic electrons (Peterson and Winckler Kane 1971), gamma-ray line and continuum emission due to nuclear interactions o energetic ions and the bremsstrahlung of relativistic electrons (Chupp et al. 1973, Ramaty et al. 1975), and direct spacecraft and ground-based observations of energetic electrons and ions which escape from the Sun (McCracken and Rao 1970, Lin 1974, Simnett 1974, McDonald, Fichtel and Fisk 1974). Other emissions such as white light continuum and impulsive EUV bursts, not directly attributable to energetic particles, also appear to be good indicators of particle acceleration (e.g. Svestka 1976).

In examining the problem of energetic particles in flares, the most striking result is the great variety of accelerated particle populations that the flare is capable of producing. The most dominant population, at least from the point of view of energetics, consists of electrons in the energy range from about 10 to 100 keV. Information on these electrons, at or close to the flare site, is derived mainly from hard X-ray observations.

The first measurement of solar flare hard X-rays (Peterson and Winckler 1959) was followed by many more from rockets, balloon gondolas, and spacecraft (notably the OSO and OGO series). Though a clean measurement of a steep photon spectrum over a wide energy interval is difficult, many reliable solar flare hard X-ray spectra and their time histories are available (Kane and Anderson 1970, Frost and Dennis 1971, McKenzie, Datlowe and Peterson 1973, Datlowe, Hudson and Peterson 1974, Datlowe, Elcan and Hudson 1974, Hoyng, Brown and Van Beek 1976).

The results are that above a lower limit roughly around 10 keV the photon spectrum is compatible with a power law spectrum. But above about 70 KeV the spectrum frequently steepens, so that an exponential form can also fit the data (Chubb 1970, Milkey 1971, Brown 1974, Crannell et al. 1978, Elcan 1978). The X-ray emission can be highly time variable, with spikes in the time profile of only a few seconds duration. The emission lasts for about 10 to 100 seconds, and in exceptional cases it may last for as long as 1000 seconds.

It is widely accepted that the radiation mechanism for producing hard X rays is bremsstrahlung from fast (10 to 100 keV) electrons. Two limiting cases exist regarding the nature of these electrons. They could belong to a nonthermal population whose number density is much lower than that of the relatively cool ambient medium with which it interacts, or they could form a quasithermal hot plasma. In the former case, the ratio of the bremsstrahlung yield (due to electron-ambient ion collisions) to nonradiative collisional losses (due to electron-ambient electron collisions) is very small ($\sim 10^{-5}$ at 25 keV); this would imply that hard X-ray production in flares should be accompanied by the deposition of large amount of energy into the solar atmosphere. The quasithermal case, on the other hand, allows the production of hard X rays with less energy loss to the solar atmosphere,

although, as we shall discuss in detail in Section 4.2, the gain in efficiency is not larger than about a factor of 20 relative to the nonthermal case.

The X-ray production models can also be distinguished by the fate of the electrons after X-ray production. In the thick target model (Brown 1971, 1972; Hudson 1972; Brown and McClymont 1975) the electrons stop in the solar atmosphere and lose all their energy there, while in the thin target case (Datlowe and Lin 1973) the electrons escape from the Sun without much energy loss. Clearly, the ratio between the bremsstrahlung yield and the total energy contained in the 10 to 100 keV electrons is lower for a thin target than for a thick target.

Even though a thick target model only requires that the 10 to 100 keV electrons lose their energy at the Sun, for example in a magnetic trap, thick target models with downward beaming into the dense chromosphere were proposed (Sweet 1969, Sturrock 1974). The inferred beam strength can be as high as 10^{36} electrons s^{-1}. For any reasonable beam area, the energy in the self magnetic field of such a beam is orders of magnitude above the total beam kinetic energy and the total flare energy. This argument has been used against beam models (Colgate, Audouze and Fowler 1977, Colgate 1978). However, other authors have pointed out that it underlines the need for a reverse current (Hoyng, Brown and Van Beek 1976, Brown and Melrose 1977, Hoyng 1977a, Knight and Sturrock 1977). We treat the existence and consequences of reverse currents in Section 4.3, and point out the conflict between the presence of a reverse current and simultaneously an induction electric field. A specific consequence of a reverse current in certain circumstances is the rapid heating of the coronal plasma which will have a specific soft X-ray spectroscopic signature. This is treated in Section 4.4.

In addition to the production of hard X rays, the acceleration of the 10 to 100 keV electrons is manifest (e.g. Lin 1974) in the simultaneous occurrence of impulsive microwave and fast drift type III radio

bursts with the impulsive hard X rays. In many cases the same energy electrons are observed at 1 AU some 20 minutes later ($\sim$ transit time to 1 AU). As discussed above, the energy contained in the 10 to 100 keV electrons may comprise a substantial fraction of the total energy of the flare. The acceleration mechanism responsible for the production of the 10 to 100 keV electrons, therefore, is likely to be catastrophic, involving the rapid conversion of magnetic into kinetic energy. We shall refer to such mechanisms as first phase acceleration, and we shall discuss them in Section 4.5.

In addition to the 10 to 100 keV electron component, solar flares also accelerate higher energy electrons which produce radio emission at various wavelengths as well as gamma-ray continuum emission. The first evidence that not all electrons can be accelerated by a single mechanism came from radio observations (Wild et al. 1963). A detailed discussion on the radio evidence on particle distribution functions in the corona following flares is given in Section 4.6.

The properties of energetic particles in flares can also be studied by directly observing the particles in space. Energetic ions from just below an MeV to energies of several GeV and electrons from tens of keV to ultrarelativistic energies have been observed (e.g. McDonald et al. 1974). These observations reveal complex spatial and temporal characteristics, many of which result from coronal and interplanetary propagation effects. In Section 4.7, we emphasize those aspects of energetic particle observations which could have a direct implication on particle acceleration in flares. These are the energy spectra of protons and electrons, the proton-to-electron ratio, and the dramatic ^{3}He enrichments. We also provide some discussion of the phenomenon of enrichments of heavy nuclei, since these appear to be closely related to events enriched in ^{3}He. A detailed discussion of heavy nuclei

enrichments, however, even though very important for the flare acceleration process, was not undertaken at the workshop.

Gamma-ray lines are the direct signature of nuclear reactions in solar flares, and these are believed to result from the interactions of energetic protons and nuclei with the ambient solar atmosphere. Continuum emission in the gamma-ray band is a superposition of relativistic electron bremsstrahlung, and Doppler and instrumentally broadened nuclear lines. Solar gamma-ray observations are therefore probing energetic particles in the flare region at energies in excess of several MeV for protons and nuclei, and above hundreds of keV for electrons. The gamma-ray observations and their theoretical interpretation can give a direct measure of the acceleration time of the nuclei and high energy electrons, can determine the ratio of protons to electrons which can then be compared to the observed ratio of these particles in the interplanetary medium, and can place important constraints on the energy content in protons and nuclei. Gamma-ray observations could also provide information on abundances, in particular those of C, O, Mg, Si and Fe. In Section 4.8 we treat the production mechanisms of gamma rays in flares, and the information derived from their observations and analysis.

In addition to emissions whose association with accelerated particles is clear and unmistakable (e.g. nuclear gamma rays, hard X rays, radio bursts, and, of course the direct detection of energetic ions and electrons), there are other emissions that mimic the time history of those above so closely that their direct association with energetic particles is unescapable. Two such

flare-associated phenomena that show promise of setting direct, strong, constraints on the flux, spectrum and place of acceleration of the energetic protons during the impulsive phase are the white-light flare and the non-thermal wings of the hydrogen Lyman-Alpha line. The former may yield information on the downward flux of protons above 20 Mev or electrons above 10 keV, while the latter may provide information on the flux of protons below 1 MeV. These phenomena are discussed in Section 4.9.

As we have already pointed out above, an examination of the radio, X-ray, gamma-ray and particle signatures for solar flares indicates that at least two distinct phases of acceleration can be distinguished in terms of their temporal behavior, the type and energy of the particles accelerated, and the likely acceleration mechanism. The first phase consists of the acceleration of electrons to energies of about 10 to 100 keV, and mechanisms for accelerating these electrons are discussed in Section 4.5. In some large flares a distinct second phase of acceleration lasting for $\sim$ 10 minutes follows the first phase. This is characterized by the acceleration of ions to energies $\geq$ 10 MeV and electrons to relativistic ($\geq$ 0.5 MeV) energies. Both ions and electrons are directly observed in the interplanetary medium; in addition, the electrons generate detectable synchrotron radio and bremsstrahlung X-ray emissions, and the protons produce gamma-ray line emission. The radio, hard X-ray, and gamma-ray observations all indicate that the particles accelerated in this second phase acceleration rise to their maximum intensity slower than do those accelerated in the first phase (Wild et al. 1963, Frost and Dennis 1971, Bai and Ramaty 1976). The interplanetary particle observations also show that the ions and relativistic electrons are likely to have been released a few minutes later than the electrons accelerated in the first phase (Lin 1970, Sullivan 1970, Simnett 1974). There appears to be a close association of this acceleration stage

with the passage of a shock wave through the solar atmosphere, as evidenced by type II and other radio emissions (McLean et al. 1971) and interplanetary shock observations, indicating that a stochastic, Fermi-type acceleration process may be operating. Second phase acceleration is discussed in Section 4.10.

A summary of the material presented in this Chapter is given in Section 4.11. There we also indicate the contributions of Team members to the various sections, as well as the contributions of other individuals to this Chapter.

4.2 ENERGY CONTAINED IN THE 10-100 keV ELECTRONS

The 10-100 keV electron population which occurs in most solar flares may contain a significant or possibly large fraction of the solar flare energy. As discussed in §4.1, this result follows from the assumption that the hard X-rays are produced by nonthermal electrons interacting with a relatively cool ambient medium. In this section we consider the observational limits on the hard X-ray producing electrons and a quasi-thermal model for hard X-ray emission in which the efficiency (the ratio of the bremsstrahlung yield to the nonradiative energy loss rate) is maximized under reasonably realistic conditions.

4.2.1. OBSERVATIONAL LIMITS ON THE ENERGY OF THE HARD X-RAY PRODUCING ELECTRONS

We consider the energy and number of electrons in the 10-100 keV range derived from observations. At these energies only bremsstrahlung due to electron-proton collisions is important. We consider two models. The first is a thick target model in which an observed X-ray flux $I(E) = aE^{-\gamma}$, where E is the photon energy, is due to an influx F of fast electrons with energies above E_0 into the target which results in an energy deposition rate P as shown in Table 4.2.1. Formulas for F and P are given in Hoyng et al. (1976). The model independent emission measure which follows directly from a and γ is Y. The second model we consider is a thermal model for which the energy deposition rate is P_{th} in Table 4.2.1. This model is 100% efficient with all of the energy supplied going into hard X rays. The large difference between P and P_{th} indicates the possible advantages which might be obtained with a thermal model, but the difference is unrealistically large because any thermal model must expand. In the

next subsection we consider this expansion and place more realistic bounds on the reduction in energy deposition rate for a thermal model as compared to a thick target model. Any thin target model is less efficient than a thick target model.

4.2.2. A QUASI-THERMAL HARD X-RAY MODEL

We consider as a model a symmetric initially constant density magnetic arch of length 10,000 km in which the electrons of a 2000 km section at the top are rapidly energized in bulk (see §4.5) to an effective temperature of 4×10^8 ^oK. The model is termed quasi-thermal because the electron and ion temperatures are unequal and the electron and ion velocity distributions are not necessarily Maxwellian. The possibility that the X-ray emission above 10 keV could be due to a multi-temperature thermal source was pointed out by Chubb (1970) and made quantitative by Brown (1974) who showed that any X-ray spectrum can be reproduced by a suitable distribution of thermal sources. Common objections to a quasi-thermal source are reviewed in Smith and Lilliequist (1978) where a more complete analysis of this model can be found. There it is concluded that there is no reason in principle why a quasi-thermal source could not work although it remains to be shown in detail that it will work. The model examined here is by no means complete in this sense and relations to other phenomena such as microwave bursts are not considered. Rather, it is meant to be an exploratory case in which dynamics are taken into account to see if more involved modeling would be justified.

For example, it might be thought that the efficiency ε of a thermal model could be evaluated from the formula

$$\varepsilon = \frac{j_B \tau_X}{\frac{3}{2} n K T_e} \qquad (4.2.1)$$

where j_B is the bremsstrahlung volume emissivity, τ_x is the duration of the hard X-ray emission, n is the density and T_e is the electron temperature. Eq. (4.2.1) gives the ratio of the energy in hard X-rays per unit volume emitted to the energy per unit volume put in when a region of the solar atmosphere is instantaneously heated. However, this assumes no more energy is put into the source after the initial instantaneous heating and the X-ray spectrum is continuously changing in time as the source expands and cools. This is in contrast to what was determined observationally in Section 4.2.1 which is the instantaneous energy deposition rate required to produce an observed emission measure in hard X-rays above 25 keV. Clearly, in contrast to Eq. (4.2.1), an instantaneous efficiency is required which we define as

$$\varepsilon = \frac{j_B}{L_{NR}} \quad , \tag{4.2.2}$$

where L_{NR} is the nonradiative loss rate per unit volume required to maintain the source emitting at the rate j_B.

When the electrons at the top of an arch are heated to $T_e = 4 \times 10^8\ ^oK$, a conduction front moves down the arch with a characteristic velocity limited by ion-acoustic instability of

$$v_o = c_s + (c_s - v_i) \left[\frac{m_i}{m_e}\right]^{\frac{1}{2}} \left[\frac{T_e}{T_i}\right]^{3/2} \exp\left[-\frac{0.5\ T_e/T_i + 1.5}{1.25}\right], \tag{4.2.3}$$

where $c_s = (kT_e/m_i)^{\frac{1}{2}}$ is the sound speed and $v_i = (kT_i/m_i)^{\frac{1}{2}}$ is the ion thermal velocity. In the idealized case that the electrons are heated instantaneously we can solve for the expansion of the source along the magnetic field analytically since the ions remain cold on the time scale of the expansion and the second term on the right hand side of Eq. (4.2.3)

is negligibly small. Because the arch is symmetric, the calculation can be restricted to a 5000 km half of the arch. Suppose that there is some cooling during the expansion so that when the conduction front reaches $\ell(t)$ = 4000 km from the top of the arch, the temperature $T_e = 10^8$ °K and the average temperature during expansion $\bar{T}_e = 2 \times 10^8$ °K. The rate energy must be supplied per unit area of the arch cross section is

$$L_{NR}\ell(t) = \frac{3}{2} n_e K \bar{T}_e v_o = \frac{3}{2} n_e K \bar{T}_e c_s \qquad (4.2.4)$$

which gives 2.3×10^{12} erg cm^{-2} s^{-1} for the above values. The bremsstrahlung emissivity per unit area, with the average effective atomic number Z determined from Tucker and Koren (1971), is

$$j_B\ell(t) = 2.86 \times 10^{-27} T_e^{\frac{1}{2}} n_e n_i \ell(t) \qquad (4.2.5)$$

With $T_e = 4 \times 10^8$ °K from 0 to 2180 km and $\bar{T}_e = 2 \times 10^8$ °K from 2180 km to 4000 km, the total bremsstrahlung emissivity is 1.8×10^9 erg cm^{-2} s^{-1}. Thus the efficiency (from Eq. (4.2.2)) is $\varepsilon = 7.8 \times 10^{-4}$, which has a $n_i T_e^{-1}$ dependence for $T_e \gg T_i$ and an n_i dependence in all cases. A 52.5 keV electron corresponding to an effective temperature of 4×10^8 °K radiates with an efficiency of 2.3×10^{-5} in a thick target so that our idealized model is 34 times more efficient.

We can justify a one-dimensional model for the 2.2 s time it takes the conduction front to move to the feet of the arch by noting that in a turbulent plasma the perpendicular diffusion coefficient cannot exceed the Bohm value

$$D_{\perp B} \approx \frac{1}{16} v_{\perp e} \rho_e = v_{\perp} D^d \qquad (4.2.6)$$

where $v_{\perp e}$ is perpendicular electron thermal velocity, ρ_e is the electron gyroradius and $v_{\perp D}$ is the perpendicular diffusion velocity of electrons in a temperature gradient of scale d. For $T_e = 4 \times 10^8$ °K and B = 800 G, $v_{\perp e} = 7.8 \times 10^9$ cm s^{-1} and $\rho_e = 0.56$ cm leading to $D_{\perp B} \approx 2.8 \times 10^8$ cm^2 s^{-1}. The hot part of the arch must have a radius of at least 10 km to give a reasonable emission measure and the scale of the temperature gradient over which the temperature returns to a coronal value d > 0.1 km. This leads to a maximum perpendicular diffusion velocity of 0.28 km s^{-1} or to a maximum expansion of 0.62 km during the time of movement of the conduction front. Considering the exploratory nature of this analysis, this maximum error of ∿7% is judged to be of little significance. On longer time scales the perpendicular expansion must be considered.

A model with a realistic heating rate of about 10^5 erg cm^{-3} s^{-1} was computed numerically using one-fluid two-temperature hydrodynamic equations which are given in Smith and Lilliequist (1978). The results of this model show that the ions are heated to about 2×10^7 °K in 0.74 s which gives rise to mass motions up to 410 km s^{-1} behind the conduction front. The ion heating also leads to a faster propagation speed for the front which reaches 2430 km in 0.74 s and neglect of perpendicular diffusion is better justified. The efficiency ($\varepsilon = 4.3 \times 10^{-4}$) for this model is 19 times greater than that of a 52.5 keV electron with the same n_i dependence as the analytic model. The decrease in efficiency of the numerical model relative to the analytic model is due to a higher average T_e and the fact that 11% of the input energy goes into mass motions.

These results underline the possible advantages of a quasi-thermal hard X-ray source.

4.3 ON THE EXISTENCE AND CONSEQUENCES OF REVERSE CURRENTS

If an electron beam is forced to pass through a plasma by a force other and a uniform DC electric field, a reverse current can be generated in the plasma, such that the total current density vanishes, while the energy flux density does not. This phenomenon is well established experimentally (Levine et al. 1971, Klok et al. 1974) and theoretically (Cox and Bennett 1970, Hammer and Rostoker 1970, Chu and Rostoker 1973). A reverse current was already postulated in beams causing type III radio emission by Melrose (1970).

In the case of solar flares, when the emergent hard X-ray flux is caused by bremsstrahlung possibly coming from a beam of fast electrons, the inferred beam strength F could be as high as $\sim 10^{36}$ electrons s^{-1}, see Table 4.2.1. The energy in the self magnetic field of such a beam [$\sim(eF/c)^2$ x beam length] is orders of magnitude above the total beam kinetic energy and the total flare energy. This argument has been used against beam models (Colgate et al. 1977). However, other authors have pointed out that it underlines the need for a reverse current (Hoyng et al. 1976, Brown and Melrose 1977, Hoyng 1977a, and Knight and Sturrock 1977).

Beams of 10-100 keV electrons of the strength required by X-ray observations can only exist if they are compensated. This can be achieved by the reverse current, which allows a net beam energy transport at zero net particle transport. On the other hand, this implies that the mechanism operative in the acceleration region itself must be such that a reverse current can be set up. This places restrictions on these regions, as discussed in Section 4.5. Possibilities for the acceleration of 10-100 keV electrons are given in Section 4.5. The analysis here is restricted to the problem of beam transport.

4.3.1 Consequences of a reverse current

The dynamics of an electron beam due to Coulomb and wave-electron interactions with the background plasma has been studied extensively (see for example Hoyng and Melrose 1977 and references therein). The existence of the reverse current adds two new elements: (a). Stability of the reverse current requires

$$v_r/v_t \leq \begin{cases} 0.47 & T_e \simeq T_i \\ 0.19 & T_e \simeq 3T_i \\ 0.063 & T_e \simeq 10T_i \end{cases} \qquad (4.3.1)$$

(Kindel and Kennel 1971), where $v_t = (kT_e/m)^{1/2}$ is the electron thermal velocity, v_r is the reverse current drift velocity and $T_{e,i}$ are the electron and proton temperatures. (b). The electric field E_{rev} that drives the reverse current (against ohmic, i.e. Coulomb losses), will decelerate the beam. For a beam electron with velocity v, this deceleration is smaller than that due to Coulomb losses (collisions) if (Hoyng and Melrose 1977):

$$(v/v_t)^2 \, (v_r/v_t) < 6.4 \qquad (4.3.2)$$

where

$$v_r \sim F/n_o A \qquad (4.3.3)$$

F = fast electron flux as inferred from hard X-rays (Hoyng et al. 1976), and n_o, A = background density, beam area. Caution is needed with relation (4.3.3) as it only holds under special conditions which are more fully discussed by Hoyng et al. (1978) [for example, since the hard X-ray flux is very insensitive to the angular velocity distribution, the fast electrons may not be streaming at all and then $v_r \simeq 0$]. In principle, (4.3.3) expresses the

requirement of zero total current.

Requirements (4.3.1) and (4.3.2) are summarized in Figure 4.3.1 in a diagnostic diagram. Application of this diagram requires knowledge of v_t (from soft X-rays) assuming soft and hard X-ray sources to be spatially coincident, beam flux F, area A and velocity distribution (from spatially resolved hard X-ray observations), the density n_o (from line intensity ratios or non-stationary ionization equilibria), and the proton temperature T_i (from linewidths). At present, we have no information at all concerning the

position of hard X-ray sources in Figure 4.3.1. One may hope that the Solar Maximum Mission will make the observations needed.

Out of the many possible scenarios, we just mention briefly two rather interesting ones (the reader is referred to Hoyng et al. (1978) for a complete discussion):

(a). It may turn out that the ambient density n_o and/or the beam area A are so small (small A means small hard X-ray image) that the position in Figure 4.3.1 is far beyond $v_r/v_t = 1$. The reverse current is then always unstable. The result is that the beam current is virtually isotropized, which decreases the actual value of v_r (but not F), and the band is moved to the left to a position of marginal stability, supposing $T_e \simeq T_i$ (Figure 4.3.1 at c or d). The result could be a (partly) thermal X-ray source, which is theoretically very attractive, see Section 4.2.

(b). Suppose a beam is initially at, say $v_r/v_t = 0.1$ and $T_e = T_i$. The beam is stable, but decelerated by the reverse current electric field E_{rev} instead of Coulomb collisions as usual. The possibility of this in the context of solar flares was first pointed out by Knight and Sturrock (1977). X-rays will therefore emerge from a relatively low density plasma. However, this situation will not last for very long, since the ambient electrons are heated to, say, $T_e = 10T_i$. As a consequence, the later stages are collision-dominated and the "classical" thick target analysis applies (Figure 4.3.1 at a and b).

If impulsive hard X-ray bursts are produced by directed streams of non-thermal electrons, reverse currents will develop such that the total current density is approximately zero. The examples discussed above illustrate that these reverse currents can have important consequences. The second of these two possibilities is analyzed more thoroughly in Section 4.4. Possible acceleration mechanisms are discussed in greater detail in Section 4.5.

4.4 THE RAPID HEATING OF CORONAL PLASMA DURING SOLAR FLARES: NONEQUILIBRIUM IONIZATION DIAGNOSTICS

Observational and theoretical evidence suggests that hard X-ray emission (10-100 keV) during solar flares may be accompanied by extremely rapid heating of coronal plasma. If this hard X-ray emission is thermal electron-ion bremsstrahlung (Section 4.2.2), then very hot plasma ($kT_e \gtrsim 50$ keV) must be created in a very short tim Alternatively, if the hard X-rays are non-thermal electron-ion bremsstrahlung resulting from the streaming of energetic non-Maxwellian electrons from the corona to the chromosphere, a reverse current is required to balance the beam current (Section 4.3). This reverse current can lead to extremely rapid heating (Knight and Sturrock 1977).

If the temperature of coronal electrons increases during flare hard X-ray bursts on a time scale which is shorter than the characteristic ionization times of plasma ions, a lack of equilibrium between ionization and recombination results which can dramatically affect the emergent X-ray line spectrum (Shapiro and Moore 1977). The effect of non-equilibrium ionization of coronal

flare plasma on selected X-ray line intensities has been illustrated by Kafatos and Tucker (1972) and Mewe and Schrijver (1975). Recently, the effect on the complete line and continuum spectrum from 1 to 250 Å has been calculated in detail for a model in which a magnetic loop of preflare coronal plasma initially in ionization equilibrium at a typical quiet coronal temperature ($\sim$2 x 10^6 K) and at a density of between 10^{10} and 10^{11} cm^{-3} is heated within a fraction of a second to a temperature close to 10^8 K (Shapiro and Moore 1977). Among the non-equilibrium effects found for this model was a burst-like enhancement of the soft X-ray flux from the loop. It was argued there that such effects are likely to be common to a fairly general class of scenarios involving rapid coronal heating.

The magnitude of such soft X-ray enhancements as a function of wavelength should reflect the particular temperature to which the plasma electrons are heated, while the decay time for the enhancements should depend upon both the temperature and the density after heating as reflected in the ionization times of the line-emitters. This suggests that observations of such non-equilibrium ionization effects may provide a useful diagnostic of the temperature and density of rapidly heated coronal flare plasma. Since the reverse current mentioned above may imply rapid heating, such effects may provide observational confirmation of theoretical reverse current models, or at least place constraints on them.

The rate for collisional excitation of the i to j transition of a positive ion by Maxwellian electrons of temperature T and number density n_e, where i is the ground level and j is the upper level, can be written as

$$n_e C_{ij} = 1.70 \times 10^{-3} n_e E_{ij}^{-1} f_{ij} \bar{g}(E_{ij}/kT) T^{-\frac{1}{2}} \exp(-E_{ij}/kT) \text{ sec})^{-1}, \quad (4.4.1)$$

where E_{ij} is the energy difference (in eV) between the ground level and level j, k is the Boltzmann constant, f_{ij} is the absorption oscillator strength, and $\bar{g}$ is the integrated effective Gaunt factor (Van Regemorter 1962). We shall be particularly interested here in situations in which E_{ij}/kT is a small number. In that case, the Bethe approximation is valid and we can replace $\bar{g}$ by the asymptotic form of the actual integrated Gaunt factor for high electron energies. If we define $y \equiv E_{ij}/kT$, then this gives (for $y \lesssim 0.01$)

$$g(y) \cong (\sqrt{3}/2\pi)(-0.57722 - \ln y). \quad (4.4.2)$$

(cf. Van Regemorter 1962). For low electron energies ($y \gtrsim 1$), on the other hand, at least in the case of the optically allowed transitions in which we are primarily interested, $\bar{g}$ can be taken as constant and roughly equal to 0.2 (Van Regemorter 1962).

The line emission rate for spontaneous radiative decay of the upper level j into a level k subsequent to the collisional excitation described by equation (4.4.1) is given by

$$\Lambda_{jk} = n_e n_H A(Z) y_{Z,z} E_{jk} C_{ij} B_{jk} \text{ eV cm}^{-3} \text{ s}^{-1}, \quad (4.4.3)$$

where n_H is the hydrogen number density, A(Z) is the abundance of element Z relative to hydrogen, $y_{Z,z}$ is the fraction of atoms of atomic number Z which are in the zth ionic stage, and B_{jk} is the branching ratio indicating the fraction of decays of level j which end in level k. This ignores the typically minor contributions to the line emission rates considered here from such

things as cascades from upper levels, dielectronic recombination, and the collisional depopulation of nearby mestastable levels. The temperature dependence of this line emission rate is then contained entirely in the product $y_{Z,z}\,\bar{g}(y)T^{-\frac{1}{2}}\,e^{-y}$. What happens to the rate if T is instantaneously increased by a factor α?

Since $y_{Z,z}$ is a quantity which varies on a time scale comparable to the ionization time for that species, any increase in T which occurs faster than this will leave $y_{Z,z}$ unaffected. Accordingly, if we define β as the factor of change in the line emission rate resulting from the factor α increase in T, then

$$\beta = (\bar{g}(y/\alpha)/\bar{g}(y))\;\alpha^{-\frac{1}{2}}\,e^{-y(1/\alpha-1)}. \qquad (4.4.4)$$

For small values of y/α, where $y \gtrsim 1$, we can use equation (4.4.2) for $\bar{g}(y/\alpha)$ and replace $\bar{g}(y)$ by 0.2. In that case,

$$\beta \cong 1.38(-0.577 - \ln y + \ln\alpha)\;\alpha^{-\frac{1}{2}}e^{-y(1/\alpha-1)}. \qquad (4.4.5)$$

As an example, let y=1. Then for α=10, β=1.8, and for α=100, β=1.5. As we shall see when we consider selected lines, β can sometimes be quite large. For a given y, β has a maximum as a function of α given by $\beta_{max} = \beta(\alpha_{max})$, where

$$\alpha_{max} \cong 17y. \qquad (4.4.6)$$

When y=5.88, for example, α_{max}=100, and the corresponding β_{max}=105!

Equation (4.4.5) suggests a simple temperature diagnostic for the rapidly heated coronal plasma: For a given initial, pre-flare (i.e. prior-to-heating), coronal temperature, an X-ray line can be chosen which is fairly prominent in the spectrum of the ionization equilibrium at that T (using a tabulation such as that of Kato, 1976). A measurement of β at the time of heating then permits the use of equation (4.4.5) to solve for α and, hence, the post-heating temperature, αT.

At the very least, two lines with different y-values must be considered since the existence of a maximum in β as a function of α implies that, in some neighborhood of α_{max}, α is a double-valued function of β.

We present in Table 4.4.1 a representative selection of thirteen lines suitable for measuring α as described above, for the case in which the initial electron temperature before heating is 3×10^6 K, a value typical of the corona above an active region (Noyes 1971). We have limited our selection to optically allowed transitions, for which the density-dependent effects described, for instance, by Mewe and Schrijver (1975) do not occur. Table 4.4.1 gives the enhancement factor β for these lines for a variety of temperature increases. Results range from an enhancement factor of 133 for the Mg XI line at 7.85 Å for α=100 to a factor less than one for the Fe XVI line at 76.60 Å for α=1000. The ease with which these enhancement factors can be measured depends on a variety of things including the duration of the enhancements relative to instrumental time resolution, instrumental wavelength resolution and the confusion caused by nearby lines, and the strength of the line relative to the continuum. Shapiro and Knight (1978) discuss the thermal bremsstrahlung continuum and show how it may provide an independent temperature diagnostic as well.

The time scales on which the non-equilibrium-enhanced X-ray lines decay are just the ionization times of the species responsible for the lines; the lines disappear when the ionic stages which produce them are

ionized away. This suggests an electron density diagnostic for the rapidly heated coronal plasma as follows: The ionization time is a function of both T and n_e. Once T is determined by the prescription given above, however, the ionization times determined from the line emission decay times are just inversely proportional to the electron density.

The thermal electron collisional ionization time for an ion of nuclear charge Z in the corona is given by Lotz (1968, 1969) as

$$\tau_I = 1.39\times10^4\, n_e^{-1} T^{\frac{1}{2}} \left(\sum \xi^{-1} a^{-1} I_{Z,z} \left(E_1(y_I) - be^c \frac{y_I}{c+y_I} E_1(c+y_I)\right)\right)^{-1}, \quad (4.4.7)$$

where $y_I = I_{Z,z}/kT$, $I_{Z,z}$ is the ionization potential in eV of one shell of the z^{th} stage of element Z, and a, b, c, and ξ are tabulated constants (where, in general, $a \approx 5$, $0 \leq b \leq 1$, $0 \leq c \leq 1$, and $1 \leq \xi \leq 10$), and where the summation is over all contributing n, l subshells. When y_I is small, we can ignore the second term inside the innermost parentheses in equation (4.4.7) and replace $E_1(y_I)$ by $(-0.577 - \ln y_I + y_I)$.

Table 4.4.2 shows the collisional ionization times and, hence, the expected line-enhancement decay times for the ions included in Table 4.4.2 for the same selected temperature increases, using equation (4.7). These times are normalized to the case of $n_e = 10^9 cm^{-3}$, a typical value for the corona above an active region (Noyes 1971). The timescale to produce a maxwellian distribution may not, in fact, be short enough in some cases, to justify our assumption of a well-defined electron temperature after heating. This can be accommodated by interpreting αkT as a characteristic mean energy of the heated electrons. For instance, the ionization times given by equation (4.4.7) and shown in Table 4.4.2 are simply uniformly 20% higher than would be calculated for a monoenergetic distribution of electrons of energy E_o

roughly equal to $\frac{1}{2}\alpha kT$. It should be noted that autoionization is important for a few of the ions and, in a more accurate treatment, this would slightly reduce the time scales shown in Table 4.4.2 for these ions. Inasmuch as τ_I is just inversely proportional to n_e, measurement of the decay times of the line enhancements is much more sensitive a diagnostic of n_e than the measurement discussed earlier was of T.

In conclusion, we mention another more commonly known temperature diagnostic which, while not based upon a non-equilibrium effect, takes a particularly simple form in the case discussed here. Using equations (4.4.1), (4.4.2), and (4.4.3), and the fact that y/kT is small for the lines considered, it can be shown that the ratio of line intensities of a pair of lines produced by the same ion gives the electron temperature T after heating according to the equation

$$T = \exp(((9.94 + \ln E_2)R - (9.94 + \ln E_1)C)/(R - C)), \qquad (4.4.8)$$

where

$$C = (f_1 B_1 E_2 \lambda_2)/(f_2 B_2 E_1 \lambda_1),$$

and where $f_{1,2}$, $B_{1,2}$, $E_{1,2}$, and $\lambda_{1,2}$ are the oscillator strengths, branching ratios, excitation energies (ev), and wavelengths, respectively, of the lines and R is the measured ratio of line 1 and line 2. This diagnostic has the particular virtue of allowing the "monitoring" of the electron temperature both during and after the rapid heating, in the event that either the heating is not much faster than characteristic ionization times or the temperature continues to change rapidly even after the heating takes place. For details on how electron beams and return currents can lead to rapid heating see Shapiro and Knight (1978).

4.5 ACCELERATION AND ENERGIZATION MECHANISMS FOR THE 10-100 keV ELECTRONS

The demands on the acceleration mechanism for the 10-100 keV electrons are not presently completely clear and range from supplying a direct flux of 10^{36} electrons s^{-1} above 25 keV (Hoyng et al. 1976) to supplying $\lesssim 10^{34}$ electrons s^{-1} above 25 keV with a power-law distribution (Lin 1974). The former requirement comes from the interpretation of hard X-ray bursts as due to a nonthermal flux of electrons streaming into a thick-target, whereas the latter comes from electrons directly measured near the earth which thus leads to an escape probability $\sim$ 1% assuming that the electrons were injected over the duration of the flash phase and that the X-rays were produced by thick-target processes. The above numbers do not necessarily refer to very large flares. It may also be possible to interpret the hard X-rays as due to a quasi-thermal distribution of electrons (cf. Section 4.2), in which case the nonthermal electron requirement from directly measured electrons becomes applicable. In this case all of the electrons in a small volume must be heated to a temperature $T_e \gtrsim 4 \times 10^8$ K by a process of bulk energization. We can divide possible acceleration and energization processes into bulk energization, direct electric field acceleration, and wave acceleration which are interrelated and which will be considered in turn. Second order Fermi acceleration processes which are considered in §4.10 probably are not efficient enough to be of interest for the 10-100 keV electrons.

4.5.1. BULK ENERGIZATION

The heating of the electrons and/or ions of the plasma by the conversion of stored magnetic energy into thermal energy is quite easy to obtain and partictically unavoidable under solar conditions. The term heating as used here is synonymous with bulk energization and is meant

to imply an increase in the energy content of the nearly isotropic, but not necessarily Maxwellian, electron velocity distribution.

Confirmation of this conclusion comes from both laboratory experiments (Hirose and Skarsgard 1976) and numerical simulations (Boris et al. 1970) of the effect of applying a direct electric field to a plasma as in Subsection 4.5.2. At first the electrons are freely accelerated. However, as soon as a critical velocity is reached, an instability occurs and waves are generated which transfer the directed motion of the electrons into heat. When the plasma is heated sufficiently, the criterion for instability is no longer satisfied, the electrons are again freely accelerated until they reach a new critical velocity and so on. Thus it is only possible to give the electrons a directed velocity to the extent that the electrons are heated since $v_D = v_e$ on the average, where v_D is the directed velocity and v_e is the electron thermal velocity. This means that 50-75% of the energy that would otherwise go into acceleration must be expended for heating depending upon how many thermal degrees of freedom are present. Although there are other possibilities for bulk energization, the one considered here is just direct electric field acceleration in the presence of intense wave scattering which inevitably arises if the acceleration is sufficiently strong.

4.5.2. DIRECT ELECTRIC FIELD ACCELERATION

By direct electric field acceleration we mean the acceleration of particles along the magnetic field either by an induced electric field due to magnetic field line motion or a polarization electric field due to charge separation. Since the medium in which the acceleration occurs is presumably the highly conducting coronal plasma, polarization electric fields are extremely hard to maintain because according to

$$j_{||} = \sigma E_{||} \tag{4.5.1}$$

only a very small current is required to eliminate any $E_{||}$. Here $j_{||}$ and $E_{||}$ are the current and electric field parallel to the magnetic field, respectively and σ is the conductivity. This situation changes if the value of σ is reduced significantly due to an instability such as the Buneman instability. However, conditions for the Buneman instability are quite difficult to satisfy under coronal conditions, requiring extremely large current concentrations and small dimensions. In these cases even the 10^5 reduction factor in the conductivity is typically not sufficient to account for the energy release in solar flares (Smith and Priest 1972). Thus, for solar conditions, the induced electric field must be due to magnetic field line motion in the frame in which the acceleration occurs. The most favorable configurations for acceleration in which such motion occurs are tearing mode instabilities (Drake and Lee 1977) and reconnecting current sheets (Vasyliunas 1975).

The manner in which this acceleration occurs and the gain in energy is summarized in Smith (1974) neglecting thermal velocities, polarization fields and microinstabilities such as the ion-acoustic instability. Thermal velocities will lead to a spread of the energy gain and microinstabilities will have two effects. The first is to scatter the directions of particles which again will lead to a spread of the energy gain since some particles will leave the field reversal region prematurely while others will be retained longer and experience additional acceleration. The other effect is to provide a dynamic change in the conductivity which may dramatically increase the energy gain via Equation (4.5.1). This effect could be used to explain some pulsating phenomena in solar flares

(Smith 1976a). However, it should be noted that as soon as the velocity v_D and density of the accelerated component become large enough to cause microinstabilities, v_D will be limited to v_e as in §4.5.1. The values of v_D and v_e can become quite large locally and the resulting hot drifting plasma will appear as a distinct nonthermal component when it interacts with the cool plasma outside (Smith 1977b).

Finally, the transverse dimensions of any direct electric field acceleration region are restricted by the requirement that the magnetic energy carried by the accelerated electrons which form a current must not significantly exceed the kinetic energy of the electrons (Section 4.3 on reverse currents). Assuming the current has a circular cross section of radius R, this requirement becomes

$$R \lesssim \left(\frac{m_e c^2}{90 n_b e^2}\right)^{\frac{1}{2}} , \qquad (4.5.2)$$

where n_b is the density of the accelerated electrons. The factor 90 can vary within a factor of 2 for typical solar parameters. For example, for $n_b = 3 \times 10^9$ cm^{-3}, $R \lesssim 13.5$ cm which means many small regions must be involved (Hoyng 1977a).

4.5.3. WAVE ACCELERATION

Since an efficient acceleration mechanism may be required and electric field acceleration is very efficient, we restrict our discussion to electron plasma and electron cyclotron waves (whistlers) which carry a large fraction of their energy in electric fields. Since whistlers are not easy to excite except by anisotropic distributions of already accelerated electrons (Melrose 1974), their main function tends to be isotropization and redistribution of accelerated electrons. Thus electron

plasma waves which can resonantly interact with particles from $\sim 2v_e$ up to c are the best candidate for wave acceleration (Benz 1977; Hoyng 1977a,b, Smith 1977a,b).

The principle problem with electron plasma wave acceleration is again the wave generation although the conditions are generally much less stringent than for whistlers. The possibilities summarized in Smith (1977a) and Tsytovich, Stenflo and Wilhelmsson (1975) are:

a. Electron-electron and electron-ion two-stream instabilities which require at least one streaming component.

b. Quasilinear relaxation of a low density stream.

c. Extended nonthermal tails and gap distributions of isotropic electrons.

d. Conversion of anisotropic ion-acoustic wave energy into electron plasma wave energy by a nonlinear amplification process.

The first three mechanisms require streaming particles of velocity greater than v_e which can occur when hot streaming plasma (Subsections 4.5.1 and 4.5.2) interacts with cool plasma. The single mechanism which may be able to produce electron plasma waves with particles streaming at velocities less than v_e is amplification by an anisotropic distribution of ion-acoustic waves. However, shock and turbulent heating experiments with high levels of anisotropic ion-acoustic waves have been carried out in a number of laboratories throughout the world over the past 15 years with high intensities of electron plasma waves measured only in cases where a suspected or confirmed runaway electron stream with velocities greater than v_e was present.

Given a large energy density W_p in electron plasma waves, the most efficient acceleration sequence is the following (Hoyng 1977a,b, Smith

1977a,b). The waves are likely to be produced with large wavenumbers k or low phase velocities. Nonlinear scattering processes (Tsytovich 1970) will transform the waves to small k until the condition

$$\frac{W_p}{n_e K T_e} > k^2 \lambda_{De}^2 \text{ or } (\Delta k)^2 \lambda_{De}^2 \qquad (4.5.3)$$

is satisfied where $\lambda_{De} = v_e/\omega_{pe}$ is the electron Debye length and Δk is the width of the plasma wave spectrum in k space. At this point the ponderomotive force of the plasma waves overcomes the dispersive properties of the plasma which forces the plasma waves to form spatially isolated regions of depleted density and high wave intensity called solitons (Zakharov 1972). The subsequent development of the solitons is for the density depletion and wave intensity to increase which drives the plasma waves trapped in the solitons to large k or low phase velocity where they are heavily Landau damped by the tail of the electron distribution. This results in the nearly complete conversion of wave energy into an accelerated electron tail which extends up to several tens of keV for typical solar conditions. This process is especially effective when a moderate magnetic field is present with $\omega_{ce} \lesssim \omega_{pe}$, where ω_{ce} is the electron cyclotron frequency. In this case both the nonlinear scattering processes and the modulational instability occur almost one-dimensionally in two cones along the magnetic field (Smith 1976b, 1977b).

4.6. Radio Evidence on the Particle Distribution Functions in the Corona Following Flares

The purpose of this Section is to summarize the results of radio studies and the information they give on the distribution functions (number, energy distribution and pitch angle distribution) of the energetic particles produced at the time of solar flares. We discuss the distribution functions of the particles resulting from I) first phase acceleration, II) first and/or second phase and III) second phase acceleration. Table 4.6.1 summarizes the results.

4.6.1. First Phase Acceleration

Two kinds of radio bursts are caused by particles accelerated in the first phase: Type III bursts and microwave impulsive bursts.

Type III bursts provide evidence that 10^{32} to 10^{33} electrons in the energy range ~10 to ~100 keV are often accelerated in the initial phases of a flare. Type III bursts occur in the corona above 1.1 R_0 during the flash phase of about 30% of all Hα flares (e.g. Svestka 1976); similarly, many Type III bursts have no chromospheric counterpart. When they occur together, they are highly correlated with the time variations in microwave and X-ray impulsive bursts.

It is now reasonably certain that the Type III bursts result from the conversion of Langmuir waves into electromagnetic radiation, and that the intense Langmuir waves result from nonthermal electrons propagating outward from the flare region. Both the particles and the waves have now been observed directly in interplanetary space (e.g. Lin 1974, Gurnett and Anderson 1977). The observed electron energies are again ~10 to ~100 keV and their pitch angles favor the forward direction. Spacecraft observations show a "forward-cone" distribution in "scatter-free" events (Lin 1974); in "diffusive events" where the majority of electron velocities are nearly isotropic, there seems to be a "scatter-free" core of streaming electrons (Kurt, Logachev and Pissarenko 1977). From theory, it seems necessary to

have both a gap distribution in velocity space (attributed simply to the faster electrons outpacing the slower ones) and a strongly anisotropic, forward-cone pitch angle distribution to give sufficiently intense Langmuir waves to account for the observed brightness temperatures of $\gtrsim 10^{11}$ K (e.g. Smith 1977C; Melrose 1978). Also as shown recently by Melrose, Dulk and Smerd (1977), the observed sense of polarization of harmonic Type III bursts (which Suzuki and Sheridan 1978 have shown to be o-mode) implies that the Langmuir waves, and presumably the particles which generate them, are confined to a forward cone of angle 10° to 30°.

In the acceleration region, the information we can deduce from Type III bursts about the electron energy and pitch angle distribution is quite limited. We have no direct information from the radio observations on electrons with energy less than several keV. This is because the collisional slowing-down time varies as v^3, and only the faster particles can escape. The total number of first phase electrons at low heights can be any number greater than 10^{33} insofar as type III bursts are concerned. Also their energy distribution could be power law or thermal with $T \gtrsim 10^8$ K. Regarding their pitch angles, the observed pitch-angle distributions must be determined by propagation effects and cannot reflect conditions at the source; some pitch-angle scattering must occur to produce the observed pitch-angle distribution at the Earth.

Microwave impulsive bursts are believed to be due to gyrosynchrotron emission from basically the same particles which produce the impulsive hard X-ray bursts except that most of the radio emission is produced by electrons with energies greater than 100 keV and most X-ray emission is produced by electrons with energy less than 100 keV (e.g. Takakura and Kai 1966, Ramaty 1969, Ramaty and Petrosian 1972, Takakura 1972).

The possibility that microwave impulsive bursts are radiated by quasi-thermal electrons (with near-Maxwellian velocity distribution) has not yet been investigated thoroughly, (see, however, Matzler 1978) but the radio observations

seem to be compatible with the idea of a small source in which the electron temperature is between 10^8 and 10^9 K, the density is $\sim 10^{10}$ cm^{-3} and the magnetic field is a few hundred gauss.

Comparing the implications of microwave impulsive vs. Type III bursts, we infer that the microwave, X-ray and Type III bursts stem from the same electron population, accelerated by the same acceleration mechanism, and that the electrons have access to both closed field lines of low loops where the majority are trapped and radiate microwaves and open field lines where they produce Type III bursts.

It is important to note that if the individual Type III electron streams are discrete by acceleration, rather than modulation, then the acceleration mechanism has to explain repeated (quasi-periodic at ~10 sec), impulsive (lasting ~1 sec) electron acceleration. Taking into account decimeter wavelength fast drift bursts, both the impulsiveness (~0.1 sec) and the repetition rate (~1 sec) must be even shorter.

4.5.2. First and/or Second Phase Acceleration

There are two kinds of radio bursts whose origin cannot be attributed unambiguously to the particles of first- or second-phase acceleration: Type II bursts and the early meter-wave continuum designated FCM.

Type II bursts have two different aspects which need to be carefully distinguished: a) Type II's as indicators of a shock front and second phase acceleration and b) the Type II radiation itself. Following the work of Wild, Smerd and Weiss (1963) it is widely accepted that Type II bursts are indicators of shock fronts and second phase acceleration. This belief, which we share, relies on radio, particle and X-ray evidence: 1) the spectral drift rate of Type II bursts suggests a disturbance which originates at the place and time of the flash phase of flares and which travels faster than the Alfvén speed (Wild, Murray and Rowe 1954), 2) there is a close association between Type II bursts and the high-energy phase of other

coronal events (e.g. microwave IV's, strong, stationary meter-wave IV's) which require relativistic particles, and 3) there is a close association between Type II bursts (and the other bursts just enumerated) with relativistic particles producing PCA's and "cosmic ray events" as detected on spacecraft. As discussed in Section 10, Fermi acceleration by the shock or in shock-produced turbulence may be the agent for the second phase acceleration.

The Type II radio emission however, may not result from the relativistic electrons produced in the second phase acceleration. In fact, the occasional presence of "herringbone structure" in Type II bursts, i.e. Type III−like extensions from the slow drift "backbone" toward higher and/or lower frequencies, indicates that Type II radiation too results from 10 to 100 keV electrons. These electrons could be accelerated in or near the shock front and then outpace the slower ones to form the gap distribution and the forward-cone anisotropy which are required for the Type III-like bursts. Note, however, that despite their similarity, these electrons are accelerated at a later time and in a different location than the first phase particles.

The early flare continuum, FCM, is probably initiated by first phase electrons, but its characteristics give evidence of subsequent acceleration. FCM is usually weak, continuum radiation that starts during the flash phase, persists about 10 min in a given location, and then disappears (usually in association with the appearance of a moving Type IV burst; hence the name FCM). The relatively long duration and the occasional brightening of the source in association with a Type II burst suggests that secondary acceleration is important (Robinson and Smerd 1975; see also the discussion of FC II below).

4.6.3. Second Phase Acceleration

There are three kinds of radio bursts which are related to second phase acceleration and from which we can derive some properties of the

particle distribution functions: Microwave Type IV, Flare Continuum and Moving Type IV.

Microwave Type IV bursts (IVμ), it is generally accepted, result from gyro-synchrotron radiation emitted by electrons trapped in low coronal loops, as suggested by Takakura (1960). To distinguish weak IVμ bursts from the tails of impulsive bursts, it is important to note a delayed rise to maximum intensity, taking $\gtrsim 3$ min, and the "U-shaped spectrum" which peaks at wavelength of 3 cm or less (e.g. Wild, Smerd and Weiss 1963; Castelli and Aarons 1968; Croom 1971). When distinguished in this way there is a strong correlation between IVμ bursts and the observation of relativistic particles near the Earth.

Studies of IVμ bursts have led to the conclusion that about 10^{31} to 10^{33} electrons are accelerated to relativistic energies by the second phase process, i.e. about 10^{-3} of the first phase electrons are accelerated to about 100 times their energy. The energy distribution is inferred to be a power law of index $\gamma \approx 2$ to 3 (e.g. Kai 1968). The radio observations do not require a strong anisotropy for the radiating particles. Because they are trapped in coronal loops we would expect them to have a loss cone distribution, but this probably has little effect on the radio emission.

Moving Type IV bursts (IVM) appear to be of several varieties (e.g. Wild 1970; Smerd and Dulk 1971), only two of which are of interest here. The first is the rare "Advancing Front" which is closely associated with a Type II burst and indicates that relativistic electrons are produced in the vicinity of the shock. The radiation occurs over about a 2:1 frequency range, the sources occur considerably higher in the corona than the plasma level for the frequency of observation, and the only acceptable radiation mechanism seems to be synchrotron emission. Only a half-dozen or so bursts of this kind have ever been recorded: examples were given by Boischot and Clavelier (1967, 1968), Warwick (1968), and Kai (1970), while ideas on their interpretation were given by Ramaty and Lingenfelter (1967, 1968) and Lacombe and Mangeney (1969),

Smith (1971, 1972a, b). Because the source regions are large and the magnetic fields are small (approximately the ambient fields), it is inferred that about 10^{33} electrons of energy $\approx$1 to 3 MeV are required (Boischot and Daigne 1967). The frequency spectrum of the emission implies that the electron energy distribution is a steep power law, with index $\gamma \approx 5$ to 10. We know little about the pitch-angle distribution, but a strong anisotropy does not seem to be required.

The second variety of IVM burst is the "Isolated Source", which is much more common and is probably a self-contained configuration of electric currents, magnetic field and mildly-relativistic electrons (termed a "plasmoid"), which moves outward from the low or middle corona. The properties of these bursts and their interpretation have been given by Smerd and Dulk (1971), Schmahl (1972), Dulk (1973) and Robinson (1977). Again, the only acceptable radiation mechanism seems to be gyrosynchrotron emission. The observed characteristics, especially the high degree of circular polarization usually observed, imply a strong magnetic field (3-10 G) and relatively low particle energies. About 10^{33} electrons with energies greater than 100 keV are required; the inferred energy distribution is a power law with index $\approx$4. The pitch angle distribution is uncertain; only an extreme type of anisotropy would lead to observable effects, i.e. to maser-like emission.

Flare Continuum, especially the FCII variety, closely associates with Type II bursts and second phase acceleration. FCII differs from the moving Advancing Fronts in that at a given observing frequency, the sources typically appear at a given height at about the time that the Type II passes and then remain at the same height for some tens of minutes afterwards. At lower frequencies the sources appear at greater heights. This characteristic and the arch-shaped structure sometimes observed, indicates that the radiation comes from electrons trapped in high coronal loops. Although a definitive study has not yet been carried out, it

appears that FCII bursts are very closely associated with long-decay X-ray events and proton events observed by spacecraft. The characteristics and interpretation of these bursts have been given by Pick (1961), Akinyan et al. (1971), Böhme (1972), Robinson and Smerd (1975), Magun, Stewart and Robinson (1975) and Robinson (1977).

The radiation mechanism for FCII bursts is not known; plasma radiation and gyrosynchrotron radiation are possible. If plasma radiation, it is necessary to have many more than one fast electron per cubic Debye length throughout the source volume (e.g. Melrose 1978), which is typically 10^{32} to 10^{33} cm^3. Because the Debye length is about 1 cm, this implies that $\gtrsim 10^{34}$ electrons of energy $\gtrsim 10$ keV are required. The plasma mechanism allows, but does not require the electrons to be relativistic, but it does require the energy distribution to be either a gap or a plateau and it requires the pitch angle distribution to be anisotropic; a loss-cone distribution of opening-angle 20° to 30° will suffice (Robinson 1977). Such a distribution could result from scattering of particles into the loss cone (Melrose and Brown 1976) followed by their thermalization due to Coulomb interactions in lower, denser regions.

Alternatively, if gyrosynchrotron emission, it is necessary to have about 10^{33} electrons with energies $\gtrsim 0.5$ MeV in order to account for the observed intensity from a region with the relatively low magnetic field strength of the ambient corona ($\lesssim 1$ G at the heights involved). From the spectrum, it is inferred that the energy distribution is a steep power law, of index $\gamma \approx 7$. The pitch angle distribution is not required to be anisotropic for this radiation mechanism to work, but a loss-cone distribution is likely for electrons trapped in coronal loops.

4.6.4. Summary and Conclusions

Scanning Table 4.6.1, we note that the short wavelength radio bursts emanating from the low corona generally require a harder electron energy spectrum than do the long wavelength bursts from higher up.

Most bursts are consistent with a power-law distribution; the exceptions are Type III (where the fast electrons have outpaced the slow), the Type II radiation itself (which is not understood), and the Flare Continuum if interpreted in terms of plasma radiation.

4.7 ENERGETIC SOLAR PARTICLES AT 1 AU

Acceleration processes in solar flares can be studied by observing flare associated energetic particle events in the interplanetary medium, generally at 1 AU. After the particles have been accelerated and released from the Sun, the charge composition and energy spectra can be measured in interplanetary space as a function of time. Contained in these measurements is information on the acceleration process and the properties of the source region, as well as on the transport of the energetic particle in both the corona and the interplanetary medium.

In this Section we discuss the observed energy spectra of protons and electrons over a wide range of energies, the ratio of protons-to-electrons, and the observations of energetic particle events which are rich in ^{3}He. Information on the spectra of protons and electrons and their ratio can give important clues for unravelling the properties of the acceleration mechanism. Knowledge of the proton and electron spectra as deduced from particle observations in space is also required for the interpretation of information derived from X-ray and gamma-ray data discussed elsewhere in this Chapter. The ^{3}He enrichments pose a considerable challenge to particle acceleration theories in flares, and indeed to the entire flare process itself. The ^{3}He enhancements are strongly correlated with enhancements of heavy nuclei in solar energetic particles. In the present Section we give a brief review of these enhancements, and in Section 4.8 we evaluate their effects on solar gamma-ray spectra.

4.7.1 PROTON AND ELECTRON ENERGY SPECTRA AND RATIOS

The energy spectra observed at 1 AU represent the combined effects of acceleration, coronal transport, release into interplanetary medium and interplanetary propagation. As a result of the propagation conditions, the observed spectra vary considerably from one event to another and during

the course of a given event. For example, near the onset of the particle event, the spectrum should be harder than that near the acceleration site, because the higher energy particles arrive first; in the decay phase, on the other hand, the fluxes of higher energy particles are already decreasing while the lower energy particles fluxes are still increasing, and this effect produces a softer energy spectrum than that released from the flare. It has been shown (Lin 1974, Van Hollebeke, Ma Sung and McDonald 1975) that the propagation effects can be minimized if the energy spectra are observed at a time of maximum particle intensity. Furthermore, the direct magnetic connection of the observer to the flare is also important for obtaining an energy spectrum representative of flare acceleration; if the associated flare is at a substantial azimuthal angle from the preferred connection site (i.e. separated by more than 60° of longitude), the particle distributions are expected to be significantly modified by coronal propagation. And finally, for obtaining an unbiased flare acceleration spectrum, it is important that no strong interplanetary disturbances, such as shocks, exist between the particle release site and the point of observation.

Proton Spectra

An extensive study for determining the energy spectrum of protons from solar flares was made by Van Hollebeke et al. (1975). By analyzing some 32 particle events associated with flares that were well connected magnetically to the observing spacecraft, these authors found that over the limited energy range from 20 to 80 MeV the spectrum of the proton number density can be expressed as a power law in kinetic energy $N(E) \propto E^{-s}$. It was also found that for these well connected flares the values of s displayed only a small dispersion, with 90% of the events in the range $2.5 \leqslant s \leqslant 3.7$. Steeper spectra (i.e. larger values of s) are observed from flares which are not well connected to the observer, and this steepening may result from the energy dependence of particle escape from the corona.

Below $\sim$ 10 MeV, the observed spectrum is generally flatter than at higher energies (McKibben 1972, Van Hollebeke et al. 1975). These authors have shown that the spectrum cannot be represented by a single power law over an extended energy interval ($\sim$ 4 to 80 MeV) even when the velocity dispersion of the particles is taken into account. An exponential in rigidity also does not give a good fit to the data. This indicates that either there is an intrinsic flattening in the spectrum of protons escaping from the Sun, or different propagation conditions apply at low and high energies. That the flattening is intrinsic to the acceleration mechanism is supported by the finding that a similar change of spectral slope is required also by the gamma ray data (Section 8).

Above 100 MeV, reported measurements have shown a steepening of the spectrum. However, these measurements are often the result of indirect observations which present both uncertainties and limitations. Ground level detectors, such as neutron monitors, need to be corrected for geomagnetic cutoff fluctuations or variation of the cone of acceptance; rocket measurements are limited to brief samples; balloon experiments have limitation in the low energy threshold. Intercalibration between the various parts of experiments covering a larger energy interval is not easy. It is expected that measurements of protons from large flares in solar cycle 21 (to be made by detectors on IMP 8, ISEE A and C) will help define the proton spectrum at high energies. Meanwhile, we tentatively summarize the observational evidence as indicative of a proton spectrum which is a power law in kinetic energy from about 20 to 80 MeV, with a flattening at lower energies, and a possible steepening at energies exceeding about 100 MeV.

Electron Spectra

A detailed analysis of a large number of nonrelativistic electron events was made by Lin (1971). In this study the spectrum was determined from measurements of the maximum intensity at two energies, > 22 keV and > 45 keV, and the number density was fitted to a power law in kinetic energy, E^{-s}, with s between 3 and 4.5. In a subsequent study (Lin 1974), the electron events were analysed according to whether they were or were not accompanied by > 10 MeV protons above a given flux threshold ($0.3\ cm^{-2}sec^{-1}sr^{-1}$). This analysis revealed the existence of two groups of electron events: "pure electron events", i.e. those which were not accompanied by protons, and mixed events in which both protons and electrons were observed. It was found that pure electron events generally exhibited power law spectra from 5 to 100 keV with s ranging from 2 to 5, and a rapid steepening above $\sim$ 100 keV. For mixed events, the spectrum tends to be harder and does not seem to steepen above 100 keV.

Based on observations on the timing of the arrival of the particles, and related observations of optical, radio and X-ray phenomena, first phase acceleration should be responsible for the pure electron events, while second phase acceleration could produce the protons and more energetic electrons in mixed events (Lin 1974).

Relativistic electron events occur much less frequently than do non-relativistic events, and they are accompanied by large fluxes of energetic protons. The spectra of relativistic electrons are also power laws: in the energy range from 3 to 12 MeV, s = 3.2 $\pm$0.2 (Simnett 1971), while from 12 to 45 MeV, s has a median value of 3.5 (Datlowe 1971).

For only a few solar energetic particle events has the electron spectrum been measured over a wide energy range. Spectra determined from some 20 keV to beyond 10 MeV are generally the result of a compilation from different

experiments. For example, Lin (1974), by combining electron spectra from various measurements found that the spectrum of the May 28, 1967 event is consistent with a power law in kinetic energy with spectral index s=3. However uncertainties in some of the measurements used to determine this spectrum were as large as 100%. Quite recently, Lin et al. (1978) have determined the electron spectrum for several events from tens of keV to about 10 MeV (Figure 4.7.1) A break at $\sim$ 100 keV is clearly evidenced in these spectra. Above this energy, an unbroken power law can be seen out to the highest observed energies.

Correlations Between Electrons and Protons

An important parameter in the study of particle acceleration mechanisms is the ratio of the protons to electrons. In Figure 4.7.2 we compare the intensities of 0.5 to 1.1 MeV electrons with proton intensities at 10 MeV for 42 events detected by the Goddard Space Flight Center experiment on IMP 4 and IMP 5 from May 1967 to October 1972. Both the electron and proton intensities are taken at times of maximum intensity. As can be seen, for large events (proton intensity greater than 5×10^{-2} protons/(cm^2sec sr MeV)) there is an almost constant ratio between the electrons and protons. This result suggests that for such events 0.5 to 1.1 MeV electrons and 10 MeV protons are accelerated by the same mechanism; this mechanism could operate during second phase acceleration.

For small size events (proton intensity less than 5×10^{-2} protons/(cm^2sec sr MeV)), the results of Figure 4.7.2 show that there is no good correlation between the electron and proton intensities. These events probably belong to the same class as Lin's (1974) "pure electron events". They are characterized by an overabundance of electrons which are likely to be accelerated by the first phase mechanism.

Because of uncertainties in the value of the geometric factor of the GSFC electron detectors, it was not possible to obtain a numerical relationship between the proton and electron intensities for large events in Figure 4.7.2. To overcome this problem, we have used results from the Caltech cosmic ray experiment on IMP 7 (E. Stone, R. Mewaldt, private communication 1977). In Figure 4.7.3 we compare the intensities of 0.2 to 1 MeV electrons from the Caltech experiment with the 10 MeV proton intensity from the GSFC cosmic ray telescopes on IMP 7. We again see a good correlation between the proton and electron intensities. From this correlation we can deduce that I_e ($\sim$ 0.4 MeV)/I_p (10 MeV) $\simeq$ 100.

Assuming a spectral index s=3 for electrons above 0.2 MeV (Figure 4.7.1), we find that for second phase acceleration the electron-to-protnn ratio at 10 MeV is about 10^{-2}. This result is qualitatively consistent with that of Datlowe (1971) who also found very small electron-to-proton ratios at high energies. As we shall see in Section 4.8 an essentially similar result can be obtained from the analysis of gamma-ray data. Second phase acceleration, therefore, should produce many more protons than electrons at the same energy.

4.7.2 ^{3}He IN ENERGETIC SOLAR PARTICLES

The first attempt to measure the ^{3}He abundance in energetic solar particles was made by Schaeffer and Zahringer (1962). By using mass spectroscopy of material from the Discoverer 17 satellite, these authors found that the ^{3}He/^{4}He ratio at about 70 MeV/nucleon was $\sim$ 0.2 for the 1960, November 12 flare. Subsequent measurements (Hsieh and Simpson 1970, Anglin, Dietrich and Simpson 1973, Dietrich 1973, Garrard, Stone and Vogt 1973) have revealed the existence of a class of solar particle events in which the ^{3}He/^{4}He ratio is substantially larger than in the ambient solar atmosphere. In the solar wind, for example, ^{3}He/^{4}He is of the order of a few times 10^{-4} (Geiss and Reeves 1972), while Hall (1975) determined spectroscopically a ^{3}He/^{4}He ratio

of $(4 \pm 2) \times 10^{-4}$ in a solar prominence. There is no direct observation of the ^{3}He in the photosphere, but the 2.2 MeV gamma-ray line sets an upper limit on the photospheric ^{3}He abundance consistent with that measured in the solar wind (Wang and Ramaty 1974).

The basic characteristics of the ^{3}He rich events can be summarized as follows: (a) The ^{3}He/^{4}He ratio measured over the energy range from 1 to 20 MeV/nucleon is fairly variable ranging from about 10^{-2} to more than 1. (b) The enhancement in ^{3}He is not accompanied by a similar enhancement in ^{2}H or ^{3}H. The upper limits on ^{2}H/^{3}He and ^{3}H/^{3}He can be as low as a few times 10^{-3}. (c) Large enhancements of ^{3}He usually accompany small proton events. These events are not always identified with solar flares. (d) ^{3}He rich events are always associated with enhancements of Fe nuclei, the range of variability of the ratio Fe/^{4}He being similar to that of ^{3}He/^{4}He. The opposite, however, is not true, i.e. there are events rich in Fe with no ^{3}He enhancements (Anglin et al. 1977; Zwickl et al. 1978).

Enrichments of ^{3}He in energetic particle populations (for example the galactic cosmic rays) have been generally attributed to nuclear reactions between the energetic particles and the ambient medium. But as first pointed out by Garrard et al. (1973), this interpretation of the solar ^{3}He enrichments, in its simplest form, is inconsistent with much of the ^{3}He data. If the ^{3}He enrichments are due to nuclear reactions of the energetic particles, then they should be accompanied by similar enrichments in ^{2}H and, to a lesser degree, in ^{3}H. Such enrichments, however, are not observed.

To resolve this difficulty, Ramaty and Kozlovsky (1974) and Rothwell (1976) have pointed out that the kinematical prpperties of the ^{2}H and ^{3}He producing reactions are such that ^{2}H is preferentially emitted in the forward direction, i.e. the direction of the primary projectile. Thus, if energetic particles in the flare are beamed, fractionation effects among ^{3}He and ^{2}H could arise, provided that the escape of the particles from the interaction region is not

along the beam direction. Moreover, ^{3}H is more readily destroyed after its production than ^{3}He. These effects can lead to an enhanced $^{3}He/^{2}H$ ratio, but no larger than about 30 (Ramaty and Kozlovsky 1974), while there are cases where the observed ratio is larger than about 600 (Serlemitsos and Balasubrahmanyan 1975). In a different nuclear model, Colgate, Audouze, and Fowler (1977) have proposed that the energetic products of the primary nuclear reactions, by being confined to thin filaments in their flare model, interact thermonuclearly with each other to destroy ^{2}H and ^{3}H. Such destruction in addition to the kinematical selection, can lead to a $^{3}He/^{2}H$ ratio greater than 10^{3}.

As opposed to the above nuclear models, plasma models for ^{3}He enrichments were proposed (Fisk 1978, Ibragimov and Kocharov 1978), In the model of Fisk (1978) it is suggested that a common current instability may excite electrostatic ion cyclotron waves which could heat coronal ^{3}He to a temperature significantly higher than that of the ambient ^{4}He. Then, if ions from the high-energy tail of a Maxwell-Bolzmann distribution are directly accelerated to energies in excess of an MeV, ^{3}He would be preferentially injected into the acceleration mechanism, and hence would show up overabundant at high energies. This interpretation of the ^{3}He-rich particle events predicts no enhancements of ^{2}H and ^{3}H, since these isotopes are essentially absent from the solar atmosphere.

The requirements of Fisk's model are that (a) the β of the plasma be less than 10^{-3}, (b) the electron temperature be less than 10 times the ion temperature, and (c) $^{4}He/^{1}H \geq 0.2$ in the ambient medium. Requirement (a) is plausible in the low corona while (c) could result either from thermal diffusion or from the consideration that the solar wind removes, on the average, more protons than helium from the corona. If only (a) and (b) are satisfied, the waves can be excited, but their frequency is above the ^{1}H

cyclotron frequency. If, in addition, (c) is also satisfied, the wave frequency is between the $^4He^{+2}$ and ^1H cyclotron frequencies. Electrostatic ion cyclotron waves can then resonate with ambient coronal ^3He, thereby raising its temperature. If the acceleration process has an injection threshold (Section 4.10), only particles in the high energy tail of the Maxwell-Boltzmann distribution are accelerated. The heating, and hence the acceleration, of the ^3He is preferential, because this isotope is the only stable one with fundamental cyclotron frequency between those of $^4He^{+2}$ and ^1H. However, as pointed out by Fisk, (1978), resonance at the second cyclotron harmonic is also possible, in particular for heavy ions. To have the right cyclotron frequency, these ions must be partially stripped; preferential heating is expected for $^{12}C^{+4}$, $^{16}O^{+5}$ and $^{56}Fe^{+17}$. Since the concentration of these ions in the ambient medium is strongly temperature dependent, not all of them should be simultaneously enhanced together with ^3He. The observation that the ^3He enrichments are best correlated with Fe enrichments (see below) suggests, in Fisk's model, that the temperature is around a few million degrees. At this temperature there is an appreciable concentration of ^{17}Fe with essentially no $^{12}C^{+4}$ and $^{16}O^{+5}$ present (Jordan 1969). Furthermore, the preferential heating of ^3He and Fe by electrostatic ion cyclotron waves has the implication that the charge state of enhanced Fe in ^3He-rich events should be around +17.

To compare the above proposed theories with observations, we have compiled and analyzed the available data on energetic particle events which are rich in ^3He.

A list of all known ^3He-rich events with $^3He/^4He \geq 0.1$ is given in Table 4.7.1. The first and second columns give the dates and time intervals of the measurements (for some events there are no published time intervals and these are indicated by dashes). In the third column we give the location

of the flares which are expected to be associated with the observed enrichments. But, as can be seen, there are many ^{3}He rich events which are not associated with known flares and these are indicated in this column by dashes. Columns 4 through 7 give the observed ^{3}He/^{4}He, ^{4}He/^{1}H, ^{2}H/^{3}He and ^{3}H/^{3}He ratios and the energy intervals in which these ratios are measured. The values of ^{2}H/^{3}He and ^{3}H/^{3}He are given for only 19 events and for all of these only upper limits are available. This shows that the ^{3}He enrichments are not accompanied by corresponding ^{2}H and ^{3}H enrichments. Column 8 gives the actual number of nuclei observed, when this information is available and column 9 gives the proton intensity of the time of maximum intensity of the event. Column 10 gives information on the association of the ^{3}He rich events with radio and X-ray emission and column 11 cites the appropriate references.

The ^{3}He/^{4}He ratio as a function of the maximum proton intensity at 10 MeV is plotted in Figure 4.7.4. In addition to the data of Table 4:7.1, this figure also includes 10 events with $^3\overline{\text{He}}/^4\text{He} < 10^{-1}$ in the energy range 5 to 8 MeV/nucleon (Anglin et al. 1977, J. A. Simpson private communication 1978). It can be seen that there is a general trend for the smaller events to be richer in ^{3}He. Small events also tend to have larger ^{4}He/^{1}H ratios as can be seen from Figure 4.7.5. This figure is also based on data from Table 4.7.1, from Anglin et al. (1977), and from J. A. Simpson (private communication 1978). It can be seen from Figure 4.7.4 and 4.7.5 that the higher ^{3}He/^{4}He ratio occur for small events with high ^{4}He/^{1}H ratio. A consequence of this result is that the large ^{3}He/^{4}He ratio reflects a genuine ^{3}He enhancement rather than a ^{4}He depletion. Figure 4.7.6 is taken from the work of Anglin et al (1977) and shows a plot of Fe/^{4}He as a function of ^{3}He/^{4}He. As can be seen, ^{3}He rich events are also rich in Fe, confirming the initial observation of Hovestadt et al. (1975). There are, however, several Fe-rich events which do

not show an enhancement in ^{3}He.

A summary of the models proposed to explain the ^{3}He rich events has been given above. The result that ^{2}H and ^{3}H are not enhanced together with ^{3}He is a problem faced by all nuclear models. However if ^{3}He enhancements are due to preferential heating (Fisk 1978) no ^{2}H and ^{3}H enhancements are expected.

The mechanism of Fisk (1978) requires an enrichment of ^{4}He in the ambient medium (^{4}He/^{1}H $\geq$ 0.2). In order to check this requirement we have plotted in Figure 4.7.7 the ratio ^{3}He/^{4}He as a function of ^{1}H/^{4}He, using data given in the Figures 4.7.4 and 4.7.5. As can be seen the ^{3}He overabundance is associated with an enhancement of ^{4}He in the energetic particles and this enhancement might be due to the enrichment of ^{4}He in the ambient medium, as required. Another requirement of the mechanism is that the temperature of the ambient electrons be sufficiently low ($T_e < 10\ T_{ion}$). This could also be consistent with at least part of the data, since, as can be seen from Figure 4.7.4, many of the ^{3}He rich events are not associated with identified flares and this may be due to the low temperature of the electrons. Finally, preferential heating of ^{3}He could be accompanied by preferential heating of partially stripped Fe (Fisk 1978), consistent with the association of ^{3}He and Fe enhancements (Figure 4.7.6).

There is however a group of events with ^{3}He/^{4}He ratio in the range 0.1 to 0.2 for which ^{4}He/^{1}H $\simeq 10^{-2}$ or less (Figure 4.7.7). These events cannot be easily explained by Fisk's model because, as mentioned above, the mechanism requires a large ambient ^{4}He abundance. Furthermore, as we have already discussed in connection with Figure 4.7.6 the events for which ^{3}He/^{4}He is about a few percent, do not show any clear correlation between the ratios ^{3}He/^{4}He and Fe/^{4}He. Furthermore, we have been able to find one ^{3}He-rich event for which the charge state of Fe has been measured, and it is not +17 as required by

the preferential heating model. This is the May 14, 1974 event for which $^3He/^4He \simeq 0.18$ (Table 4.7.1). Gloeckler et al. (1976) have detected overabundant Fe from this event ($Fe/O \sim 1$), and they find that its mean ionization is 11.6. It is possible, therefore, that the origin of ^3He in the moderately enriched events ($^3He/^4He \leqslant 0.1$) is nuclear, while the plasma mechanism could be responsible for the ^3He enhancement in the extreme cases where $^3He/^4He \geqslant 1$.

There is additional data to support the hypothesis that there could be two classes of ^3He rich events. This is shown in Table 4.7.2 where we have compiled data on energy spectra of ^3He and ^4He. Such spectra are available in only a few cases, but even the limited data of this table shows that the ^3He and ^4He spectra are parallel if $^3He/^4He$ is large, while the ^3He has a flatter spectrum than ^4He if $^3He/^4He$ is smaller. If preferenti heating and injection are responsible for the large $^3He/^4He$ ratios, then the parallel ^3He and ^4He spectra could simply result from the common mechanisms which accelerates these two isotopes after injection. In the nuclear models, however, the ^3He is expected to have a flatter spectrum than its parent ^4He, qualitatively consistent with the results of Table 4.7.2.

4.7.3 HEAVY NUCLEI IN FLARES

Nuclei heavier than He in energetic solar flare particles were first detected by Fichtel and Guss (1961), and since then numerous measurements of such particles have been made (e.g. Fan, Gloeckler and Hovestadt 1975 and references therein). While the earlier results of the composition of solar energetic particles have indicated rough agreement with photospheric composition, during the last few years, it became quite obvious that in many instances the energetic particle composition can depart drastically from the expected composition of the solar atmosphere. In addition to the ^3H enhancements mentioned above, there are very dramatic enhancements of

heavy nuclei, in particular Fe; the largest Fe enhancements are observed at low energies (< 10 MeV/nucleon), where Fe/He ratios close to unity have been seen (see previous subsection). But these enhancements are not limited to only the low energies. In the 15 to 30 MeV/nucleon range, Bertsch and Reames (1977) have reported on Fe/O ratio close to 40% for the 1974, July 4 flare, while Dietrich and Simpson (1978), report on Fe/O ratio close to unity up to about 200 MeV/nucleon for the 1977, September 24 event. It is outside the scope of this Chapter to discuss these enrichments in great detail. In Section 4.8, however, we evaluate the effects of heavy nuclei enrichments on solar gamma ray spectra.

4.8. SOLAR GAMA RAYS

Solar gama ray lines were first observed from the 1972, August 4 and 7 flares by a detector employing a NaI(Tℓ) crystal flown on OSO-7 (Chupp el al. 1973, 1975). Lines at 2.22, 0.51, 4.44 and 6.13 MeV, and continuum in the 0.35 to 8 MeV range were reported from the August 4 flare, with fluxes of $(2.8 \pm 0.22) \times 10^{-1}$, $(6.3 \pm 2.0) \times 10^{-2}$, $(3 \pm 1) \times 10^{-2}$ and $(3 \pm 1) \times 10^{-2}$ photons/cm^{2}sec in the above 4 lines, respectively, and about 1 photon/cm^{2}sec in the continuum above 1 MeV. Line emission at 2.22 and 0.51 MeV, with fluxes of $(6.9 \pm 1.1) \times 10^{-2}$ and $(3.0 \pm 1.5) \times 10^{-2}$ photons/cm^{2}sec, respectively, was also detected from the August 7 flare, but only upper limits could be set on the 4.4 and 6.1 MeV lines and on the continuum from this flare. Gamma-ray emission in the MeV region was also reported from the 1967, May 21 and 23 events, but because of poor energy resolution, no line emission could be resolved from these flares (Gruber, Peterson and Vette 1973). It is worthwhile to note, however, that the flux of MeV gamma rays from the May 23 flare was comparable to that from the 1972, August 4 event, and that the upper limit set on the 2.2 MeV line was larger by only about a factor of 2 than the observed flux of this line from the 1972, August 4 flare. Very recently, gamma-ray line observations were reported from the flares of 1977, November 22 (Chambon et al. 1978) and 1978, July 11 (Hudson et al. 1978). Solar gamma rays are the most direct probe of the nucleonic component of energetic particles in flares.

4.8.1. GAMMA RAY EMISSION MECHANISMS

The strongest gamma-ray line from flares is expected at 2.223 MeV resulting from the radiative capture of neutrons on protons ($n + p \rightarrow {}^2H + \gamma$). The neutrons are produced mostly in spallation reactions of He and heavier nuclei in the chromosphere or lower corona. The nuclear cross sections were summarized by Ramaty et al. (1975). After their production, the neutrons propagate rectilinearly with typical initial energies of $\sim$ 10 MeV, until they either decay or are captured. Wang and Ramaty (1974), employing a detailed

Monte Carlo simulation, have shown that the neutrons whose velocity vectors at production point toward the photosphere have a good chance (probability $\gtrsim 0.2$) of being thermalized and captured before they decay. The resultant gamma-ray line, at 2.223 MeV is extremely narrow (FWHM $\simeq$ 100 eV), its width determined by the photospheric temperature.

Because of the finite capture time, the 2.223 MeV gamma rays are emitted after the production of the parent neutrons. This delay, $\sim$100 sec, has to be taken into account in the comparison of the time profile of the 2.2 MeV line with hard X-ray and microwave time profiles. Such a comparison has been done by Bai and Ramaty (1976), and forms the basis for present studies of the temporal relationship between proton and electron acceleration in solar flares.

The second strongest line from flares is expected at 0.511 MeV from positron annihilation. The most important sources of positrons are radioactive nuclei (e.g. ^{11}C, ^{13}N, ^{14}O, and ^{15}O), the first excited state of oxygen, $^{16}O^{*}6.052$, and π^{+} mesons. The positrons are produced with initial energies ranging from several hundreds keV to tens of MeV (depending on the production mode), but if trapped by magnetic fields close to the Sun, the positrons can be slowed down to energies of tens of eV on time scales less than $\sim 10^{2}$ sec (if the ambient density is about $10^{11} cm^{-3}$). The positrons then annihilate, either freely or from a bound positronium atom. The latter annihilation mode dominates if the temperature is greater than $\sim 10^{6}$K and the density is $>10^{15} cm^{-3}$ (Crannell et al. 1976). Positronium formation leads to a characteristic 3-photon continuum just below 0.511 MeV. The width at the 0.511 MeV line depends on the temperature, state of ionization and density of the ambient medium, and is expected to

be less than about 20 keV for solar flares.

In addition to the 2.223 and 0.511 MeV lines, nuclear interactions in flares lead to many other lines resulting from deexcitations of nuclear levels. Figure 4.8.1 shows the spectrum from these deexcitations calculated by employing a Monte Carlo simulation for an energetic particle population interacting with an ambient medium. The energetic particle spectrum is proportional to E^{-2}, where E is energy per nucleon. Both the ambient medium and the energetic particles at the same E have a photospheric composition (Ross and Aller 1976). The calculations are based on close to 100 nuclear lines derived from either labotatory measurements or theoretical interpolations and evaluations (Ramaty, Kozlovsky and Lingenfelter 1979). The shapes of the lines are evaluated by taking into account nuclear kinematics and data on the differential cross sections of the reactions. The results of the simulations are binned into energy intervals ranging from 2 to 5 keV, as indicated in the figure, consistent with the resolution of a high purity Ge detector.

Two line components can be distinguished in Figure 4.8.1: a narrow component resulting from the deexcitation of ambient heavy nuclei excited by energetic protons and alpha particles, and a broad component from the deexcitation of energetic heavy nuclei interacting with ambient H and He. The widths of some of the narrow lines are about 5 keV at 0.847 MeV, 18 keV at 1.369 MeV, 13 keV at 1.434 MeV, 100 keV at 4.44 MeV, and 150 keV at 6.129 MeV. The spallation features at $\sim$5.2 and $\sim$6.3 MeV are a few hundred keV wide. There are many other weaker lines, which together with the Doppler broadened nuclear emission produced by heavy

accelerated particles, merge into the underlying continuum. Above ∿4 MeV most of the radiation is from C, N and O, while below about 3 MeV the principal contributions are Mg, Si and Fe. At higher energies, an important line is at 15.11 MeV from ^{12}C deexcitation (Crannell, Ramaty and Crannell 1977). Even though its intensity is less than 2% of the 4.44 MeV line intensity, its high energy could make this line detectable above background for large flares.

4.8.2 CONSEQUENCES ON ENERGETIC IONS AND RELATIVISTIC ELECTRONS

Solar gamma rays, being produced by protons and nuclei of energies greater than several MeV and by electrons above about 0.5 MeV, provide unique information on these particles at or near the flare region. In what follows, we discuss the information on the timing of the acceleration of high energy particles in flares, the spectrum and energy content of the nucleonic component, the enrichment of heavy nuclei in the accelerated particles, and the proton-to-electron ratio.

Timing of the Acceleration of High Energy Particles

Gamma-ray observations of the 1972, August 4 flare have pinpointed the acceleration time of the nucleonic component of solar energetic particles with an accuracy on the order of 1 minute. In Figure 4.8.2 the three upper curves are the measured time profiles of X rays (29 to 41 keV), gamma rays (0.35 to 8 MeV), and microwaves (37 GHz). The error bars in the lower part of the figure represent the measured intensities of the 2.22 MeV lines (Chupp et al. 1975). The solid, dashed, and dotted curves are calculated time profiles of the 2.22 MeV line (Bai and Ramaty 1976); the solid curve is obtained by assuming that the instantaneous number of energetic nuclei in the flare region has the same time dependence as that of the observed 0.35 to 8 MeV gamma rays, while the dashed and dotted curves are obtained by assuming that the time dependence of

the nuclei is the same as that of the 29 to 41 keV X-rays. Thus, there appears to be a delay between the appearance of the ∿10-100 keV electrons which produce the 29 - 41 keV X rays and the energetic nuclei which are responsible for the gamma-ray line emission. For the solid and dotted curves we use a photospheric ^{3}He abundance ^{3}He/H = 5×10^{-5}, and for the dashed curve we use ^{3}He/H = 0. On the other hand, there seems to be no delay between the time profile of the nuclei and that of the gamma rays above 0.35 MeV or the 37GHz microwaves. The microwaves are produced by electrons of energies from several hundred keV to about 1 MeV and the gamma rays are a combination of bremsstrahlung from such electrons and nuclear radiation. We therefore conclude that nuclei of tens of MeV and electrons of several hundred keV should have similar time profiles. In Section 4.10 we show that this result could be consistent with Fermi acceleration.

The Spectrum and Energy Content of the Nuclei

The spectrum of energetic particles in the 1972, August 4 flare has been estimated by comparing the calculated and observed ratios of the intensities of the 4.44 and 2.22 MeV lines (Ramaty et al. 1975), or of the total 4 to 8 MeV radiation and the 2.22 MeV line (Ramaty et al. 1977). We define spectral parameters s and E_c, such that the instantaneous number of particles per unit energy per nucleon around E is proportional to E^{-s} for $E > E_c$ and to a constant for $E < E_c$. Figure 4.8.3, taken from Ramaty et al. (1977), shows the ratio of the nuclear radiation from 4 to 8 MeV to the 2.223 MeV line intensity as a function of these parameters. The shaded area is the measured ratio of the total 4 to 8 MeV radiation to the 2.22 MeV line intensity. The comparison of this ratio with the calculated

ratios yield the spectral information: for $E_c \lesssim 10$ MeV/nucleon $s \simeq 1.8$, while for $E_c \simeq 30$ MeV, $s \simeq 2.5$. Steep spectra ($E_c \lesssim 10$ MeV/nucleon, $s \gtrsim 2$) are inconsistent with the gamma-ray data because they produce too much radiation in the 4 to 8 MeV range relative to the 2.22 MeV line intensity.

The production of gamma rays by nuclear collisions is accompanied by energy deposition due to Coulomb collisions of the accelerated particles. Using the energy loss rates for protons in an ionized medium (Ginzburg and Syrovatskii 1964) we have calculated the ratio of the energy deposition rate, $\dot{W}$, to the narrow 4.44 MeV line production rate, $Q_{4.44}$. The results are shown in Figure 4.8.4. The ordinate on the left side of this figure shows $\dot{W}/Q_{4.44}$, while the right side ordinate shows $\dot{W}$ for the 1972, August 4 flare; to calculate $\dot{W}$ we have used the measured 4.44 MeV line flux of 0.03 photons/cm^2 sec (Chupp et al. 1975).

As can be seen, $\dot{W}/Q_{4.44}$ is a strong function of the spectral parameters; for steep energetic particle spectra the energy deposited per gamma ray is large because the particles below a few MeV per nucleon deposit energy efficiently by Coulomb collisions but do not produce gamma rays. However, using the previously derived constraints on the spectral parameters, we see that the energy deposited by the protons and nuclei in the 1972, August 4 flare could not have exceeded about 10^{28} erg/sec. While this is an upper limit, a more probable value of $\dot{W}$ would be that corresponding to $s = 2.5$, $E_c = 30$ MeV/nucleon, a set of parameters which fit the data in Figure 4.8.3. For this spectrum, $\dot{W}$ is about 6×10^{26} erg/sec. Since the duration of proton acceleration should be similar to that of

electron acceleration, about 10^3 sec, the total energy deposited by the nucleonic component was about 6×10^{29} erg for the 1972, August 4 flare.

If the energetic protons and nuclei produce the gamma rays by interacting with a thick target, the total energy in the nucleonic component is just the deposited energy as calculated above. However, for a thin target, the total energy is the sum of the deposited energy and the energy carried away from the Sun by escaping particles. This energy is given approximately by (W_i/t_{esc}) T, where W_i and t_{esc} are the average instaneous energy content and escape time from the Sun of energetic particles, and T is the total duration of particle acceleration.

In Figure 4.8.5 we show the production rate of the narrow 4.44 MeV line, $Q_{4.44}$, for W_i = 1 eV and unit ambient density as a function of s and E_c. For the spectral parameters derived above, $Q_{4.44}/W_i$ is about 10^{-26} photons/sec eV. The observed 4.44 MeV line flux, $\sim$0.03 photons/cm^2 sec, and T $\simeq 10^3$sec imply that the escaping particles carry away about 10^{43} ergs/(nt_{esc}), where n is in cm^{-3} and t_{esc} in seconds.

The value of nt_{esc} can be best determined from observations of energetic particle species with low abundance in the ambient solar atmosphere (e.g. ^{2}H, ^{3}H, Li, Be, B). Such species therefore, if observed in the energetic particles, must be of secondary nuclear origin. ^{3}He can only place upper limits on nt_{esc} in flares, because, as implied by the anomalously rich ^{3}He events, (Section 4.7), at least part of the energetic ^{3}He nuclei could be due to preferential heating rather than nuclear spallation.

^{3}He was observed from the 1972, August flares (Webber et al. 1975),

and these observations imply that $nt_{esc} \lesssim 1.5 \times 10^{13} cm^{-3} sec$ (Ramaty and Kozlovsky 1974). While ^2H and ^3H was not observed from the 1972, August events, Anglin et al. (1973) have presented average $^2H/^1H$ and $^3H/^1H$ ratios for other flares which at 10 MeV/nucleon are about 8×10^{-5} and 2×10^{-5}, respectively. For these ratios nt_{esc} is about $10^{13} cm^{-3} sec$. Hurford, Stone and Vogt (1975a) detected ^2H in data from several flares, and found an $^2H/^1H$ ratio consistent with this value. Thus, while the ^3He abundance seems anomalous for many flares, for the 1972 August events the observed ^3He flux could be consistent with nuclear reactions of energetic particles, and the implied value of nt_{esc} is about 10^{13} $cm^{-3} sec$. When this value is compared with the range-energy relations of Barkas and Berger (1964), it follows that protons above $\sim$15 MeV escape without much energy loss (thin target), and that below this energy they lose a large fraction of their energy (thick target). Most of the gamma rays are in fact produced by particles above 15 MeV, and, moreover, for the spectral parameters deduced above, more than half of the energy resides in these particles.

For $nt_{esc} \simeq 10^{13} cm^{-3} sec$, the escaping particles carry away about 10^{30} ergs. This is comparable to the total energy deposited, $\sim 6 \times 10^{29}$ erg, but it is less by almost an order of magnitude than the estimated energy $\sim 8 \times 10^{30}$ erg, in the interplanetary medium in particles above 10 MeV (Lin and Hudson 1976). A possible reason for this discrepancy could be the acceleration of particles in the interplanetary medium by shock waves (e.g. Otaola, Gall and Perez Enriquez 1977). The total energy in energetic protons and nuclei at the Sun is therefore about 1.5×10^{30} ergs, or about 1% of the total flare energy.

The Effect of Heavy Nuclei Enrichments on the Gamma Ray Spectrum

The gamma ray spectrum of the 1972, August 4 flare, after the subtraction of the observed lines at 0.51, 2.22, 4.44 and 6.13 MeV is shown by the data points (Suri et al. 1975) in the left panel of Figure 4.8.6. The solid line in all three panels is the bremsstrahlung spectrum (Bai 1977) produced by electrons with number spectrum proportional to $E^{-3.5}$ which fits the X-ray data of Van Beek et al. (1973) above 100 keV. The data points in the central and right panels were obtained from those in the left panel by subtracting the contribution of unresolved nuclear lines. This nuclear radiation is calculated for photospheric abundances for the ambient medium, and is normalized to the observed total radiation in the 4 to 7 MeV region. This emission is believed to be entirely of nuclear origin for the 1972, August 4 flare (Ramaty et al. 1977). For the central panel the energetic particles have the same composition as the ambient medium, and for the right panel the energetic particles are enriched in heavy nuclei. We have used the recent results of Dietrich and Simpson (1978) for the 1977, September 24 flare at high energies, C:N:O:Ne:Mg:Si:Fe = 0.3:0.1:1:0.17:0.23:0.35:0.89:, where the Mg, Si and Fe abundances combine the data for Na and Mg, Al, Si and S, and $17 \leq Z \leq 28$, respectively.

If both the energetic particles and the ambient medium have photospheric abundances (central panel) the gamma-ray data requires more bremsstrahlung above ~ 0.7 MeV than is produced by a single power law electron spectrum. Based on this result Suri et al. (1975) and Bai and Ramaty (1976) have suggested that the electron spectrum should flatten above ~ 0.7 MeV, but as shown in Section 4.7 (see Figure 4.7.1) there is no evidence for such flattening in observed electron spectra from other flares. If, however the energetic particles are rich in heavy nuclei (right panel) all the gamma ray data are consistent with nuclear radiation and bremsstrahlung from a single

electron power law. (The excess between 2 and 2.4 MeV is probably due to the incomplete subtraction of the 2.2 MeV line, A. N. Suri private communication 1978). The energetic particles from the 1972, August 4 flare could have been enriched in heavy nuclei as were those from the 1977, September 24 event, eventhough the measurements of Webber et al. (1975) indicate only moderate enrichments; as we have already discussed, a major fraction of the energetic particles from the 1972, August events were probably accelerated in the interplanetary medium, and therefore their composition could differ from the composition of the flare accelerated particles.

The issue of whether the excess gamma rays are mostly from nuclear reactions or bremsstrahlung produced by a flat electron spectrum could potentially be resolved by microwave observations. The data of Croom and Harris (1973), at 71 GHz, indicate a flattening in the radio spectrum at high frequencies, and this would imply a corresponding flattening in the electron spectrum (Bai and Ramaty 1976), but the reliability of these millimeter wave data is somewhat in doubt. High resolution nuclear spectroscopy could also resolve this issue, since the fine structure of a Doppler-broadened nuclear spectrum should be quite different from that of bremsstrahlung, but no such data are available from solar flares at the present time.

The Proton-to-Electron Ratio

In Figure 4.8.7 we show nN(E) for protons and electrons as derived from the analysis of gamma ray and X-ray observations. The protons are normalized to $nW_i = 10^{40}$ erg cm^{-3}. The electron spectrum shown by the solid line produces the bremsstrahlung spectrum of Figure 4.8.6. As we have just discussed, this spectrum cannot account for the observed gamma rays and hence requires an enrichment of heavy nuclei. This enrichment could be in the energetic particles, in the ambient medium or in both. The electron

spectrum shown by the dashed line would produce the required excess bremsstrahlung without such enrichments, but the flattening implied by this spectrum is not seen in the particle data.

The temporal evidence for a second phase acceleration phase for the protons and relativistic electrons different from that which accelerates the lower energy electrons was shown in Figure 4.8.2. The flattening of the electron spectrum above 0.7 MeV would be another manifestation of second phase acceleration. If, however, there is no such flattening, then second phase acceleration should produce electrons with a single power law above about 100 keV. The two acceleration phases also manifest themselves in different proton-to-electron ratios. Whereas at low energies ($\lesssim$ 100 keV) this ratio is quite low (Canfield and Cook 1978), above about 10 MeV, the instantaneous number of protons must exceed that of the electrons by a large factor, as can be seen from Figure 4.8.7. Measurements of relativistic electrons in the interplanetary medium (Section 4.7) lead essentially to the same conclusion. In Section 4/10 we show that Fermi acceleration can lead to a large proton-to-electron ratio at high energies.

4.9 OTHER MANIFESTATIONS OF PARTICLE ACCELERATION

4.9.1 WHITE-LIGHT FLARES

These are short-lived, localized brightenings in the optical continuum sometimes observed during the impulsive stage of energetic flares. The light curves of these events have been observed to coincide with hard X-ray bursts, and there is evidence that they are associated with the proton flares with the hardest spectra, although the sample of observed events is small.

A number of possible explanations of white light flares have been proposed (e.g. Svestka 1976). We consider here only those mechanisms for producing optical continua that depend directly on energetic particles and which might serve as useful diagnostics. a) Synchrotron emission from highly relativistic electrons (e.g. Stein and Ney 1963); b) thermal emission from the photosphere produced by the thermalization of energetic flare protons (or electrons) penetrating from above; c) free-bound emission from the recombination of chromospheric material non-thermally ionized by energetic flare electrons (Hudson 1972, Lin and Hudson 1976); d) self-absorbed thermal synchrotron emission from hot filaments (Colgate 1978). We shall not attempt here to compare the merits and difficulties of these four mechanisms, except to note that the relativistic synchrotron mechanism would require many more relativistic electrons (10 to 1000 MeV) than there is other evidence for. More observations of the color and polarization of white light flares are needed, as well as more detailed theoretical modeling. It may be that more than one process is operative. Here we shall only consider the second proposed mechanism, since it is simplest to interpret, less model-dependent, and leads to the most useful diagnostics.

The suggestion was made and discussed independently by Najita and Orrall (1970) and Svestka (1970) that white light flares are due to the heating of the photosphere by a flux of energetic flare particles deposited from above. Protons (or electrons) with energies above ∿20 MeV can reach the photosphere. Because of the rapid increase of column density with depth there, particles of between 20 and 1000 MeV will deposit most of their energy in a thin layer about 100 km thick and the temperature will rise in the region of impact. Because of the short radiative relaxation time in the photosphere (∿1 sec), an equality will be quickly set up between the incoming particle energy flux and the excess radiative flux from the slightly heated region of impact. The white-light flare of 1967, 23 May (Demastus and Stover 1967) was a factor 1.16 brighter than the nearby photosphere, corresponding to a temperature increase of 220°K, and an excess radiative flux of $\sim 10^{10}$ erg cm^{-2} sec^{-1}. This is the flux that must be provided by particles with energies of 20 MeV or more. The larger of the two flare patches had an area of 2×10^{17} cm^2, so that a total deposition rate of 2×10^{27} erg sec^{-1} would be required to maintain it.

An early objection to this model was that it required particles of MeV energy to be accelerated early in the impulsive phase. But it is now known from the gamma-ray observations from OSO-7 of the 1972, August 4 flare (Chupp et al. 1973 and Section 4.8) that such protons are indeed produced in the impulsive phase only slightly later than the hard X-rays (Bai and Ramaty 1976). From Section (4.8), the rate of energy deposition for the August 4 flare from protons and nuclei above 20 MeV was about 5×10^{26} erg sec^{-1}, and this is about a factor of 4 too small to have

maintained the 1967, May 23 event.

No white light event was reported during the 1972 August 4 flare, but a well observed white light event occurred during the 1972, August 7 flare that coincided with the impulsive hard X-ray burst. Rust and Hegwer (1975) estimate that the total optical emission rates from the 4 bright knots of the event was 4.6×10^{27} ergs sec^{-1}. Unfortunately OSO-7 was in earth-shadow during the impulsive phase, although gamma ray observations were obtained during the later stages of the flare (Chupp et al. 1973).

From a comparison of the delayed emission at 2.2 MeV with microwave emission in the late stages of the flare, Wang and Ramaty (1975) find that the gamma-ray production during the unobserved impulsive portion might have been an order of magnitude greater than for the 4 August flare, provided that the delayed emission was due to the finite capture time of neutrons in the photosphere. If this is indeed true, the gamma-ray data are presently consistent with a proton-heated model of white light flares, since the total proton energy would have just supplied the events of 1967, May 23 and 1972, August 7. But Wang and Ramaty (1975) point out that this delayed emission might also be produced by protons trapped in the region of interaction. Further discussion probably must await new observations.

4.9.2 NON-THERMAL WINGS OF HYDROGEN LYMAN ALPHA

It has been pointed out by Orrall and Zirker (1976) that a beam of fast nonthermal flare protons impacting into the chromosphere will produce some equally fast neutrals (mostly by charge exchange). These will radiate Doppler-shifted photons, so that the hydrogen Lyman-alpha line

from the region of impact will have asymmetric, polarized, non-thermal wings, whose asymmetry depends on the flux and energy spectrum of the protons. The effect has been studied in some detail by Orrall and Zirker (1976), who find that protons with eneggies less than about 300 keV should be detectable, if the proton beam has a flux and spectrum comparable to the impulsive non-relativistic electrons.

The interpretation of the effect is not greatly model-dependent. It is uncertain how rapidly the thermal flare Lyman-alpha, produced by the thermalization of the fast protons and electrons themselves, will increase to mask the non-thermal effect. For this reason, observations early in the impulsive phase are required. Spectra of the Lyman-Alpha line in flares including the extended line wings, were obtained by the NRL experiment on Skylab but not in the early impulsive phase. These have been studied independently by Canfield and by Orrall at this workshop. No asymmetry has yet been detected that is certainly associated with the flare. Canfield and Cook (1978) place an upper limit of 2×10^{-2} on the ratio of the energy flux of nonthermal protons-to-electrons injected into the chromosphere at energies above 20 keV.

4.10 SECOND PHASE ACCELERATION

Ideas on second phase acceleration are closely related to older concepts of the acceleration of galactic cosmic rays. From an historical viewpoint these arose as follows. Swann (1933) proposed acceleration due to the "betatron" effect, and his idea was modified by Schluter (1957) and Berger et al. (1958) who called it "magnetic pumping." Fermi (1949, 1954) proposed acceleration from moving magnetized blobs, and Thompson (1955) and Kaplan (1956) applied the same idea to acceleration by hydromagnetic waves. It was recognized by Thompson (1955), Davis (1956) and by Parker and Tidman (1958) that effective acceleration requires effective scattering of the particles. Parker (1958) suggested that the scattering could be due to hydromagnetic waves with wavelength equal to the Larmor radius of the scattered particles. The theory of this co-called "resonant scattering" has since been developed in detail, and it is an important ingredient in present-day theories of acceleration by hydromagnetic turbulence. In this section we review some of the theoretical ideas of particle acceleration, and we discuss the plausibility of the Fermi mechanisms for second phase acceleration of energetic particles in flares.

4.10.1 Brief Review of Theoretical Ideas

Provided the turbulence can be regarded as stationary on time-scales shorter than the acceleration time (e.g., excluding advancing shock fronts) detailed balancing applies. This was implicit in some earlier theories, e.g. Parker and Tidman (1958), and was made explicit by Tverskoi (1967). It then follows that the acceleration of a distribution of particles f(p) may be described by an equation of the form

$$\frac{\partial f(p,t)}{\partial t} = \frac{1}{p^2} \frac{\partial}{\partial p} \left[p^2 d(p) \frac{\partial f(p,t)}{\partial p} \right], \qquad (4.10.1)$$

where p is particle momentum. This equation can be rewritten as a Fokker-

Planck equation (e.g., Chandrasekhar 1943)

$$\frac{\partial N(E,t)}{\partial t} = \frac{\partial}{\partial E}\ [A(E)\ N(E,t)] + \frac{1}{2}\frac{\partial^2}{\partial E^2}\left[D(E)N(E,t)\right], \qquad (4.10.2)$$

where E is particle kinetic energy, $N(E,t) = f(p,t)p^2dp/dE$, and there is a relationship between A(E) and D(E),

$$A(E) = \frac{1}{p^2}\ \frac{\partial}{\partial p}\left[p^2 d(p)\ \frac{dE}{dp}\right],\ D(E) = 2d(p)(dE/dp)^2. \qquad (4.10.3$$

In the presence of advancing shock fronts there is an additional contribution to A(E) but not to D(E). The rate of change of the mean energy of the particles is given by A(E).

Kulsrud and Ferrari (1971) treated acceleration by hydromagnetic turbulence in a general way. They showed that d(p) in equation (4.10.1) could be written in the form

$$d(p) = p^2 \int \frac{d^3\underline{k}d\omega}{(2\pi)^4}\ \gamma(\underline{k},\omega)\ \frac{<\delta B(\underline{k},\omega)\delta B^*(\underline{k},\omega)>}{B_o{}^2}\ , \qquad (4.10.4)$$

where B_o is the magnitude of the ambient magnetic field and $\delta B(\underline{k},\omega)$ is the Fourier transform of the magnetic fluctuations associated with the turbulence. The scattering rate $\gamma(\underline{k},\omega)$ depends explicitly on the assumed collision rate ν. Kulsrud and Ferrari found simple limiting expressions for the acceleration rate $\gamma(\underline{k},\omega)$. They take $\omega/k \approx v_A$, i.e., that the turbulence consists of compressions and rarefactions propagating at the Alfvén speed. The limiting cases are then as follows: (i) For $\omega/\nu << v_A/v$ and $v << v_A$ the acceleration corresponds to magnetic pumping. The particles can be regarded as trapped in localized regions subjected to compressions and rarefactions which change the energy of the particle due to conservation of the magnetic moment. The scattering tends to keep the pitch-angle distribution isotropic and provides a frictional drop which causes the compressions to damp by transferring their energy to the particles. (ii) For $\omega/\upsilon << v_A/v << 1$ the acceleration corresponds to transit acceleration as discussed by Shen (1965). In this case the particles diffuse out of the

region of compression at a rate, $\omega_D = \omega(v/v_A)^2$, which is faster than the compression rate ω. (iii) For $\omega/\nu >> v_A/v$ the acceleration corresponds to Fermi acceleration in the sense defined by Parker (1958). The particles are reflected by the moving magnetic compressions and the scattering counteracts the tendency of the pitch angles to decrease systematically.

Following Kulsrud and Ferrari's treatment Melrose (1971, 1974) showed that the scattering rate υ can adjust itself to a value which corresponds to Fermi acceleration in the Kulsrud and Ferrari theory. The underlying idea is that the turbulence causes the particles to become anisotropic, and such particles generate the resonant waves which scatter them. This idea is most familiar in connection with trapped particles in the magnetosphere (Wentzel 1961, Dragt 1961, Dungey 1963, Kennell and Petschek 1966). The conditions for the anisotropic particles to generate their own resonant waves are relatively mild, and the resulting acceleration rate (for $\omega/k = v_A$) is

$$\gamma(\underline{k},\omega) = \frac{\pi}{2}\,\omega\,\frac{v_A}{v}\,. \qquad (4.10.5)$$

This is essentially the same as the rate which occurs in the early theories of Fermi acceleration, e.g., Thompson (1955), Davis (1956), Parker and Tidman (1958), and Hall and Sturrock (1967).

The requirement that resonant scattering be effective provides several limitations on the acceleration. The most important is a threshold condition. The scattering is possible only when the gyroradius of the particle is comparable with the wavelength of the resonant wave and the speed of the particle is much greater than the phase speed of the wave (so that the wave looks like a stationary spatially periodic magnetic fluctuation to the particle). These conditions can be satisfied for nonrelativistic ions only for $v >> v_A$. Nonrelativistic electrons can resonate only with whistlers and only for $v >> 43\ v_A$ (ignoring the electron-cyclotron branch of the whistler mode at frequencies above half the electron gyrofrequency).

Other restrictions are that the particles must become sufficiently anisotropic to generate their own waves, and that the resonant waves grow fast enough, a condition which places a lower limit on the number density of the accelerated particles (Melrose 1974).

4.10.2 Fermi Acceleration in Solar Flares

In this subsection we wish to investigate the plausibility of the Fermi mechanism for second phase acceleration of energetic particles in solar flares. We consider the rate of change of the mean energy, A(E), given by equation (4.10.3). By using equations (4.10.4) and (4.10.5) we obtain

$$A(E) = 2\pi\langle\omega\rangle(\delta B/B)^2(\frac{v_A}{c})pc \qquad (4.10.6)$$

where

$$\langle\omega\rangle(\frac{\delta B}{B})^2 = \frac{1}{B_o^2}\int d^3k\, d\omega\, \omega\, \langle B(\underline{k},\omega)B^*(\underline{k},\omega)\rangle. \qquad (4.10.7)$$

A result similar to equation (4.10.6), i.e. that A(E) is proportional to particle momentum, can be obtained from the simple consideration of interactions with "moving magnetic mirrows" (Fermi 1949, Davis 1956). If the particles are assumed to collide with such mirrors moving with velocity v_A, the mean energy gain per collision is $\langle\Delta E\rangle = \xi(v_A/c)^2 W$, where ξ is a numerical constant of order unity, and W is the total energy of the particle. The mean reate of energy gain is then given by

$$A(E) = \xi(v_A^2/\ell c)pc, \qquad (4.10.8)$$

where ℓ is the mean free path between collisions. We denote by α the constant of proportionality in front of pc in either equation (4.10.6) or equation (4.10.8); these equations can be solved for E as function of time, yielding

$$E(t) = [A_o\exp(\alpha t) - mc^2]^2/[2A_o\exp(\alpha t)], \qquad (4.10.9)$$

where $A_o = mc^2 + E_o + [E_o(E_o+2mc^2)]^{1/2}$ and E_o is the initial or injection energy.

In order to satisfy the injection conditions $v >> v_A$ for protons and $v >> 43\ v_A$ for electrons, the particles must have energies greater than at least 0.5 keV. But acceleration also requires that the rate of energy gain be larger than the energy loss rate due to Coulomb collisions with the ambient medium.

The dashed lines in Figure 4.10.1 show the energy loss rates of protons and electrons in an ionized medium of unit density and temperature $T = 2 \times 10^6$K. The proton loss rate is from Ginzburg and Syrovatskii (1964). For the assumed temperature, $(dE/dt)_p$ peaks at about 0.5 MeV, where the proton velocity equals the thermal speed of the ambient electrons. The loss rate for electrons is from Trubnikov (1965). At nonrelativistic energies $(dE/dt)_e$ varies as $E^{-1/2}$ for $E >> kT$, while in the MeV region synchrotron losses (not shown in Figure 4.10.1) could become important. If these losses were taken into account, $(dE/dt)_e$ would vary as E^2 at relativistic energies.

The solid curves in Figure 4.10.1 are the energy gain rates, $A(E) = \alpha(pc)$, where α was chosen such that $A_e(E)$ exceeds $(dE/dt)_e$ for $E > 100$ keV. Thus, electrons from the high energy tail of the first phase mechanism could be injected into the second phase accelerator at about this energy, as suggested by hard X ray and electron observations. The comparison of $A_e(E)$ with $(dE/dt)_e$ yields $\alpha(\text{sec}^{-1}) \simeq 1.5 \times 10^{-12} n(\text{cm}^{-3})$.

We can estimate α independently from equation (4.10.9), since the second phase mechanism should be capable of accelerating electrons to about an MeV in less than ~ 1 minute, as evidenced by radio, hard X ray and gamma ray continuum observations (Sections 4.6 and 4.8). For $E_o = 100$ keV, $E = 1$ MeV and $t \simeq 60$ sec, equation (4.10.9) yields $\alpha = 0.02\ \text{sec}^{-1}$. This value could result from large amplitude turbulence, $(\delta B/B)^2 \simeq 0.5$, with periods around 1 second, and an Alfven speed of ~ 300 km/sec (equation 4.10.6). There is radio evidence for such hydromagnetic turbulence (Abrami 1970, McLean et al. 1971,

Gotwolds 1972). For $\alpha = 0.02$ sec^{-1}, the density that satisfies the injection condition derived above is $n \sim 1.3 \times 10^{10}$ cm^{-3}, and this value is reasonable for the region of second phase acceleration of electrons in flares (e.g. Bai and Ramaty 1976).

The energy gain rate for protons, $A_p(E)$, is plotted in figure 4.10.1 with the same value of α as for electrons. Since $A_p(E)$ is greater than $(dE/dt)_p$ at all energies, the only injection condition for protons is $v \gg v_A$, and this can in principle be satisfied by ambient protons in the high energy tail of the Maxwell-Boltzmann distribution, provided of course that the temperature is sufficiently high.

Acceleration of ambient ions from the high energy Maxwell-Boltzmann tail is consistent with the enhancement mechanisms of ^{3}He and heavy ions that rely on preferential heating (Fisk 1978, and Section 4.7). As we have discussed in subsection (4.7.2), for events with very large ^{3}He/^{4}He ratios, these two isotopes have similar energy spectra. This result strongly suggests that the same mechanism accelerates both isotopes, in which case the ^{3}He enrichment cannot be due to the acceleration process itself. If, however, only particles above an energy threshold ($v \gg v_A$) are accelerated, preferential heating of ^{3}He would greatly increase the number of ambient ^{3}He nuclei above the threshold, and hence would drastically alter the abundance of this isotope in the observed energetic particles. On the other hand, if the ambient ions undergo first phase acceleration, for example by bulk energization (Section 4.5), it would appear that the different ^{3}He and ^{4}He temperatures could have no significant effect on the ratio of these isotopes at high energies.

We note, however, that $v \gg v_A$ and $\beta < 10^{-3}$ (a condition required in Fisk's 1978 model for ^{3}He-rich flares) would allow the acceleration of only an insignificant number of ^{3}He nuclei unless very substantial ^{3}He preheating

takes place. There are, of course, other versions of statistical accelerations where the scattering is not self-generated but comes from external sources; these could work when the particle speed is small compared with v_A.

A strong result of the analysis of the particle and gamma-ray observations (Sections 4.7 and 4.8) is that more protons than electrons are accelerated to MeV energies in flares. Fermi acceleration is quite consistent with this result, the overabundance resulting mainly from the more rapid energy gain of protons than electrons (see Figure 4.10.1). For example, if we inject protons into the second phase accelerator at a few keV and the electrons at ~ 100 keV, then, from equation (4.10.9) with $\alpha = 0.02$ sec^{-1}, we see that the mean energy of the protons can increase to tens of MeV in a few tens of seconds, while the mean energy of the electrons increases to only a few hundred keV in this time interval. Since the acceleration lasts for only a finite time, we expect a large proton-to-electron ratio at high energies. The proton-to-electron ratio is also affected by the different injection conditions of these two particle species as discussed above, but in any event fewer electrons than protons are expected to reach MeV energies because of their lower rate of energy gain. On the other hand, since the acceleration time of protons of tens of MeV is similar to that of electrons of hundreds of keV, the nuclear lines produced by such protons should have a time dependence similar to that of gamma-ray continuum produced by electrons of several hundreds keV energy. This result is consistent with the data discussed in Section 4.8.

We do not attempt to evaluate the spectrum of protons and electrons resulting from second phase acceleration. As was shown by Wentzel (1965), even in a steady state, different spectral shapes can result, depending on the escape conditions of the particles from the acceleration region. Moreover, acceleration in solar flares can only be poorly approximated by a steady state.

4.11. SUMMARY

We have examined the various manifestation of energetic particles in solar flares as well as the possible mechanisms for the acceleration of these particles.

Electrons in the 10 to 100 keV range are energetically the dominant component of flare accelerated particles. These electrons are manifest in hard X-ray bursts, type III radio bursts, and they are directly observed in the interplanetary medium. In the nonthermal, thick-target interpretation of hard X-rays, electrons above 20 keV could contain up to 50% of the total flare energy. The possibility that these electrons are thermal has recently been reconsidered by Colgate (1978); Crannell et al. (1978) and Elcan (1978) have shown that at least some of the data are consistent with thermal bremsstrahlung In this Chapter (Section 4.2) we have discussed a quasithermal model in which the ratio of bremsstrahlung yield to nonradiative energy loss rate is maximized under reasonably realistic conditions. In such a model, the X-ray emission efficiency is increased, and therefore a given hard X-ray flux requires a smaller nonradiative energy loss (by about a factor of 20) than that deduced from the nonthermal thick target case (see also Smith and Lilliequist 1978).

A promising mechanism for producing the 10 to 100 keV electron component is bulk energization. An additional result of the analysis of Sections 4.2 and 4.5 is that in such energization the protons are heated to an energy lower by at least an order of magnitude than the electrons. There is no direct observational evidence for a 10 to 100 keV proton component in flares, and the analysis of the nonthermal wings of hydrogen Ly α places only upper limits on the proton-to-electron ratio in this energy range (Canfield and Cook 1978, and Section 4.9). However, bulk energization on the short time scales implied by the X-ray observations most likely involves direct electric field acceleration coupled with a wave isotropization process. Moreover, direct electric field and wave acceleration processes are the most likely candidates for producing the electrons observed in interplanetary space. These electrons, however, comprise only a small fraction of the 10 to 100 keV electron component.

In Sections 4.3 and 4.4 we have discussed the existence and consequences of reverse currents. Such currents are required to neutralize beams of fast electrons which have been invoked to account for energetic solar phenomena such as type III radio bursts and nonthermal hard X-ray emission. Without reverse currents, the energy in the self magnetic fields of the postulated beams is orders of magnitude above the total flare energy (Colgate 1978). The reverse current allows beam transport, but it cannot exist in acceleration region itself thereby placing restrictions on the acceleration regions (see Section 4.5).

In Section 4.4 a method is presented for the diagnosis of the electron temperature and density of a rapidly heated coronal plasma (see also Shapiro and Knight 1978). Such heating is implied by the hard X-ray observations, and may result from the energy dissipated by either the fast electrons that produce the X-rays or the reverse current which neutralizes the electron beam.

Particles of energies higher than about 100 keV are a genuine nonthermal manifestation of solar flares. The existence of such particles is manifest in radio observations (Section 4.6) which show evidence for electrons up to energies of a few MeV, in gamma-ray continuum measurements (Section 4.8) which define the electrons spectrum in the 100 keV to $\sim$ 1 MeV region, and nuclear gamma-ray observations which indicate that flares accelerate protons and nuclei to tens of MeV in reasonably close temporal association with the bulk energization in the 10 to 100 keV region. The temporal behavior of the gamma-ray continuum above $\sim$ 100 keV, of the nuclear gamma rays and of the high frequency ($\geq$ 20 GHz) microwave emission, nevertheless, indicates that a phase of acceleration, distinct from that responsible for the bulk energization, is required for the acceleration of the high energy particle component. We have referred to these two acceleration phases as first phase (10 to 100 keV electrons) and second phase mechanisms. Second phase acceleration is discussed in Section

(4.10) where it is suggested that it could be due to a stochastic, Fermi-type process closely related to the passage of shock waves through the solar atmosphere. Some of the observed features of the high energy particle component, such as the proton-to-electron ratio, are consistent with this type of acceleration. The proton-to-electron ratio above several MeV is found to be very large ($\geq 10^2$); this result is deduced from both particle (Section 4.7) and gamma-ray (Section 4.8) observations. An acceleration mechanism in which the rate of energy gain is proportional to particle momentum would produce this result.

One of the most puzzling aspects of energetic particle observations from solar flares has been the tremendous compositional variability of these particles. The species that have shown the greatest variability are ^{3}He and Fe (Section 4.7). The theories proposed to account for the ^{3}He enhancements are discussed in subsection (4.7.2). We feel that particle events in which ^{3}He/^{4}He exceeds about 10% could be best explained by a model such as proposed by Fisk (1978), in which ambient solar ^{3}He is preferentially heated by electrostatic ion cyclotron waves. No specific acceleration mechanism is suggested in this model, but as we have discussed in Sections (4.7) and (4.10), second order Fermi mechanism could be a viable candidate. We point out (Section 4.10) that if the rate of energy gain is determined from the requirement that first phase electrons are injected into the second phase mechanism at about 100 keV, then protons and nuclei could be accelerated directly from the high energy tail of the thermal ($\sim 2\times10^6$K) ambient medium. In this way, minor constituents of the ambient gas (e.g. ^{3}He and Fe), if preferentially heated, would show up over-abundant at high energies, as occasionally observed (Section 4.7).

We have found that not all ^{3}He-rich events can be easily explained by the preferential heating model, and, therefore, nuclear reactions may be required to account for such events. These events have ^{3}He/^{4}He ratios of a few percent to $\sim$ 10%. The limit set on the amount of matter traversed by

energetic particles as they escape from the Sun (from ^{2}H observations, Section 4.8), however, is not sufficient to account for these observed ^{3}He/^{4}He ratios. But as discussed in Section (4.7), the nuclear models that have been proposed can suppress ^{2}H by kinematical effects (Ramaty and Kozlovsky 1974, Rothwell 1976) or by thermonuclear burning (Colgate et al. 1977).

The most clear cut evidence for nuclear reactions in solar flares comes from gamma-ray studies. Gamma rays above an MeV have by now been observed from several solar flares, and nuclear lines from at least two (See Section 4.8). The reactions which produce nuclear gamma rays are mostly inelastic collisions between the energetic particles and the ambient solar atmosphere. If the ^{3}He nuclei, in at least some of the ^{3}He-rich events, result from such collisions, then these events should be accompanied by gamma rays and this will be tested by observations on the Solar Maximum Mission. As we have seen in Section (4.8), the gamma rays provide information on the timing of the acceleration of protons and nuclei and on the energy content in the nucleonic component. In Section (4.9) we have discussed the origin of white light flares, and we have found that the energy contained in protons and nuclei above 20 MeV is lower by only a small factor than the energy required to produce white light emission by fast ions impinging upon the photosphere. Simultaneous observations of white-light and gamma-ray emissions are required, since the above conclusion is based on the comparison of observations from different flares.

The enhancement of heavy nuclei which is so evident in the particle fluxes from flares, may also be manifest in gamma-ray spectra. We have found that a broad feature between $\sim$ 0.8 to 2 MeV in the spectrum of the 1972, August 4 flare could be due to an overabundance of Mg, Si and Fe nuclei in the energetic particles from this flare. This result is consistent with new observations of particle events in solar cycle 21 (Dietrich and Simpson 1978), and seems to indicate that the enrichment of heavy nuclei in energetic particle events occurs in

both small and large flares. With this interpretation, essentially all gamma rays above $\sim$ 1 MeV are of nuclear origin, i.e. produced by the interactions of energetic ions with the solar atmosphere.

The material presented in this Chapter has been discussed by the authors at 4 separate one-week meetings of the Second Skylab Workshop on Solar Flares, Boulder, Colorado, 1976-1977. Section (4.2) has been written by P. Hoyng and D. Smith, Section (4.3) by P. Hoyng, J. Knight, and D. Smith, Section (4.4) by J. Knight and P. Shapiro, Section (4.5) by P. Hoyng, J. Knight and D. Smith, Section (4.6) by G. Dulk and D. Melrose in collaboration with S.F. Smerd, Section (4.7) by C. Paizis, R. Ramaty and M. Van Hollebeke in collaboration with R. McGuire and A. T. Serlemitsos, Section (4.8) by R. Ramaty, Section (4.9) by F. Orrall, and Section (4.10) by D. Melrose and R. Ramaty. The Introduction and Summary, Sections (4.1) and (4.11), have been written by the Team Leader, R. Ramaty, with inputs and suggestions from all Team Members. S. A. Colgate and R. P. Lin have contributed to various sections of this Chapter. Colgate to Sections (4.3), (4.5) and (4.7), and Lin to Sections (4.1), (4.2), (4.5), (4.7), (4.8), (4.9) and (4.10). The editing of Sections (4.2) through (4.5) was done by D. Smith, and that of that of the rest of the Chapter by R. Ramaty with assistance from C. Paizis. T. Bai, a member of Team IV of the Workshop, participated in the meetings of the present Team, and contributed to the discussion on the time dependences of hard X-ray production in solar flares. L. A. Fisk participated in one of the Workshop meetings and presented the ^{3}He enrichment model discussed in this chapter. The data used in Section (4.7) has been kindly provided by E. C. Stone, R. Mewaldt, J. A. Simpson, F. B. McDonald and T. von Rosenvinge. The team leader is grateful to the referees, H.S. Hudson and L.A. Fisk, for the careful review of the manuscript and the many helpful suggestions that they made.

References

Abrami, A. 1970, Solar Phys. 11, 40.

Akinyan, S. T., Mogilevsky, E. I., Böhme, A. and Krüger, A. 1971, Solar Phys. 20, 112.

Anglin, J. D. 1975, Ap. J., 198, 733.

Anglin, J. D., Dietrich, W. F. and Simpson, J. A. 1973, High Energy Phenomena on the Sun, Symposium Proceedings, ed. R. Ramaty and R. G. Stone (NASA SP-342), p315.

Anglin, J. D., Dietrich, W. F., and Simpson, J. A. 1977, Conference Papers, 15th International Conf. Cosmic Rays, 5, 43.

Bai, T. 1977, Studies on Solar Hard X-rays and Gamma Rays: Compton Backscatter Anisotropy, Polarization and Evidence for Two Phases of Acceleration, Univ. of Maryland Ph.D. Dissertation.

Bai, T. and Ramaty, R. 1976, Solar Physics, 49, 343.

Balasubrahmanyan, V. K. and Serlemitsos, A. T. 1974, Nature 252, 260.

Barkas, W. H. and Berger, M. J. 1964, Tables of Energy Losses and Ranges of Heavy Charged Particles, NASA SP-3013 (NASA, Washington, D. C.)

Benz, A. O. 1977, Ap. J. 211, 270.

Berger, J. M., Newcomb, W. A., Dawson, J. M. Frieman, E. A., Kulsrud, R. M. and Lenard, A. 1958, Phys. Fluids, 1, 301.

Bertsch, D. L. and Reames, D. V. 1977, Solar Physics, 55, 491.

Böhme, A. 1972, Solar Phys. 25, 478.

Boischot, A. and Clavelier 1967, Astrophys. Lett. 1, 7.

Boischot, A. and Clavelier, B. 1968, Ann. Astrophys. 31, 445.

Boischot, A. and Daigne, G. 1968, Ann. Astrophys. 31, 531.

Boris, J. P., Dawson, J. M., Orens, M. H. and Roberts, K. V. 1970, Phys. Rev. Letters, 25, 706.

Brown, J. C. 1971, Solar Physics, 18, 489.

Brown, J. C. 1972, Solar Phys. 26, 441.

Brown, J. C. 1974, Coronal Disturbances, (IAU Symp. 57, Surfer's Paradise (1973), G. Newkirk, Editor, p.395.

Brown, J. C. and McClymont, A. N. 1975, Solar Phys. 41, 135.

Brown, J. C. and Melrose, D. B. 1977, Solar Phys. 52, 117.

Chambon, G., Hurley, K., Niel, M., Talon, R., Vedrenne, G., Likine, O. B., Kouznetsov, A. V., and Estouline, I. V., 1978, Gamma Ray Spectroscopy in Astrophysics, Symposium Proceedings, ed. T. L. Cline and R. Ramaty, NASA, TM 79619, p. 70.

Canfield, R. C. and Cook, J. W. 1978, Ap. J. 225, 650.

Castelli, J. P. and Aarons, J. 1968 Astronomical J. 73, S57.

Chandrasekhar, S. 1943, Rev. Mod. Phys. 15, 1.

Chu, K. R. and Rostoker, N. 1973, Phys. Fluids 16, 1472.

Chubb, T. A. 1970 Solar-Terrestrial Physics (proceeding Int. Symp. on Solar-Terrestrial Physics, Leningrad 1970), E. R. Dryer, Editor, part 1, p.99.

Chupp, E. L., Forrest, D. J., Higbie, P. R., Suri, A. N., Tsai, C., and Dunphy, P. P. 1973, Nature, 241, 333.

Chupp, E. L., Forrest, D. J. and Suri, A. N. 1975, Solar Gamma, X and EUV Radiations, S. Kane (ed) IAU Symp. 68, 341.

Colgate, S. A. 1978, Ap. J. 221, 1068.

Colgate, S. A., Audouze, J. and Fowler, W. A. 1977, Ap. J. 213, 849.

Cox, J. L. and Bennett, W. H. 1970, Phys. Fluids, 13, 182.

Crannell, C. J., Joyce, G., Ramaty, R. and Werntz, C. 1976, Ap. J., 210, 582.

Crannell, C. J., Frost, K. J., Matzler, C., Ohki, K., Saba, J.L., 1978, Ap. J. 223, 670.

Crannell, C. J., Ramaty, R. and Crannell, H. 1977, Recent Advances in Gamma Ray Astronomy, Proceedings of the 12th ESLAB Symposium, Frascati, Italy ESA SP 124, ed. R.D. Wills and B. Battrick, p. 213

Croom, D. L. 1971, Solar Phys. 19, 152.

Croom, D. L. and Harris, L. D. J., 1973 World Data Center Report, UAG-28, Pt. 1, p210.

Datlowe, D. 1971, Solar Phys. 17, 436.

Datlowe, D. W., Elcan, M. J. and Hudson, H.S., 1974, Solar Physics 39, 155.

Datlowe, D. W., Hudson, H. S. and Peterson, L. E., 1974 , Solar Phys. 35, 193.

Datlowe, D. W., and Lin, R. P., 1973, Solar Phys. 32, 459.

Davis, L. K. 1956, Phys. Rev. 101, 351.

Demastus, H. and Stover, R. R. 1967, Publ. Astron. Soc. Pacific 79, 615.

Dietrich, W F. 1973, Ap. J. 180, 955.

Dietrich, W. F. and Simpson, J. A. 1978, Ap. J. (Letters) 225, L41.

Dragt, A. J. 1961, J. Geophys. Res. 66, 1641.

Drake, J. F. and Lee, Y. C. 1977, Phys. Fluids 20, 1341.

Dulk, G. A. 1973, Solar Phys. 32, 491.

Dungey, J. W. 1963, Planet. Space Sci. 11, 591.

Elcan, M. J. 1978, Dissertation, University of California, San Diego.

Fan, C. Y., Gloeckler, G. and Hovestadt, D. 1975, Solar Gamma, X-, and EUV Radiation, Ed. S. Kane, IAU Symposium 68, p.411.

Fermi, E. 1949, Phys. Rev. 75, 1169.

Fermi, E. 1954, Ap. J. 119, 1.

Fichtel, C. E. and Guss, D. E., 1961, Phys. Rev. Letters 6, 495.

Fisk, L. A. 1978, Ap. J. 224, 1048.

Frost, K. J. and Dennis, B. R. 1971, Ap. J. 165, 655.

Garrard, T. L., Stone, E. C. and Vogt, R. E. 1973, High Energy Phenomena on the Sun, Symposium Proceedings, ed. R. Ramaty and R. G. Stone (NASA SP-342) p.341.

Geiss, J. and Reeves, H. 1972, Astronomy and Astrophys. 18, 126.

Ginzburg, V. L. and Syrovatskii, S. I. 1964, The Origin of Cosmic Rays, (Macmillan, New York).

Gloeckler, G., Sciambi, R. K., Fan, C. Y. and Hovestadt, D. 1976, Ap. J. (Letters) 209, L93.

Gotwolds, B. L. 1972, Solar Phys. 24, 232.

Green, G., Wibberenz, G., Muller-Mellin, R., Wiffe, M., Kempe, H., Kunow, H., 1975, 14th ICRC Munich 12, 4257.

Gruber, D. E., Peterson, L. E. and Vette, J. I. 1973, High Energy Phenomena on the Sun, Eds. R. Ramaty and R. G. Stone, NASA SP-342, p.147.

Gurnett, D. A. and Anderson, R. R. 1976, Science 194, 1159.

Hall, D. N. B. 1975, Ap. J. 197, 509.

Hall. D. E. and Sturrock, P. A. 1967, Phys. Fluids 12, 2620.

Hammer, D. A. and Rostoker, N. 1970, Phys. Fluids, 13, 1831.

Hirose, A. and Skarsgard, H. M. 1976, Phys. Rev. Letters, 36, 252.

Hovestadt, D., Klecker, B., Vollmer, O., Gloeckler, G., Fan, C. Y. 1975 14th ICRC Munich 5, 1613.

Hoyng, P., Brown, J. C. and Van Beek, H. F. 1976, Solar Phys. 48, 197.

Hoyng, P. 1977a, Astron. and Astrophys. 55, 23.

Hoyng, P. 1977b, Astron. and Astrophys. 55, 31.

Hoyng, P. and Melrose, D. B. 1977, Astrophys. J. 218, 866.

Hoyng, P., Knight, S. W. and Spicer, D. S. 1978, Solar Phys. (to be published).

Hsieh, K. C. and Simpson, J. A. 1970, Ap. J. (Letters) 162, L191.

Hudson, H. S. 1972, Solar Phys. 24, 414.

Hudson, H. S., Baity, W. A., Gruber, D. E., Knight, F. K., Nolan, B. L., Matteson, J. L., Peterson, L. E. 1978, Paper presented at the High Energy Astrophysics Division (AAS)'s Meeting, La Jolla, California, September 1978.

Hurford, G. J., Stone, E. C. and Vogt, R. E. 1975a, Conference Papers, 14th International Cosmic Ray Conference, Munich, Germany, 5, p.1624.

Hurford, G. J., Mewaldt, R. A., Stone, E. C. and Vogt, R. E. 1975b, Ap. J. (Letters), 201, L95.

Ibragimov, I. A. and Kocharov, G. E. 1978, preprint.

Jordan, C. 1969, Mon. Mot. R. Astr. Soc. 142, 501.

Kafatos, M. C. and Tucker, W. H. 1972, Ap. J. 175, 837.

Kane, S. R. 1971, Ap. J. 170, 587.

Kane, S. R. and Anderson, K. A. 1970, Ap. J. 162, 1003.

Kaplan, S. A. 1956, Sov. Phys. JETP 2, 203.

Kato, T. 1976, Ap. J. Supplement Series 30, 397.

Kai, K. 1968, Publ. Astron. Soc. Japan 20, 140.

Kai, K. 1970, Solar Phys. 11, 310.

Kennell, C. F. and Petschek, H. E. 1966, J. Geophys. Res. 71, 1.

Klok, O. D., Kumentsov, V. K., Strelkov, P. S. and Shkvarunets, A. G. 1974, Sov. Phys. JETP 40, 696.

Knight, J. W. and Sturrock, P. A. 1977, Ap. J. 218, 306.

Kindel, J. M. and Kennel, C. F. 1971 J. Geophys. Res. 76, 3055.

Kulsrud, R. M. and Ferrari, A. 1971, Astrophys. Space Sci. 12, 302.

Kurt, V. G., Logachev, Yu. I., and Pissarenko, N. F. 1977, Solar Physics, 53, 157.

Lacombe, C. and Mangeney, A. 1969, Astron. and Astrophys. 1, 325.

Lin, R. P. 1970, Solar Phys. 12, 266.

Lin, R. P. 1971, Solar Phys. 15, 453.

Lin, R. P. 1974, Space Sci. Rev. 16, 189.

Lin, R. P. and Hudson, H. S. 1976, Solar Phys. 50, 153.

Lin, R. P., Mewaldt, R. A., Stone, E. C., Vogt, R. E., Paizis, C. and Van Hollebeke, M. A. I. 1978, Bull. Amer. Phys. Society 23, 4-AJ7

Levine, L. S., Vitkovitsky, I. M., Hammer, D. A. and Andrews, M. L. 1971, J. Applied Phys. 42, 1863.

Lotz, W. 1968, Z. Physik, 216, 241.

Lotz, W. 1969, Z. Physik 220, 466.

Magun, A., Stewart, R. T. and Robinson, R. D. 1975, Proc. Astron. Soc. Australia, 2, 367.

Matzler, C. 1978, Astron. and Astrophys. (in press)

McCracken, K. G. and Rao, U. R. 1970, Space Science Rev. 4, 155.

McDonald, F. B., Fichtel, C. E. and fisk, L. A., 1974, High Energy Particles and Quanta in Astrophysics, F. B. McDonald and C. E. Fichtel, Editors, MIT Press, p212.

McKenzie, D. L., Datlowe, D. W. and Peterson, L. E. 1973, Solar Phys. 28, 175.

McKibben, R. B. 1972, J. Geophys. Res. 77, 3957.

McLean, D. J., Sheridan, K. V., Stewart, R. T. and Wild, J. P. 1971, Nature, 234, 140.

Melrose, D. B. 1970, Austr. J. Phys. 23, 421.

Melrose, D. B. 1971, The Crab Nebula, eds. R. D. Davies and F. E. Smith (Reidel, Dordrecht), p.96.

Melrose, D. B. 1974, Solar Phys. 37, 353.

Melrose, D. B. 1978, Plasma Astrophysics, (Gordon and Breach), in press.

Melrose, D. B. and Brown, J. C. 1976, Mon. Not. Ray. Astron. Soc. 176, 15.

Melrose, D. B., Dulk, G. A. and Smerd, S. F. 1977, Astronomy and Astrophys. (to be published)

Mewe, R. and Schrijver, J. 1975, Astrophys. Space Sci. 38, 345.

Milkey, R. W. 1971, Solar Phys. 16, 465.

Najita, K. and Orrall, F. Q. 1970, Solar Phys. 15, 176.

Noyes, R. W. 1971, Ann. Rev. Astro. Ap. 9, 209.

Otaola, J., Gall, R., and Perez-Enriquez, R. 1977, Study of Travelling Interplanetary Phenomena, Eds. M. A. Shea, D. F. Smart, and S. T. Wu, Air Force Geophysics Laboratory Report, Bedford, Mass.

Orrall, F. Q. and Zirker, J. B. 1976 Ap. J. 208, 618.

Parker, E. N. 1958, Phys. Rev. 109, 1328.

Parker, E. N. and Tidman, D. A. 1958, Phys. Rev. 111, 1206.

Peterson, L. E. and Winckler, J. R. 1959, J. Geophys. Res. 64, 697

Pick, M. 1961 Ann. Astrophys. 24, 183.

Ramaty, R. 1969, Ap. J. 158, 753.

Ramaty, R. and Kozlovsky, B. 1974, Ap. J. 193, 729.

Ramaty, R., Kozlovsky, B. and Lingenfelter, R. E. 1975, Space Sci. Rev. 18, 341.

Ramaty, R., Kozlovsky, B. and Lingenfelter, R. E. 1979 (to be published).

Ramaty, R., Kozlovsky, B. and Suri, A. N. 1977, Ap. J. 214, 617.

Ramaty, R. and Lingenfelter, R. E. 1967, J. Geophys. Res. 72, 879.

Ramaty, R. and Lingenfelter, R E. 1968, Solar Phys. 5, 531.

Ramaty, R. and Petrosian, V. 1972, Ap. J. 178, 241.

Robinson, R.D. 1977, Ph.D. Thesis, University of Colorado.

Robinson, R. D. and Smerd, S. F. 1975, Proc. Astron. Soc. Australia 2, 374.

Ross, J. E. and Aller, L. H. 1976, Science 191, 1223.

Rothwell, P. L. 1976, J. Geophys. Res. 81, 709.

Rust, D. M. and Hegwer, F. 1975, Solar Phys. 40, 141.

Schaeffer, O. A. and Zahringer, J. 1962, Phys. Rev. Letters 8, 389.

Schlüter, A. 1957, Z. Naturforsch. 12a, 822.

Schmahl, E. J. 1972, Proc. Astron. Soc. Australia 2, 95.

Serlemitsos, A. T. and Balasubrahmanyan, V. K. 1975, Ap. J. 198, 195.

Shapiro, P. R. and Knight, J. W. 1978, Ap. J. 224, 1028.

Shapiro, P. R. and Moore, R. T. 1977, Ap. J. 217, 621.

Shen, C. S. 1965, Ap. J. 141, 1091

Simnett, G. M. 1971, Solar Phys. 20, 448

Simnett, G. M. 1974, Space Science Rev. 16, 257.

Smerd, S. F. and Dulk, G. A. 1971, Solar Magnetic Fields, ed. R. Howard, IAU Symposium No. 43, p616.

Smith, D. F. 1971, Ap. J. 170, 559.

Smith, D. F. 1972a, Ap. J. 174, 121.

Smith, D. F. 1972b, Ap. J. 174, 643.

Smith, D. F. 1974, IAU Symposium No. 57, Coronal Disturbances, ed. G. A. Newkirk (Dortrecht:Reidel), p.253.

Smith, D. F. 1976a, J. Geophys. Res. 82, 704.

Smith, D. F. 1976b, Astrophys. Space Sci. 42, 261.

Smith, D. F. 1977a, Ap. J. 212, 891.

Smith, D. F. 1977b, Ap. J. 217, 644.

Smith, D. F., 1977c, Ap. J. (Letters) 216, L53

Smith, D. F. and Lilliequist, C. G. 1978, Ap. J. (to be published)

Smith, D. F. and Priest, E. R. 1972, Ap. J. 176, 487.

Sturrock, P. A. 1974, Coronal Disturbances, ed. G. Newkirk, IAU Symp. 57, p437.

Sullivan, J. 1970, "Two Solar Flare Electron Components and their Relationship to the Proton Component" Ph.D. Thesis, Univ. of Chicago.

Suri, A. N., Chupp, E. L., Forrest, D. J., and Reppin, C. 1975, Solar Phys. 43, 415.

Suzuki, S. and Sheridan, K. V. 1978, Radiophysics, in press.

Stein, W. A. and Ney, E. P. 1963, J. Geophys. Res. 68, 65.

Svestka, Z. 1970, Solar Phys. 13, 471.

Svestka, Z. 1976, Solar Flares, (Reidel, Holland)

Swan, W. F. G. 1933, Phys. Rev. 43, 217.

Sweet P. A., 1969 Ann. Rev. Astron. Astrophys. 8, 149.

Takakura, T. 1960, Publ. Astron. Soc Japan 12, 325

Takakura, T. and Kai, K. 1966, Publ. Ast. Soc. Japan 18, 57.

Takakura, T. 1972, Solar Phys. 26, 151.

Thompson, W. B. 1955, Proc. Roy. Soc. A233, 402.

Trubnikov, B. A. 1965, Rev. Plasma Phys. 1, 105

Tsytovich, V. N. 1970, Non Linear Effects in a Plasma, (New York: Plenum)

Tsytovich, V. N., Stenflo, L., and Wilhelmsson, H. 1975, Physica Scripta, 11, 251.

Tucker, W. H. and Koren M. 1974, Ap. J. 170, 621.

Tverskoi, B. A. 1967, Soviet Phys. JETP, 25, 317

Van Beek, H. F., Hoyng, P. and Stevens, G. A. 1973, World Data Center Report UAG-28, Pt. II, p.319.

Van Hollebeke, M. A. I., Ma Sung, L. S. and McDonald, F. B. 1975, Solar Phys. 41, 189.

Van Hollebeke, M. A. I., Trainor, J. H., and McCracken, K. G. 1975 presented at the 14th ICRC Munich.

Van Regemorter, H. 1962, Ap. J. 136, 906.

Vasyliunas, V. M. 1975, Rev. Geophys. and Space Phys. 13, 303.

Webber, W. R., Roelof, E. C., McDonald, F. B., Teegarden, B. J. and Trainor, J. 1975, Ap. J. 199, 482.

Wang, H. T. and Ramaty, R. 1974, Solar Physics, 107, 1065.

Wang, H. T. and Ramaty, R. 1975, Ap. J. 202, 532.

Warwick, J. W. 1968, Solar Phys. 5, 111.

Webber, W. R., Roelof, E. C., McDonald, F. B., Teegarden, B. J. and Trainor, J. 1975, Ap. J. 199, 482.

Wentzel, D. G. 1961, J. Geophys. Res. 66, 359.

Wentzel, D. G. 1965, J. Geophys. Res. 70, 2716.

Wild, J. P. 1970, Proc. Astron. Soc. Australia, 1, 365.

Wild, J. P., Murray, J. D. and Rowe, W. C. 1954, Austr. J. Phys. 7, 439.

Wild, J. P., Smerd, S. F. and Weiss, A. A. 1963, Ann. Rev. Astron. Astrophys. 1, 291.

Zakharov, V. E. 1972, Soviet Phys. JETP, 35, 908.

Zwickl, R. D., Roelof, E. C., Gold, R. E., Krimigis, S. M. and Armstrong, T. P. 1977, Preprint JHU/APL 77-12.

Figure Captions

4.3.1 Figure 4.3.1 Diagnostic diagram for hard X-ray sources. The stable and unstable regimes are indicated; the former can be subdivided into a collision-dominated and a "reverse current electric field" - dominated regime. Knowledge of the absolute velocity or energy distribution results in a vertical velocity band at the relevant value of v_r/v_t. Four such bands are drawn and discussed in the text. The width of the band is a rough indication of the relative energy distribution of the beam electrons. The arrows indicate movements of the source made while positioning it on the v_r/v_t - axis.

4.7.1 Differential electron energy spectrum observed in the interplanetary medium from the 7 September 1973 flare. The spectrum is constructed from the flux maximum in each energy channel and compiled from 3 different detector systems as shown by the different symbols. Overlapping

energy in the $\sim$ 100 keV region between IMP-6 UCB and IMP 7 Caltech experiments insures a cross-checked intercalibration.

4.7.2 Correlation plot between .5 to 1.1 MeV electrons and 10 MeV protons for some 40 flare-associated events detected by the IMP 4/5 GSFC cosmic ray experiment. All these events are associated with flares well connected to the observer. The flux has been measured at its maximum for both protons and electrons. In order to detect possible bias due to difference in the proton spectra, the events have been grouped into two categories according to the shape γ of the differential energy spectrum. Such bias is not observed. There is a good correlation for events in which the proton flux is larger than $5 \times 10^{-2} (cm^2 \cdot sec \cdot sr \cdot MeV)^{-1}$ We suggest that in such events the two particle populations are from second phase acceleration. The excess electrons for small events, are probably from the high energy tail of the first phase acceleration.

4.7.3 Same as Figure 4.7.2 for a different time period, except that the electron flux from the IMP 7 Caltech experiment is given in absolute units (see text).

4.7.4 The ratio $^3He/^4He$ measured at various energies as a function of I_p, max (10 MeV), the proton intensity at 10 MeV and at the maximum intensity of the event.

4.7.5 The ratio $^4He/^1H$ measured at various energies as a function of I_p, max (10 MeV). Note that the trend in $^3He/^4He$ and $^4He/^1H$ ratios shown in figures 4.7.4 and 4.7.5 considerably exceeds the variability that might result from the fact that the measurements are at different energies.

4.7.6 The ratio $Fe/^4He$ as a function of $^3He/^4H$ (from Anglin et al. 1977).

4.7.7 The ratio $^3He/^4He$ as a function of $^1H/^4He$ for all available energies. In a few cases the same event has been measured in more than one energy interval, and then it appears more than once in this figure.

4.8.1 Prompt nuclear gamma ray spectrum from the interactions of energetic particles with the solar stmosphere. The composition of both the energetic particles at the same energy per nucleon and the ambient medium is the same as that of the photosphere. The energy spectrum of the particles is proportional to E^{-2}. Not shown in this figure are the delayed lines, at 2.223 MeV from neutron capture and at 0.511 MeV from positron annihilation. In the 1972, August 4 flare these lines were $\sim$ 10 and 2 times more intense, respectively, than the ^{12}C line at 4.44 MeV.

4.8.2 Time dependences of radiations of the 1972 August 4, flare. The three upper lines are the measured time profiles of X-rays (29 $\sim$ 41 keV), gamma rays (0.35 $\sim$ 8 MeV), and microwaves (37 GHz). The error bars in the lower part of the figure represent the measured intensities of the 2.2 MeV line. The solid, dashed, and dotted lines are calculated time profiles of the 2.2 MeV line. The solid lines is obtained by assuming that the instantaneous number of nuclei in the flare region has the same time dependence as that of the observed 0.35 to 8 MeV gamma rays. The dashed and dotted lines are obtained by assuming that the time dependence of the nuclei is the same as that of the 29 to 41 keV X-rays. For the solid and dotted lines we used a photospheric ^3He abundance $^3He/H = 5x10^{-5}$; for the dashed line, $^3He/H = 0$ (from Bai and Ramaty 1976).

4.8.3 The ratio of gamma ray production rate in the energy range 4 to 7 MeV to the production rate of the 2.2 MeV line. The shaded area represents the observed ratio for the 1972, August 4 flare (from Ramaty et al. 1977).

4.8.4 The ratio of the instantaneous energy deposition rate of protons and nuclei in a ionized medium to the instantaneous narrow 4.44 MeV gamma ray line production rate. Both the energetic particles and ambient

medium have photospheric composition. The right side ordinate is the energy deposition rate for the 1977, August 4 flare for the measured mean 4.44 MeV line intensity of 0.03 photons/cm^2sec (Chupp et al. 1975).

4.8.5 The instantaneous production rate of the narrow 4.44 MeV line by energetic particles with energy density 1eV/cm^3 in a medium of unit hydrogen density.

4.8.6 The effect of an enrichment in energetic heavy nuclei on the gamma ray spectrum (see text).

4.8.7 Instantaneous proton and electron numbers for the 1972, August 4 flare. The proton numbers are deduced from the gamma-ray line observations, while the electron numbers are obtained from the hard X rays and gamma-ray continuum.

4.10.1 Energy gains and losses of protons and electrons. The losses (dashed curves) are for a fully ionized hydrogen at T = 2×10^6K. The gains (solid curves) are given by the functions A(E) = const x momentum, where the constant has been chosen so that $A_e(E) > (dE/dt)_e$ for E > 0.1 MeV. At about this energy, a transition from first phase to second phase acceleration is observed (see Figure 4.7.3).

Table 4.2.1. Parameter summary for thick target and thermal hard X-ray source models (E_o = 25 keV)

	γ	duration (s)	F (s^{-1})	$P_{>E_o}$ (erg s^{-1})	Y (cm^{-3})	κT (keV)	P_{th} (erg s^{-1})
Largest event (August 4, 1972) (Hoyng et al., 1976)	3.5	~1000	4×10^{36}	2.3×10^{29}	3.6×10^{46}	30-60	2.8×10^{23}
Typical strong event (TD-1A; Hoyng et al., 1976)	4.5	10-100	10^{36}	5×10^{28}	6×10^{45}	30-60	2.4×10^{22}
Typical small event (OSO VII; Datlowe et al., 1974b)	5	10-100	5×10^{34}	2.5×10^{27}	2.6×10^{44}	30-60	8.3×10^{20}

TABLE 4.4.1*†

Line Enhancement Factors (β)

Ion	Transition	λ(Å)	E_{ij}(eV)	y	α_{max}	α=10	$\alpha=\alpha_{max}$	α=100	α=300	α=1000
Mg XI	$1s^2(^1S)$ -$1s3p(^1P)$	7.85	1579.6	6.110	104	56.1	133	133	117	88.2
	$1s^2(^1S)$ -$1s2p(^1P)$	9.17	1352.2	5.231	90	28.7	58.0	58.0	50.8	37.9
Fe XVII	$2p^6(^1S)$ -$2p^54d(^1P)$	12.12	1023.1	3.958	68	11.5	19.2	18.4	15.4	11.3
	$2p^6(^1S)$ -$2p^53d(^1P)$	15.26	812.6	3.143	54	6.6	9.5	8.9	7.3	5.2
O VIII	$1s(^2S)$ -$2p(^2P)$	19.00	652.6	2.524	43	4.4	5.7	5.2	4.1	2.9
	2-4	75.90	816.78	3.160	54	6.7	9.6	9.1	7.4	5.3
O VII	$1s^2(^1S)$ -$1s2p(^1P)$	21.60	574.1	2.221	38	3.7	4.5	4.0	3.2	2.2
N VII	$1s(^2S)$ -$2p(^2P)$	24.80	500	1.943	33	3.1	3.6	3.2	2.4	1.3
S XIV	$2s(^2S)$ -$3p(^2P)$	30.43	407.5	1.576	27	2.6	2.8	2.3	1.8	1.2
C VI	$1s(^2S)$ -$2p(^2P)$	33.70	368.0	1.424	24	2.4	2.6	2.1	1.6	1.1
Si XII	$2s(^2S)$ -$3p(^2P)$	40.92	303.0	1.172	20	2.1	2.2	1.7	1.3	0.9
Fe XVI	$3s(^2S)$ -$4p(^2P)$	50.50	245.5	0.95	16	1.9	1.9	1.4	1.1	0.7
	$3d(^3D)$ -$4p(^2P)$	76.60	245.5	0.95	16	1.9	1.9	1.4	1.1	0.7

*Wavelengths and excitation energies were taken from Kato (1976).

†$T_{initial} = 3 \times 10^6$K is assumed.

TABLE 4.4.2*†

Ionization Times ($\tau_I n_{e,9}$ s·cm^{-3})

ION	I_1(eV)/y_1	I_2/y_2	I_3/y_3	ξ_1	ξ_2/ξ_3	α=10	$\alpha=\alpha_{max}$	α=100	α=300	α=1000
Mg XI	1761.79/6.815			2		38.4	21.5 (α_{max}=90)	21.6	25.2	33.7
Fe XVII	1265/4.893	1397/5.404		6	2/	4.89	3.39 (α_{max}=68)	3.51	4.24	5.79
O VIII	871.39/3.371			1		17.9	15.1 (α_{max}=54)	16.3	20.5	28.7
O VII	739.316/2.860			2		6.63	5.84 (α_{max}=38)	6.57	8.37	11.8
N VII	667.029/2.580			1		11.0	9.99 (α_{max}=33)	11.5	14.7	20.9
S XIV	706.8/2.734	3076/11.899		1	2/	11.4	9.31 (α_{max}=27)	9.89	12.2	16.8
C VI	489.98/1.895			1		6.53	6.29 (α_{max}=24)	7.68	10.1	14.5
Si XII	523.3/2.024	2310/8.936		1	2/	6.63	5.96 (α_{max}=20)	6.63	8.38	11.8
Fe XVI	490/1.895	1223/4.731	1344/5.199	1	6/2	2.68	2.33 (α_{max}=16)	2.33	2.89	4.02

*Constants are taken from Lotz (1968, 1969), where a = 4.5, b = c = 0 throughout.

†$T_{initial}$ = 3x10^6 K is assumed.

TABLE 4.6.1

Burst Type	Radiation Mechanism	Total Number of Particles	Energy Range, Energy Distribution	Pitch Angle Distribution	Remarks
A. First (Flash or Impulsive) Phase					
Type III at $R \gtrsim 1.1\ R_o$	plasma	~10 bunches 10^{31}-10^{32} per bunch	10-100 kev, gap	forward cone of angle ~20°	fast electrons have outpaced slow
Microwave Impulsive	gyro-synchrotron	~10^{34}-10^{37} >10 kev	10 kev -1 Mev, power law with γ = 3 to 5	nearly isotropic?	most emission from e^- of E > 100 kev
	(thermal?)	>10^{10} cm^{-3}, thermal	T~10^8-10^9 K	isotropic	questionable
B. First and/or Second Phase					
Type II	plasma	?	plateau or gap	anisotropic	
Flare Continuum (FCM)	see	below			
C. Second Phase					
Microwave IV	gyro-synchrotron	10^{31}-10^{33}	0.5-5 Mev, power law with $\gamma \approx 2$ to 3	nearly isotropic?	e^- trapped in low coronal loops
Moving Type IV a) Advancing Front	gyro-synchrotron	~10^{33} > 1 Mev	1 -5 Mev, power law with γ ~ 5 to 10	nearly isotropic?	Rare. Close association with shock
b) Isolated Source	gyro-synchrotron	~10^{33} > 0.1 Mev	0.1-1 Mev, power law with $\gamma \approx 4$	nearly isotropic?	plasmoids with field of 3 - 10 G
Flare Continuum (FCII)	plasma	$\gtrsim 10^{34}$ $\gtrsim$ 10 kev	plateau or gap	loss cone	sometimes starts with III's (FCM)
	gyro-synchrotron?	~10^{33} > 0.5 Mev	0.5 -1 Mev, power law with $\gamma \approx 7$	nearly isotropic?	e^- trapped in high coronal loops

TABLE 4.7.1

DATE	TIME OF MEASUREMENT START	STOP	IDENTIFICATION	$^3He/^4He$ RATIO	$^3He/^4He$ ENERGY MeV/NUC	$^4He/^1H$ RATIO	$^4He/^1H$ ENERGY MeV/NUC	$D/^3He$ RATIO	$D/^3He$ ENERGY MeV/NUC	$T/^3He$ RATIO	$T/^3He$ ENERGY MeV/NUC	NO. OF EVENTS D	T	^3He	~10 MeV PROTON MAX. FLUX P/CM²-SEC-SR-MeV	REMARKS	REF.
NOV 12, 1960	—		CLASS 3 FLARE	0.2	~(50-120)	—	—	—	—	—	—	—	—	—	—	*	A
AVERAGE OVER 7 EVENTS (1967)	—		—	$(2.1\pm0.4)\times10^{-2}$	10-100	9.33×10^{-3}	10-100	—	—	—	—	—	—	—	—	—	B
APRIL 19, 1968	1800 4/22/68	0800	W 62, N 20	0.13 ± 0.04	4.6-19	$(4.2\pm0.3)\times10^{-2}$	4-19	—	—	—	—	—	—	14	9×10^{-3}	TYPE II, IV DKM RADIO, (2-12) Å X-RAYS WIGGLE LIKE PROTON EVENT	C
APRIL 23, 1968	1800 4/26/68	0800	—	0.08 ± 0.0	4.6-19	$(3.1\pm0.2)\times10^{-2}$	4-19	—	—	—	—	—	—	21	2×10^{-2}	I MeV ELECTRON ONSET AT 23/1310 UT (9.6-19.2) keV X-RAYS AT 23/1206 UT	C
APRIL 29, 1968	0700 5/1/68	2400	—	0.16 ± 0.05	4.6-19	$(1.12\pm0.1)\times10^{-2}$	4-19	≤0.36	4.6-13	≤0.20	4.6-10	≤5	2	14	5×10^{-2}	WIGGLE LIKE PROTON EVENT	C
MAY 11, 1968	0700 5/14/68	2000	—	0.14 ± 0.02	4.6-19	$(6.9\pm0.2)\times10^{-2}$	4-19	—	—	—	—	—	—	120	4×10^{-2}	CONSISTENT WITH A CO-ROTATING EVENT	C
OCT. 30, 1968*	1200 10/30/68	2400	W 12, S 16	0.17 ± 0.03	4.6-19	—	—	—	—	—	—	—	—	31	7×10^{-1}	EVENT ASSOCIATED WITH IP DISTURBANCE	C
MAY 5, 1969	1500 5/7/69	0900	W 72, N 09	0.53 ± 0.07	4.6-19	$(4.1\pm0.2)\times10^{-2}$	4-19	≤0.04	4.6-13	≤0.04	4.6-10	2	2	103	2×10^{-2}	RADIO BURST TYPE IV M, X-RAYS (1-20) Å WIGGLE LIKE PROTON EVENT	E
MAY 13, 1969	1800 5/15/69	1000	—	0.12 ± 0.03	4.6-19	$(8.1\pm0.5)\times10^{-3}$	4-19	—	—	—	—	—	—	18	4	IP DISTURBANCE DURING MEASUREMENT	C
MAY 28, 1969	1500 5/29/69	0200	W 59, N 10	1.52 ± 0.1	4.6-19	0.4 ± 0.2	4-19	$\leq3.6\times10^{-3}$	4.6-13	$\leq1.8\times10^{-3}$	4.6-10	1	0	560	1.2×10^{-2}	RADIO BURST TYPE II M, DKM, III DKM X-RAYS (2-12) Å	D,E
MAY 29, 1969	0200 5/29/69	2100	W 66, N 12	0.71 ± 0.06	4.6-19	0.15 ± 0.03	4-19	$\leq4\times10^{-3}$	4.6-13	$\leq8\times10^{-3}$	4.6-10	0	1	250	4×10^{-2}	RADIO BURST TYPE II, III X-RAYS (1-20) Å	E
MAY 29, 1969	2100 5/30/69	2000	W 76, N 12	0.35 ± 0.03	4.6-19	0.28 ± 0.01	4-19	$\leq1.6\times10^{-2}$	4.6-13	$\leq1.1\times10^{-2}$	4.6-10	3	2	300	6×10^{-2}	RADIO BURST TYPE III, X-RAYS (1-20) Å, LARGE ELECTRON FLUX	E
JUNE 8, 1969	0415 6/12/69	2300	—	0.09 ± 0.02	4.6-19	$(7.4\pm0.3)\times10^{-3}$	4-19	—	—	—	—	—	—	42	15	—	C
SEPT. 28, 1969*	0600 10/2/69	2000	E 02, N 09	0.18 ± 0.05	4.6-19	$(5.6\pm0.3)\times10^{-3}$	4-19	—	—	—	—	—	—	32	7	EVENT ASSOCIATED WITH IP DISTURBANCE	C
OCT. 14, 1969	0100 10/15/69	2100	—	0.45 ± 0.16	4.6-19	—	—	$\leq5.5\times10^{-2}$	4.6-13	2.3×10^{-2}	4.6-10	3	1	86	$\sim8\times10^{-2}$	ONSET ≥80 keV ELECTRONS AT 14/0945 AND 1912 UT MULTIPLE PARTICLE INJECTION	E
OCT. 14-15, 1969	—		—	0.26 ± 0.08	4-5	$(1.3\pm0.2)\times10^{-2}$	4-5	<0.16	4-5	—	—	0	0	12	—	FIRST ^3He RICH EVENT REPORTED FROM SATELLITE MEASUREMENTS	F
OCT 14, 1969	—		—	0.33 ± 0.08	10.5-21	1.2×10^{-2}	8.5-18.8	<0.16	10-15	<0.1	~10	—	—	—	—	—	G
NOV. 2, 1969	—		W 90, N 16	$(7.7\pm2)\times10^{-2}$	10-50	1.34×10^{-2}	10-50	—	—	—	—	—	—	—	80	RADIO BURST TYPE III M X-RAYS (1-20) Å I MeV ELECTRONS	H
NOV 6-7, 1969	—		—	$<6\times10^{-2}$	4-5	$(1.5\pm0.2)\times10^{-2}$	4-5	—	—	—	—	≤1	≤1	≤2	10	EVENT ASSOCIATED WITH IP DISTURBANCE	F
7 ^3He POOR FLARES 1970	—		SIX IDENTIFIED	$\sim3\times10^{-3}$	10.5-22.1	8.1×10^{-3}	8.5-18.8	—	—	—	—	—	—	—	—	—	H
MAY 30, 1970	1120 6/3/70	0740	W 31, S 08	0.12 ± 0.02	4.6-19	$(9.3\pm0.4)\times10^{-3}$	4-19	—	—	—	—	—	—	44	9	CM, DM, M RADIO BURSTS	C
JUNE 25, 1970	2200 6/27/70	2000	E 11, N 10	0.13 ± 0.03	4.6-19	$(7.9\pm0.5)\times10^{-3}$	4-19	—	—	—	—	—	—	21	3	DM RADIO BURSTS, X-RAYS (1-20) Å, LARGE IP DISTURBANCE DURING MEASUREMENT	C
JULY 6, 1970	2300 7/7/70	1900	W 90, N 22	$\leq.10$	4.6-19	$(6.7\pm0.5)\times10^{-3}$	4-19	—	—	—	—	—	—	2	7×10^{-2}	RADIO BURST TYPE II CM, DM, DKM, X-RAYS (1-20) A, TWO SOLAR FLARES	C
JULY 7, 1970	1900 7/8/70	0400	W 90, N 22	$\leq.06$	4.6-19	—	4-19	—	—	—	—	—	—	2	4×10^{-1}		
JULY 30, 1970	1500 7/31/70	1400	—	0.45 ± 0.06	4.6-19	0.16 ± 0.01	4-19	$\leq1.1\times10^{-2}$	4.6-13	$\leq5.3\times10^{-3}$	4.6-10	0	3	89	$\sim10^{-2}$	WIGGLE LIKE PROTON EVENT	E
JULY 30, 1970	—		—	0.54 ± 0.09	10.5-22.1	0.12 ± 0.02	8.5-18.8	$\leq5\times10^{-2}$	10-15	$\leq5\times10^{-2}$	~10	—	—	~50	—	—	G
JAN 25, 1971	—		W 50, N 19	$(2\pm1)\times10^{-2}$	10-50	5.5×10^{-3}	10-50	—	—	—	—	—	—	—	~100	RADIO BURSTS TYPE II M, DKM, III CM, DM X-RAYS (1-20) Å	H

TABLE 4.7.1 (cont.)

DATE	TIME OF MEASUREMENT START	STOP	IDENTIFICATION	$^3He/^4He$ RATIO	$^3He/^4He$ ENERGY MeV/NUC	$^4He/^1H$ RATIO	$^4He/^1H$ ENERGY MeV/NUC	$D/^3He$ RATIO	$D/^3He$ ENERGY MeV/NUC	$T/^3He$ RATIO	$T/^3He$ ENERGY MeV/NUC	NO OF EVENTS D	T	^3He	~10 MeV PROTON MAX FLUX P/CM^2-SEC-SR-MeV	REMARKS	REF
MAY 14, 1971	0430 5/14/71	2100	—	0.07±0.02	4.6–19	(8.49±0.9)x10^{-2}	4–19	≤0.20	4.6–13	≤0.20	4.6–10	1	1	10	3x10^{-2}	1 MeV ELECTRON ONSET AT 13/1930 UT	C
JUNE 30, 1971	0300 7/01/71	1200	UNCERTAIN	0.25±0.05	4.6–19	(8.3±0.4)x10^{-3}	4–19	≤0.10	4.6–13	≤0.04	4.6–10	2	0	27	10^{-1}	—	C
FLARE SUM 1969–72	—		—	(2.7±0.5)x10^{-2}	—	—	—	—	—	—	—	—	—	—	—	—	G
FEB 15, 1973	0000 2/15/73	2100	NO FLARE PATROL POSSIBLY WITH A R ~W60	0.21±0.07	2.9–15.0	0.27±0.03	2.4–12.7	—	—	—	—	0	0	12	5.3 x 10^{-3}	RADIO BURST TYPE IV M, DKM. X-RAYS: (1–20) Å AT 14/2330 UT	I,J
JUNE 29, 1973	0400 6/29/73	1400	—	~2	2.9–15.0	(6±2) x 10^{-2}	2.4–12.7	—	—	—	—	0	0	9	3x10^{-3}	WIGGLE LIKE PROTON EVENT	I,J
SEPT 05, 1973	0600 9/05/73	1200	SUBFLARES PRIOR TO THE SCR EVENT	~6	2.9–15.0	~0.1	2.4–12.7	—	—	—	—	0	0	12	<2 x 10^{-4}	—	I, J
FEB 20, 1974	1600 2/21/74	0600	—	0.41±0.07	2.1–2.6	—	—	—	—	—	—	0	0	43	—	EDGE OF CO ROTOTING EVENT	K
FEB 20, 1974	1600 2/21/74	2000	—	0.40	2.9–12.7	(8±1) x 10^{-2}	2.4–6	—	—	—	—	0	0	14	—	—	I
FEB 20, 1974	1200 2/23/74	2400	—	(8.7±2) x 10^{-2}	0.6–1.6	0.103±0.002	0.6–1.6	≤0.3	0.6–1.6	≤0.06	0.6–1.6	40	0	160	—	—	L
FEB 20, 1974	1200 2/21/74	1200	—	0.63±0.1	~4.5–19	0.19±0.02	~4–19	—	—	—	—	—	—	60	2.5 x 10^{-3}	—	C
MAY 09, 1974	0800 5/10/74	0000	—	6.3±1.6	2.1–2.6	—	—	—	—	—	—	—	—	95	—	—	K
MAY 09, 1974	1300 5/09/74	2100	—	~8	2.9–12.7	0.07	2.4–6	—	—	—	—	0	0	15	—	—	I
MAY 07, 1974	0600 5/13/74	1500	—	1.06±0.15	0.6–1.6	0.163±0.01	0.6–1.6	≤0.04	0.6–1.6	≤0.06	0.6–1.6	14	3	373	—	—	L
MAY 08, 1974	0500 5/09/74	2100	W35-40, S05	1.31±0.4	~4.5–19	0.176±0.04	4–19	—	—	—	—	—	—	21	4 x 10^{-4}	WIGGLE LIKE PROTON EVENT SEV FLARES	C
MAY 14, 1974	0100 5/14/74	1500	W66, S13	0.18±0.05	2.1–2.6	—	—	—	—	—	—	—	—	11	~1.5 x 10^{-2}	RADIO BURST TYPE II, M IV DKM	K
NOV 30, 1974	0900 12/02/74	0000	W52, N03	> 2	2.1–2.6	—	—	—	—	—	—	—	—	8	<2.0 x 10^{-4}	RADIO BURST TYPE II DM, M WIGGLE LIKE PROTON EVENT	K
NOV 30, 1974	1200 12/02/74	1700	—	0.64±0.15	0.6–1.6	0.14±0.01	0.6–1.6	≤0.09	0.6–1.6	≤0.03	0.6–1.6	10	4	125	—	—	L
JAN 19, 1975	1500 1/20/75	1800	SUBFLARES	0.8±0.5	2.1–2.6	—	—	—	—	—	—	—	—	4	~3 x 10^{-4}	WIGGLE LIKE PROTON EVENT	K
MAR 19, 1975	1800 3/19/75	2200	REGION 571	0.8 ±0.20	3.6–13	0.21±0.07	3.6–13	—	—	—	—	—	—	16	1.5 x10^{-3}	EVENTS DETECTED ONLY BY HELIOS-1 LOCATED AT W 110, +4°N AND 0.32 AU FROM THE SUN	M
MAR 19, 1975	2200 3/20/75	0600	W130, ~S13	1.7 ±0.6	3.6–13	0.16±0.06	3.6–13	—	—	—	—	—	—	20	1.1 x10^{-3}		M
MAR 19, 1975	1600 3/19/75	2400	OR 573	2.80±0.6	4.4–12.5	0.13±0.02	4.4–12.5	—	—	—	—	—	—	38	—		N
MAR 20, 1975	0600 3/20/75	1500	W 110	0.38±0.2	3.6–13	(9.7±3.4)x10^{-2}	3.6–13	—	—	—	—	—	—	5	8.0x 10^{-3}		M
APRIL 21, 1975	0000 4/22/75	0800	—	0.2±0.1	2.1–2.6	—	—	—	—	—	—	—	—	4	<2 x 10^{-4}	WIGGLE LIKE PROTON EVENT	K
OCT 29, 1976	1400 10/31/76	0800	—	0.7±0.3	2.1–2.6	—	—	—	—	—	—	—	—	11	5.5 x 10^{-4}	WIGGLE LIKE PROTON EVENT	K

NOTES FOR TABLE 4.7.1

1. References

   A. Schaeffer and Zahringer (1962).

   B. Hsieh and Simpson (1970).

   C. Present work

   D. Balasubrahmanyan and Serlemitsos (1974).

   E. Serlemitsos and Balasubrahmanyan (1975).

   F. Garrard, Stone and Vogt (1973).

   G. Anglin (1975).

   H. Dietrich (1973).

   I. Hurford, Mewaldt, Stone and Vogt (1975).

   J. Hurford, Stone and Vogt (1975).

   K. McGuire, McDonald, von Rosenvinge, private communication.

   L. Hovestadt, Klecker, Vollmer, Gloeckler and Fan (1975).

   M. Van Hollebeke, Trainor and McCracken (1975).

   N. Green, Wibberenz, Müller-Mellin, Witte, Kempe and Kunow (1975).

2. *For this event, pieces of Discoverer 17 satellite material have been used to search for ^{3}He.

3. The identification is based on the requirement of velocity dispersion in the proton component and the association with optical flares, radio bursts and X-ray bursts prior to the highest energy particle arrival.

4. The 10 MeV proton maximum intensity is determined from the Low Energy Detector (LED) from the GSFC Cosmic Ray experiments onboard OGO-V and IMP's IV, V and VII.

5. In a few cases the ratios ^{4}He/^{1}H, D/^{3}He and T/^{3}He were not given explicitly by the cited authors. The figures given here are estimated from the reported number of counts or spectra.

6. +The observations started 24 and 17 hours, respectively, after the Hα maximum and after the onset of the particle events. Moreover, there were interplanetary distrubances going on during the measurements. Thus they may not reflect the genuine solar flare particle emission.

TABLE 4.7.2

EVENT DATE	POWER LAW EXPONENT $\gamma_{^4He}$	POWER LAW EXPONENT $\gamma_{^3He}$	RATIO $^3He/^4He$	ENERGY RANGE MeV/Nucleon	REFERENCE
August 1972	2.65 ± 0.03	1.35	$(1.7 \pm 0.6) \times 10^{-2}$	50 - 70	Webber et al (1975)
Jan. 25, 1971	3.5 ± 0.3	2.1 ± 0.8	$(2 \pm 1) \times 10^{-2}$	10 - 50	Dietrich (1973)
Flare Sum	~3	1.8	$(2.1 \pm 0.4) \times 10^{-2}$	10 - 100	Hsieh and Simpson (1970)
Nov. 2, 1969	3.5 ± 0.2	1.9 ± 0.6	$(7.7 \pm 2) \times 10^{-2}$	10 - 50	Dietrich (1973)
Oct. 14, 1969	~3	~3	0.33 ± 0.08	10.5 - 22.1	Anglin (1975)
May 29, 1969	3.24 ± 0.05	3.24 ± 0.05	0.35 ± 0.03	4.6 - 19	Serlemitsos & Balasubrahmanyan (1975)
July 30, 1970	~3	~3	0.54 ± 0.09	10.5 - 22.1	Anglin (1975)
May 29, 1969	3.55 ± 0.12	3.69 ± 0.12	0.71 ± 0.06	4.6 - 19	Serlemitsos & Balasubrahmanyan (1975)
May 29, 1969	4.16 ± 0.1	4.04 ± 0.1	1.52 ± 0.1	4.6 - 19	Serlemitsos & Balasubrahmanyan (1975)

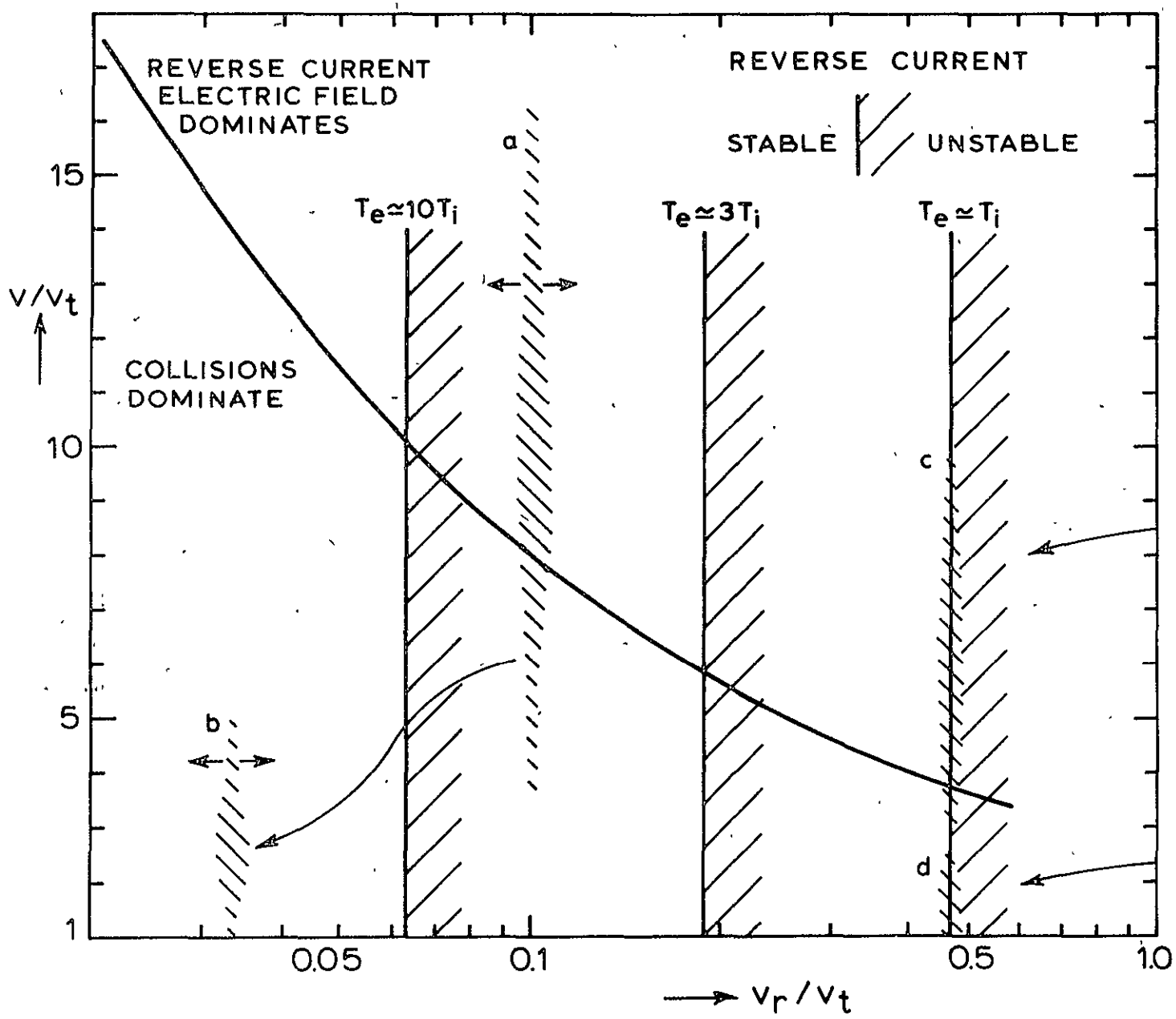
REVERSE CURRENT
ELECTRIC FIELD
DOMINATES
REVERSE CURRENT
STABLE
UNSTABLE
a
$T_e \simeq 10T_i$
$T_e \simeq 3T_i$
$T_e \simeq T_i$
V/Vt
COLLISIONS
DOMINATE
15
10
5
1
b
c
d
0.05
0.1
0.5
1.0
V_r / V_t

FIG. 4.3.1.

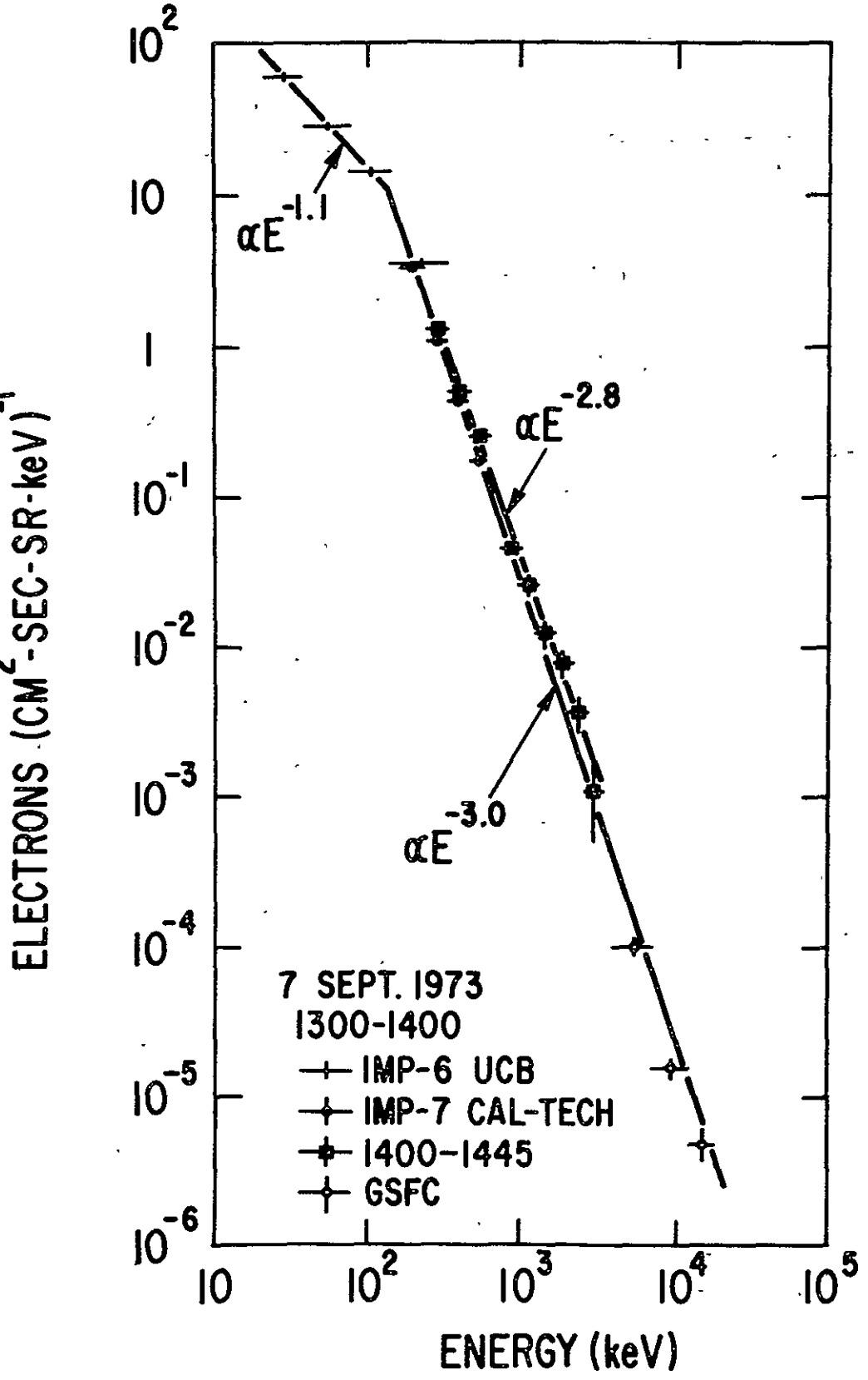

FIG. 4.7.1

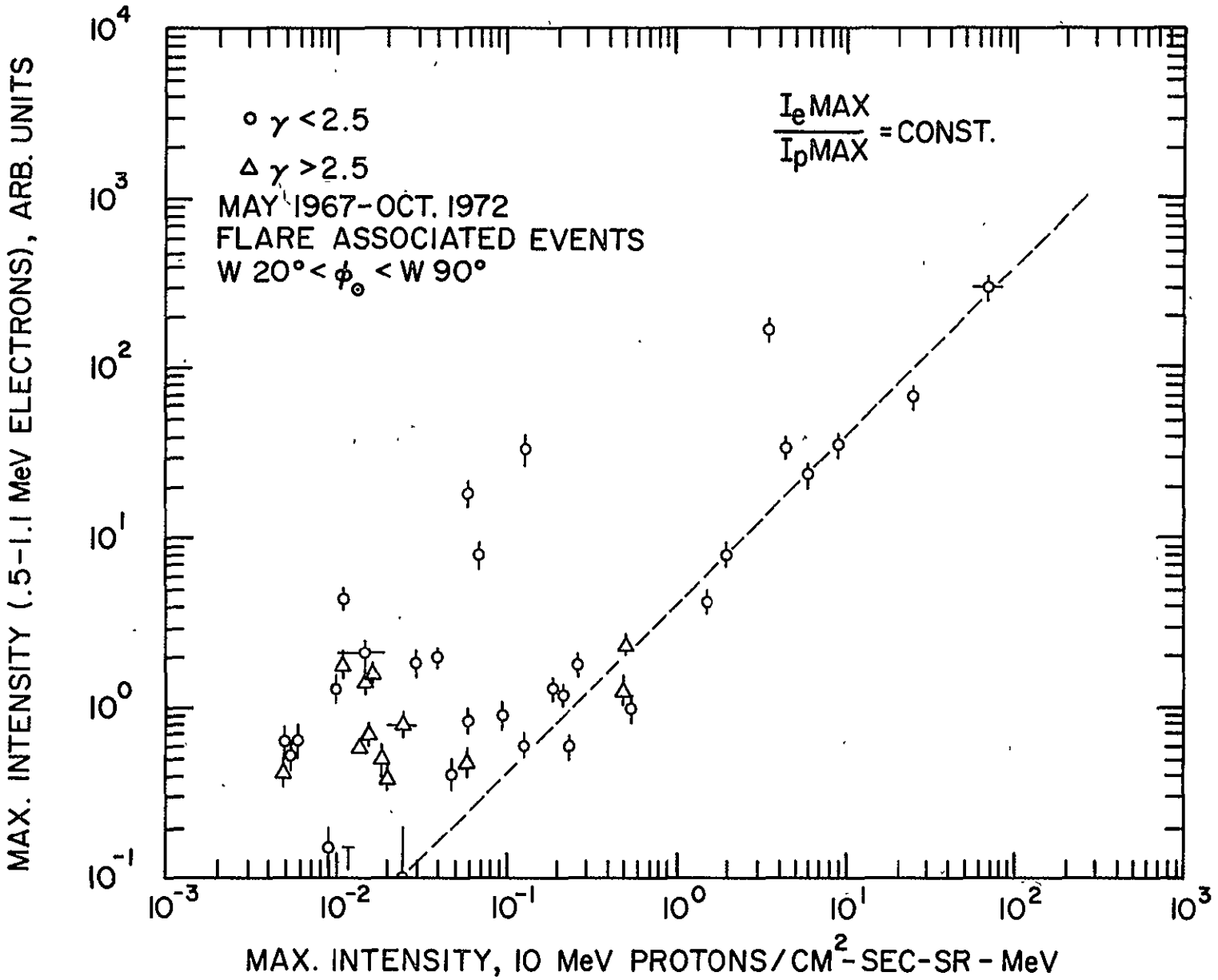
MAX. INTENSITY (.5-1.1 MeV ELECTRONS), ARB. UNITS
MAX. INTENSITY, 10 MeV PROTONS/CM²-SEC-SR-MeV
o γ <2.5
Δ γ >2.5
MAY 1967-OCT. 1972
FLARE ASSOCIATED EVENTS
W 20° < φ⊙ < W 90°
IeMAX / IpMAX = CONST.
10⁴
10³
10²
10¹
10⁰
10⁻¹
10⁻³
10⁻²
10⁻¹
10⁰
10¹
10²
10³

FIG. 4.7.2

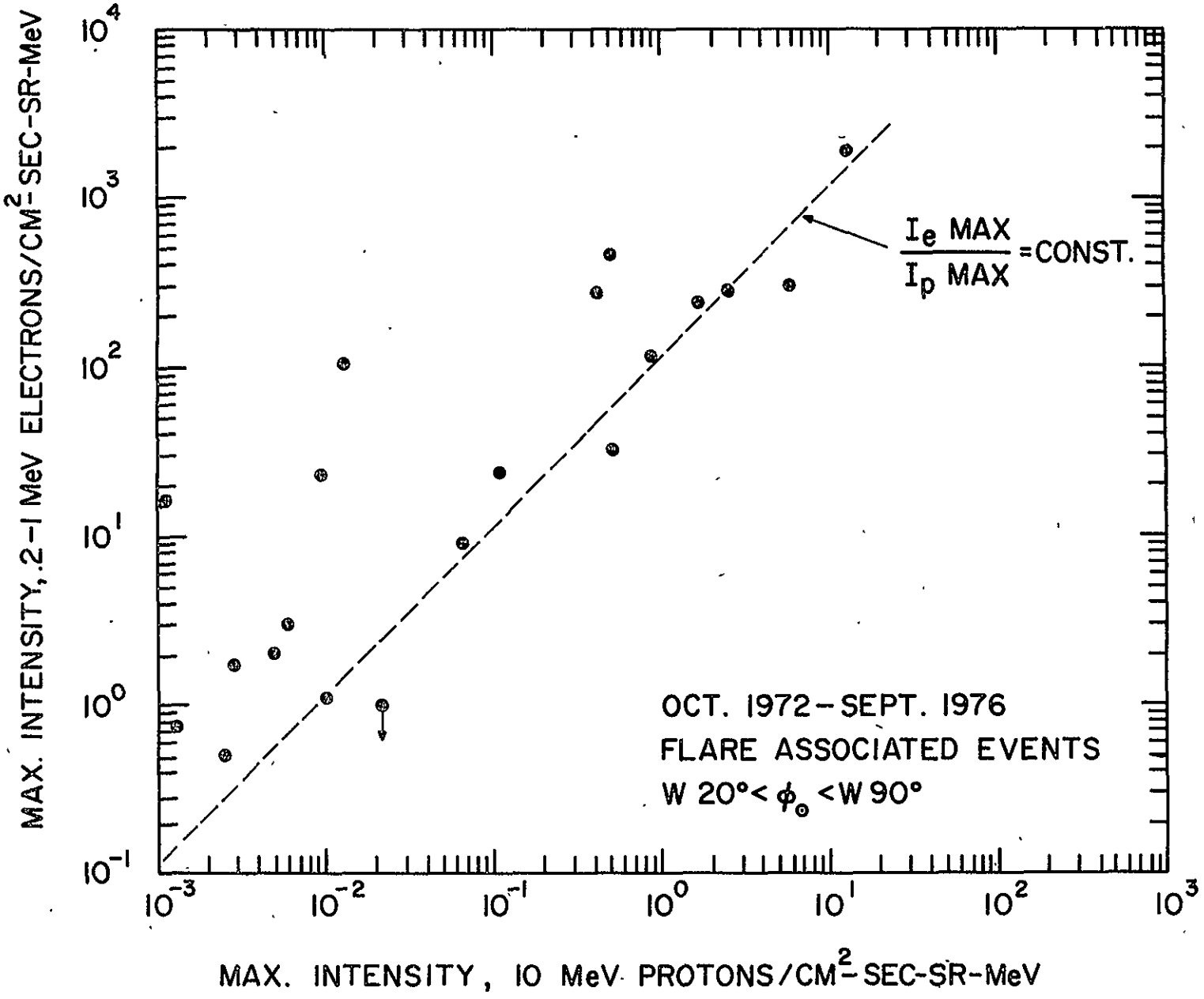
MAX. INTENSITY, .2-1 MeV ELECTRONS/CM²-SEC-SR-MeV
MAX. INTENSITY, 10 MeV PROTONS/CM²-SEC-SR-MeV
10^4
10^3
10^2
10^1
10^0
10^{-1}
10^{-3}
10^{-2}
10^{-1}
10^0
10^1
10^2
10^3
$\frac{I_e \text{ MAX}}{I_p \text{ MAX}}$ =CONST.
OCT. 1972 – SEPT. 1976
FLARE ASSOCIATED EVENTS
W 20° < $\phi_\odot$ < W 90°

FIG. 4.7.3

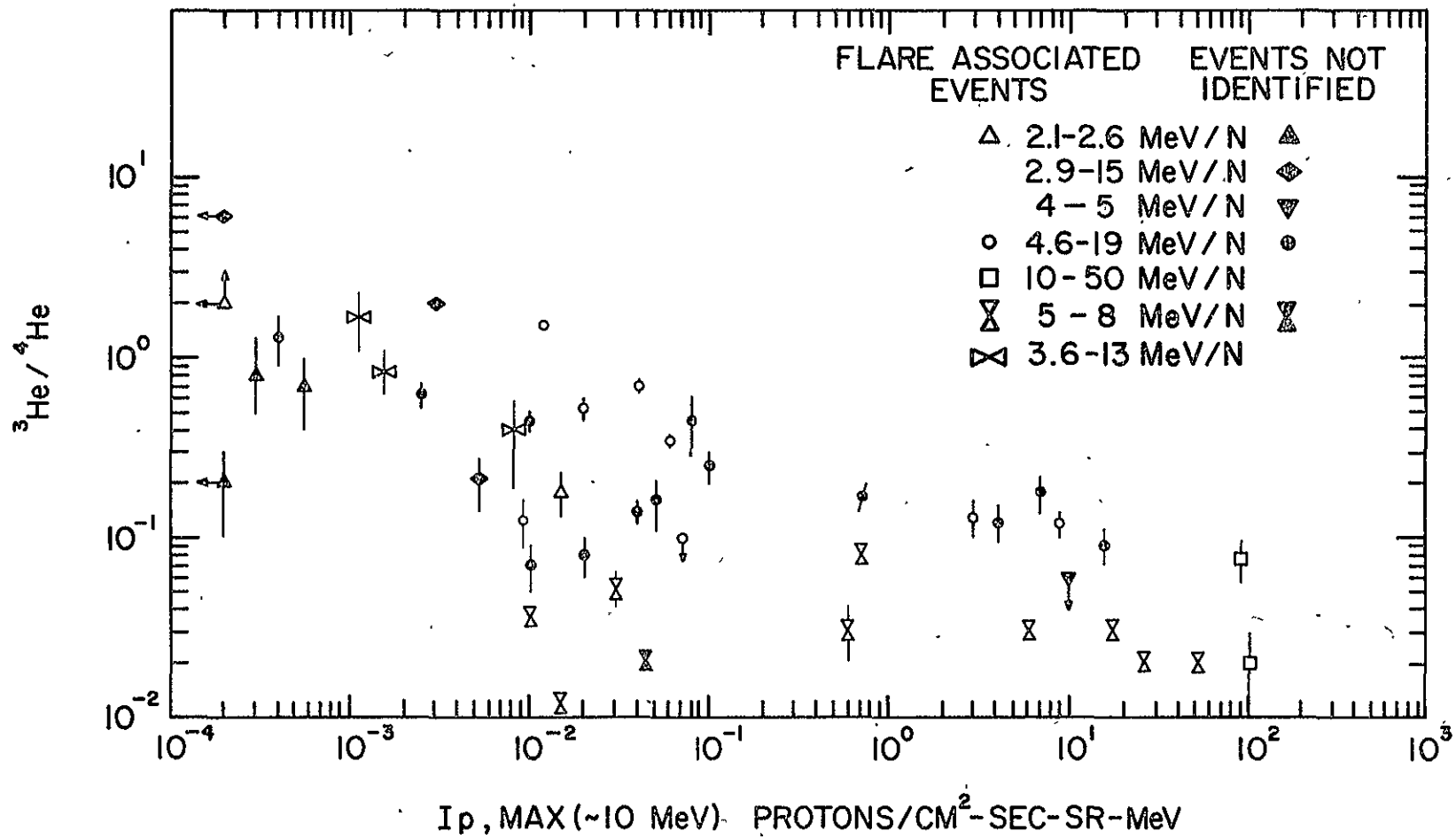
FLARE ASSOCIATED EVENTS
EVENTS NOT IDENTIFIED
2.1-2.6 MeV/N
2.9-15 MeV/N
4 - 5 MeV/N
4.6-19 MeV/N
10-50 MeV/N
5 - 8 MeV/N
3.6-13 MeV/N
$^3He/^4He$
10^1
10^0
10^{-1}
10^{-2}
10^{-4}
10^{-3}
10^{-2}
10^{-1}
10^0
10^1
10^2
10^3
Ip, MAX (~10 MeV) PROTONS/CM^2-SEC-SR-MeV

FIG. 4.7.4

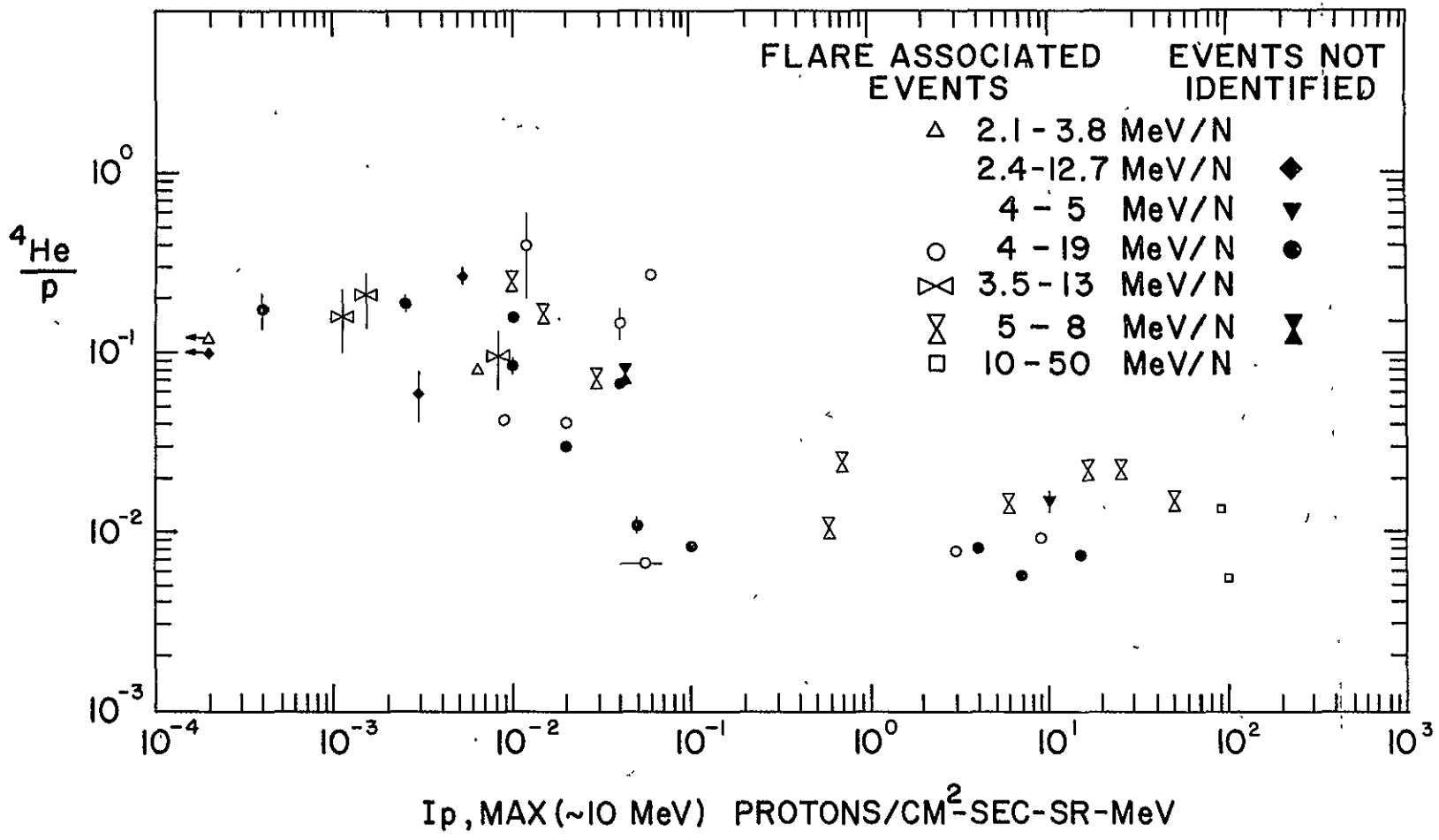
FLARE ASSOCIATED EVENTS
EVENTS NOT IDENTIFIED
2.1 - 3.8 MeV/N
2.4-12.7 MeV/N
4 - 5 MeV/N
4 - 19 MeV/N
3.5 - 13 MeV/N
5 - 8 MeV/N
10 - 50 MeV/N
$\frac{^4He}{p}$
10^0
10^{-1}
10^{-2}
10^{-3}
10^{-4}
10^{-3}
10^{-2}
10^{-1}
10^0
10^1
10^2
10^3
Ip, MAX (~10 MeV) PROTONS/CM^2-SEC-SR-MeV

FIG. 4.7.5

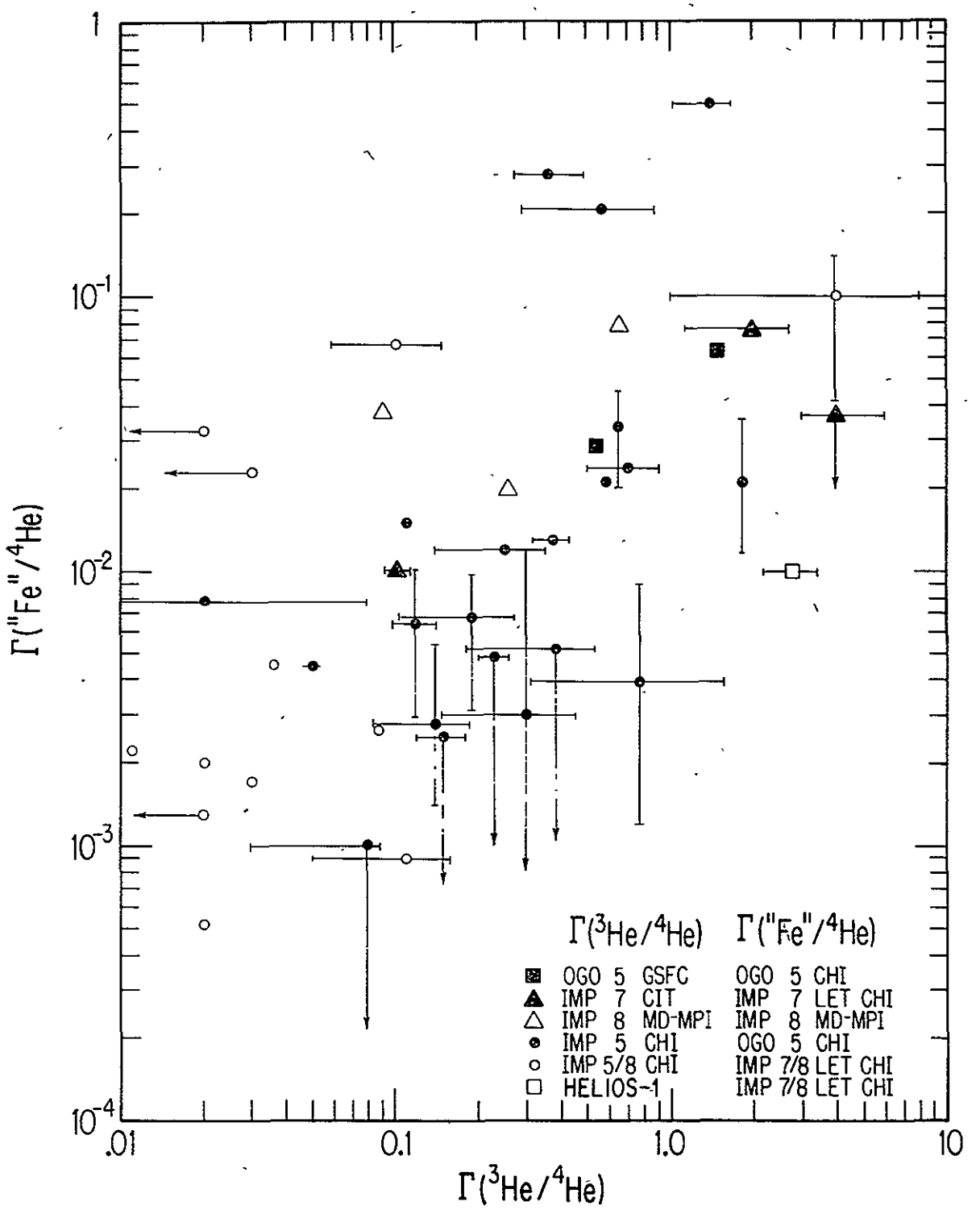
1
10^{-1}
10^{-2}
10^{-3}
10^{-4}
.01
0.1
1.0
10
$\Gamma(^{3}He/^{4}He)$
$\Gamma("Fe"/^{4}He)$
$\Gamma(^{3}He/^{4}He)$ $\Gamma("Fe"/^{4}He)$
OGO 5 GSFC OGO 5 CHI
IMP 7 CIT IMP 7 LET CHI
IMP 8 MD-MPI IMP 8 MD-MPI
IMP 5 CHI OGO 5 CHI
IMP 5/8 CHI IMP 7/8 LET CHI
HELIOS-1 IMP 7/8 LET CHI

FIG. 4.7.6.

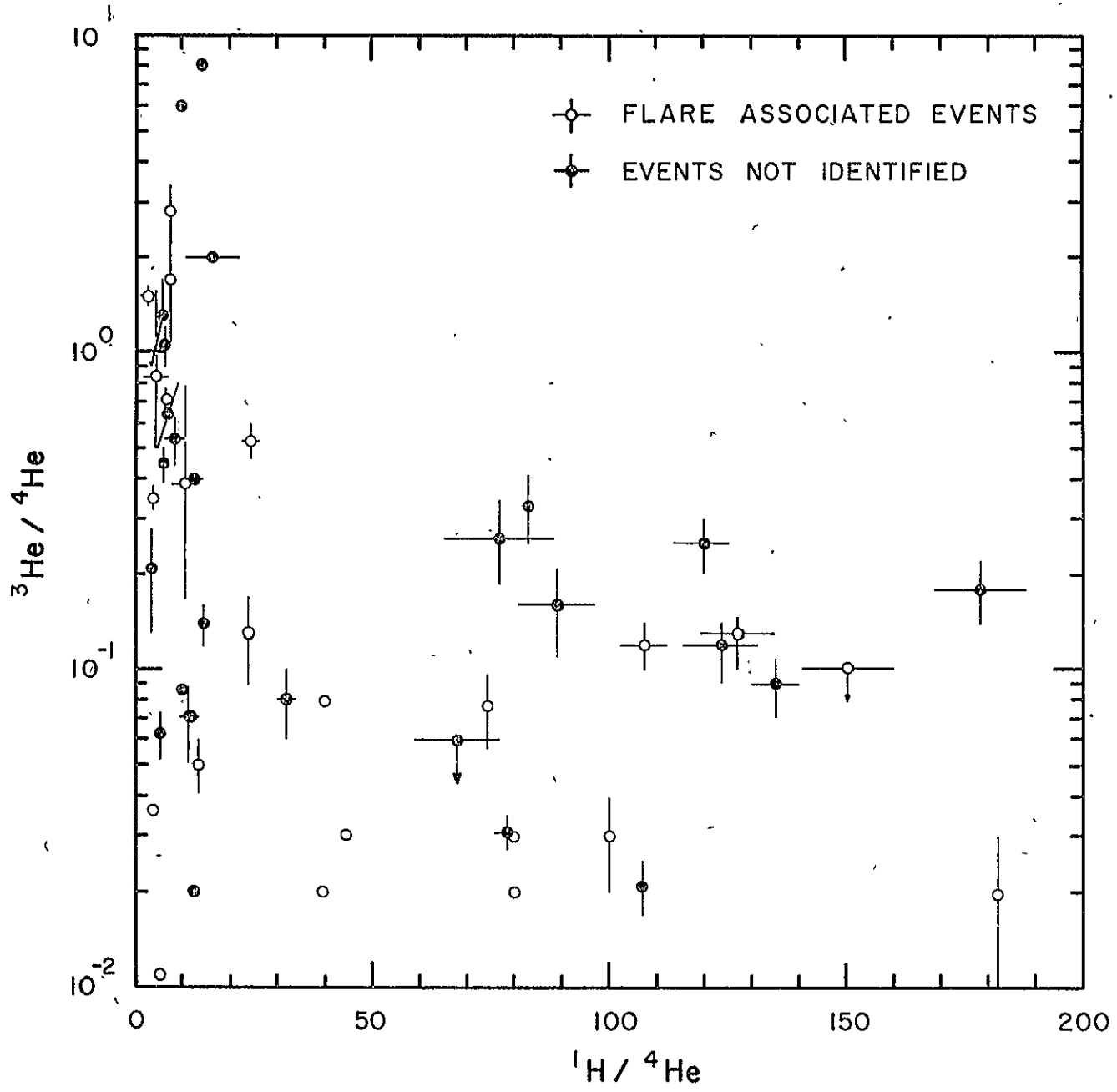
FLARE ASSOCIATED EVENTS
EVENTS NOT IDENTIFIED
10^{1}
10^{0}
10^{-1}
10^{-2}
$^{3}He / ^{4}He$
0
50
100
150
200
$^{1}H / ^{4}He$

FIG. 4.7.7

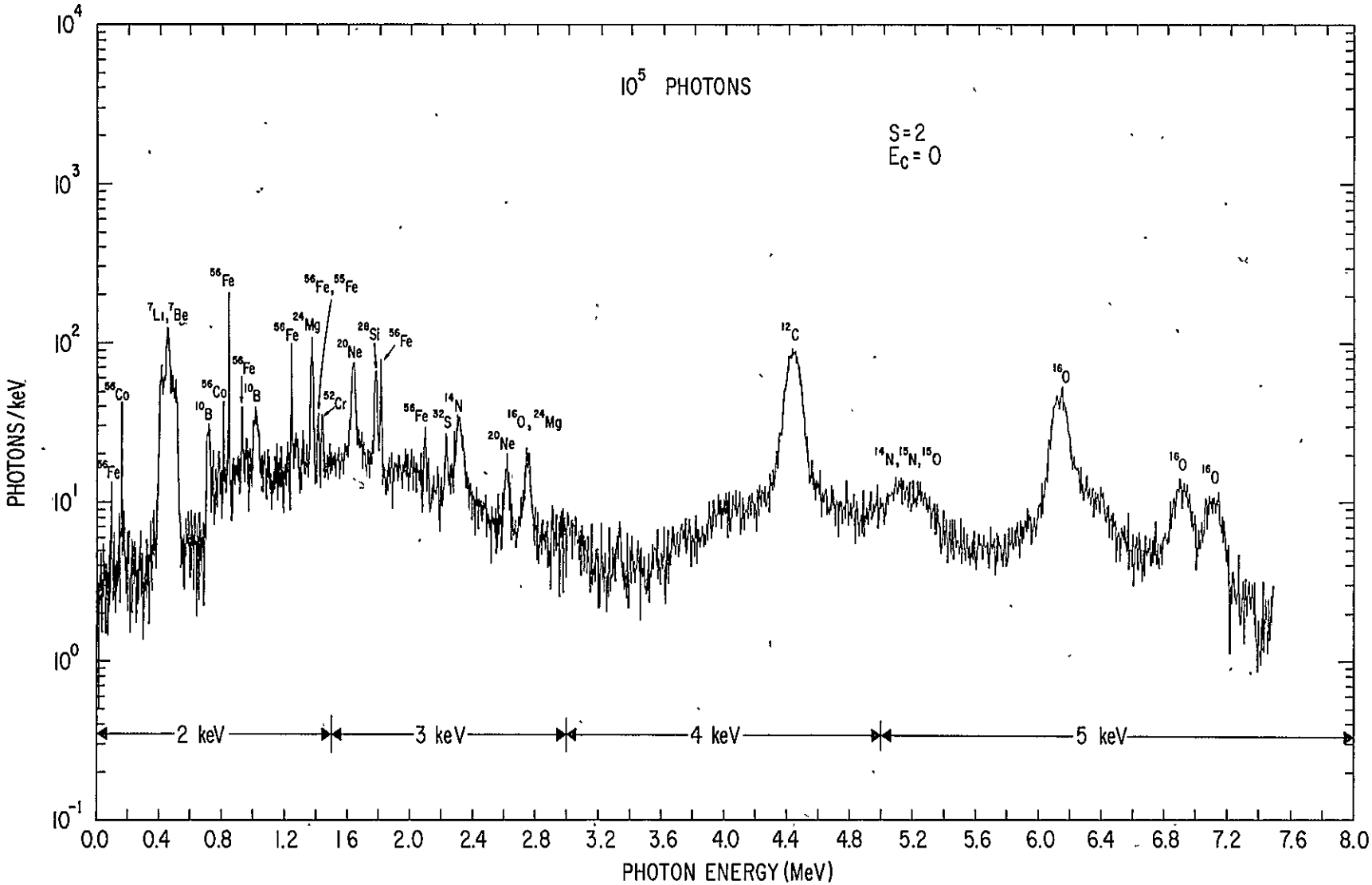

FIG. 4.8.1

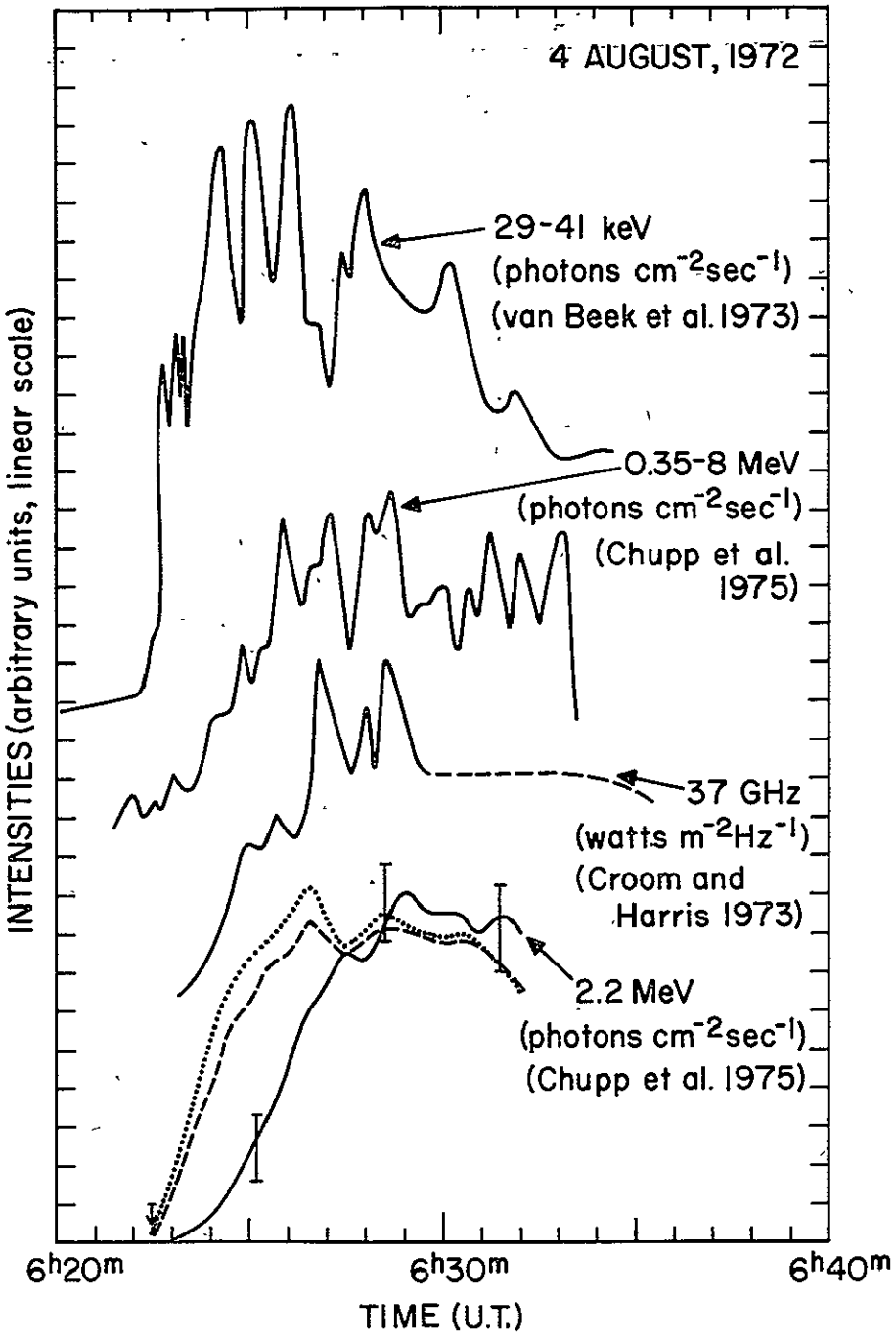
4 AUGUST, 1972
29-41 keV
(photons cm⁻²sec⁻¹)
(van Beek et al. 1973)
0.35-8 MeV
(photons cm⁻²sec⁻¹)
(Chupp et al. 1975)
37 GHz
(watts m⁻²Hz⁻¹)
(Croom and Harris 1973)
2.2 MeV
(photons cm⁻²sec⁻¹)
(Chupp et al. 1975)
INTENSITIES (arbitrary units, linear scale)
6h20m
6h30m
6h40m
TIME (U.T.)

FIG. 4.8.2.

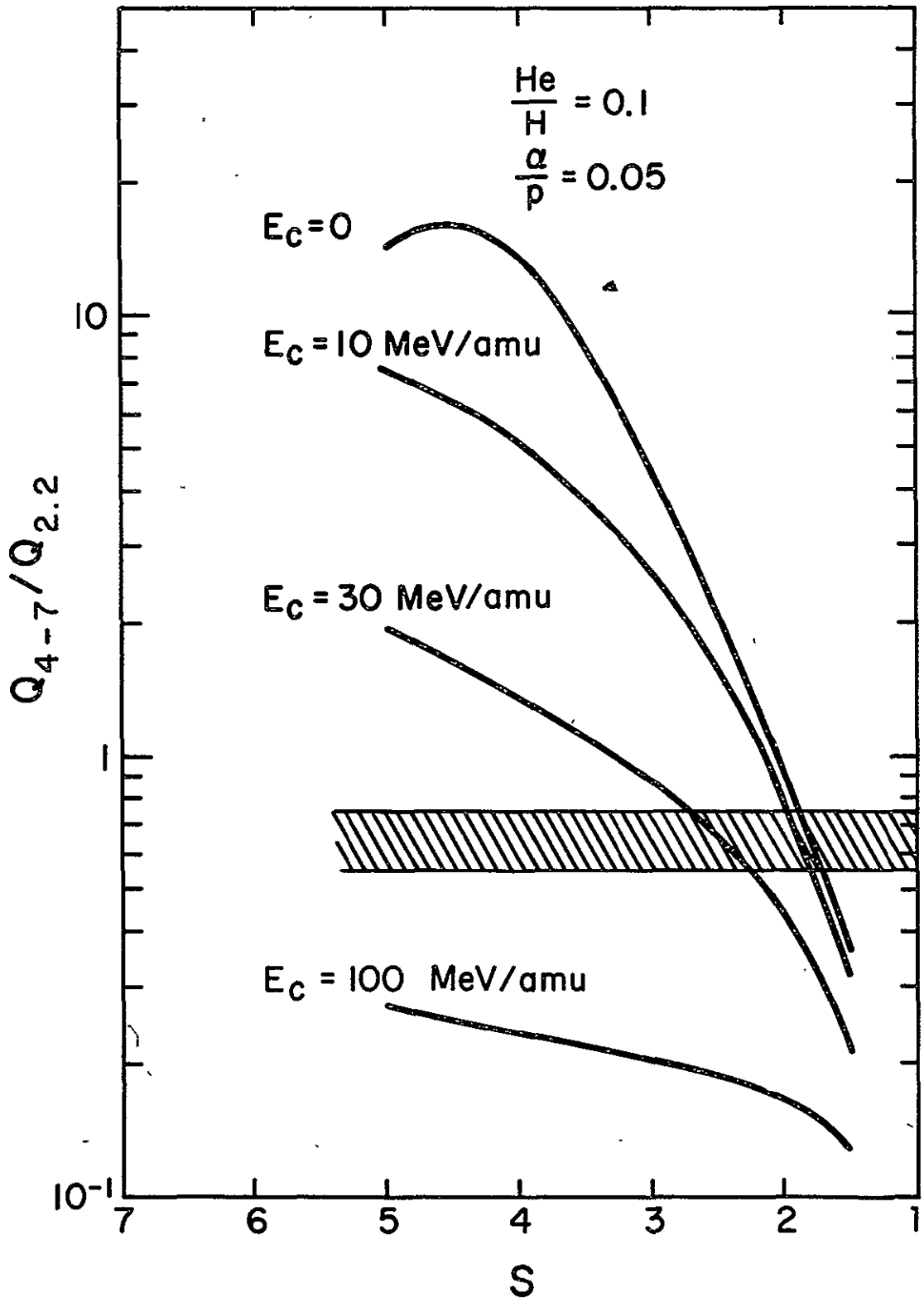
He/H = 0.1
α/p = 0.05
E_C = 0
E_C = 10 MeV/amu
E_C = 30 MeV/amu
E_C = 100 MeV/amu
Q4-7/Q2.2
10
1
10^-1
7
6
5
4
3
2
1
S

FIG. 4.8.3

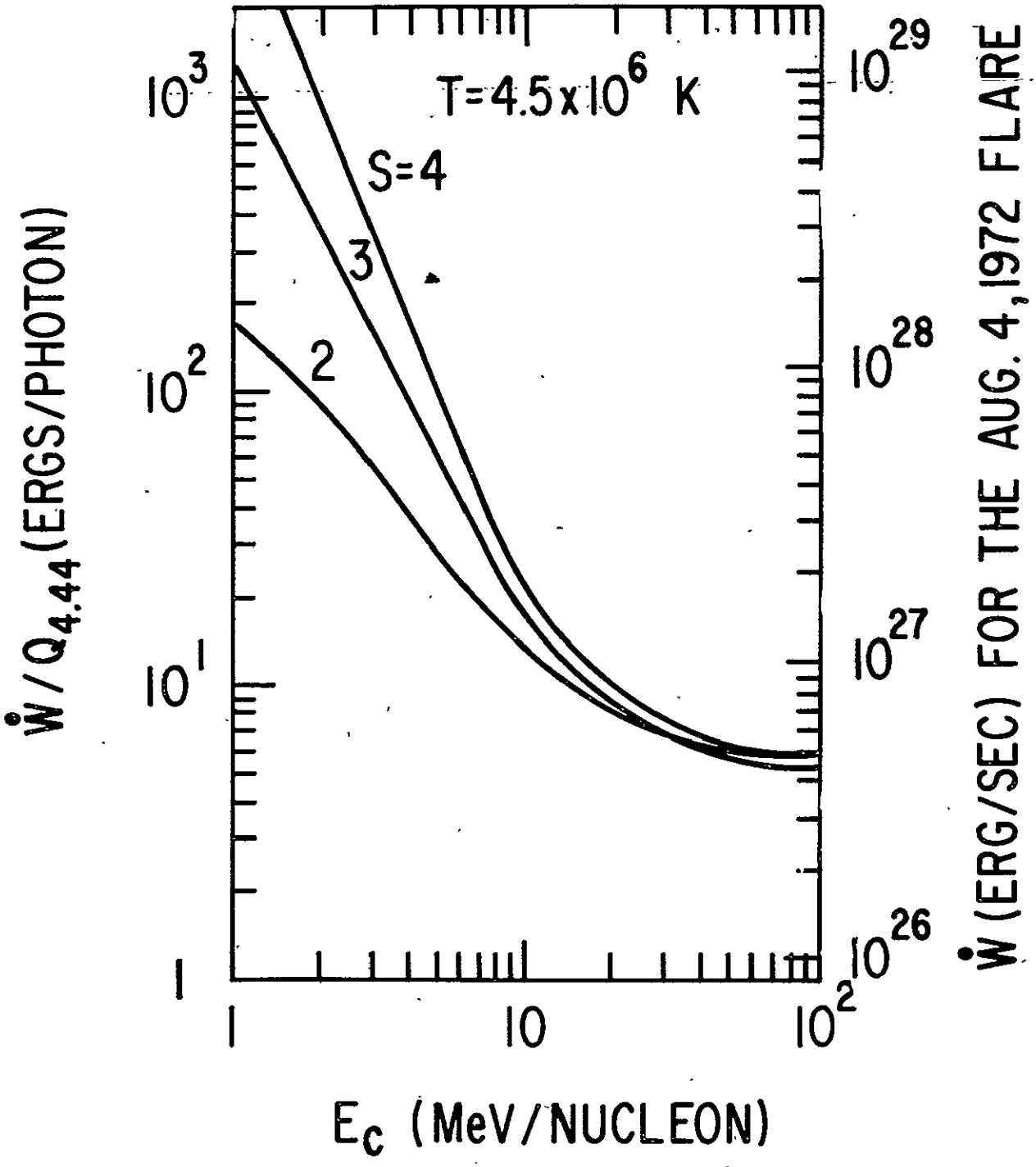
T=4.5x10^6 K
S=4
3
2
10^3
10^2
10^1
1
10^29
10^28
10^27
10^26
1
10
10^2
Ẇ/Q4.44 (ERGS/PHOTON)
Ẇ (ERG/SEC) FOR THE AUG. 4, 1972 FLARE
Ec (MeV/NUCLEON)

FIG. 4.8.4

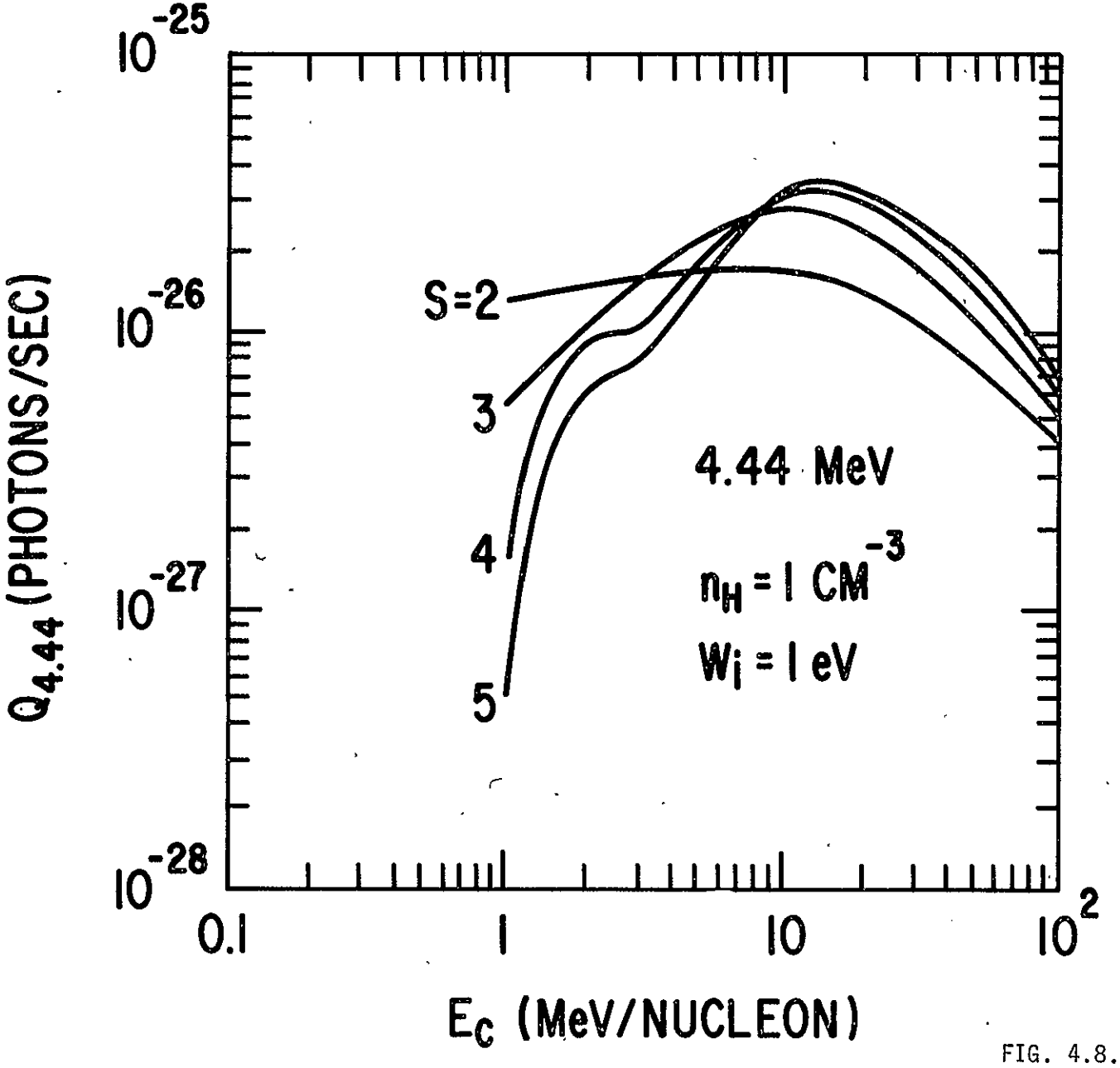
10^{-25}
10^{-26}
10^{-27}
10^{-28}
$Q_{4.44}$ (PHOTONS/SEC)
S=2
3
4
5
4.44 MeV
$n_H = 1\ CM^{-3}$
$W_i = 1$ eV
0.1
1
10
10^2
E_C (MeV/NUCLEON)

FIG. 4.8.5

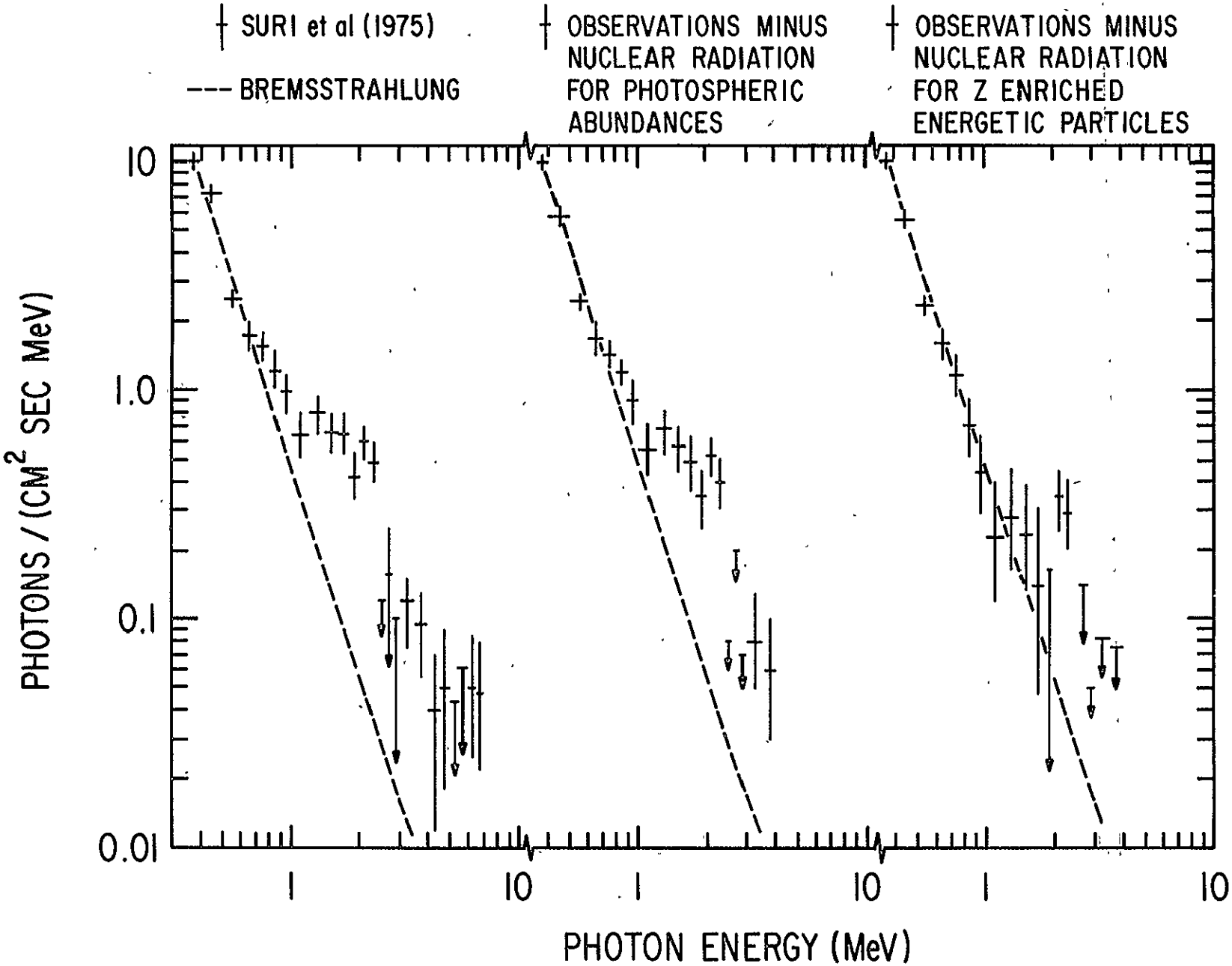
SURI et al (1975)
--- BREMSSTRAHLUNG
OBSERVATIONS MINUS NUCLEAR RADIATION FOR PHOTOSPHERIC ABUNDANCES
OBSERVATIONS MINUS NUCLEAR RADIATION FOR Z ENRICHED ENERGETIC PARTICLES
PHOTONS / (CM^2 SEC MeV)
10
1.0
0.1
0.01
1
10
1
10
1
10
PHOTON ENERGY (MeV)

FIG. 4.8.6

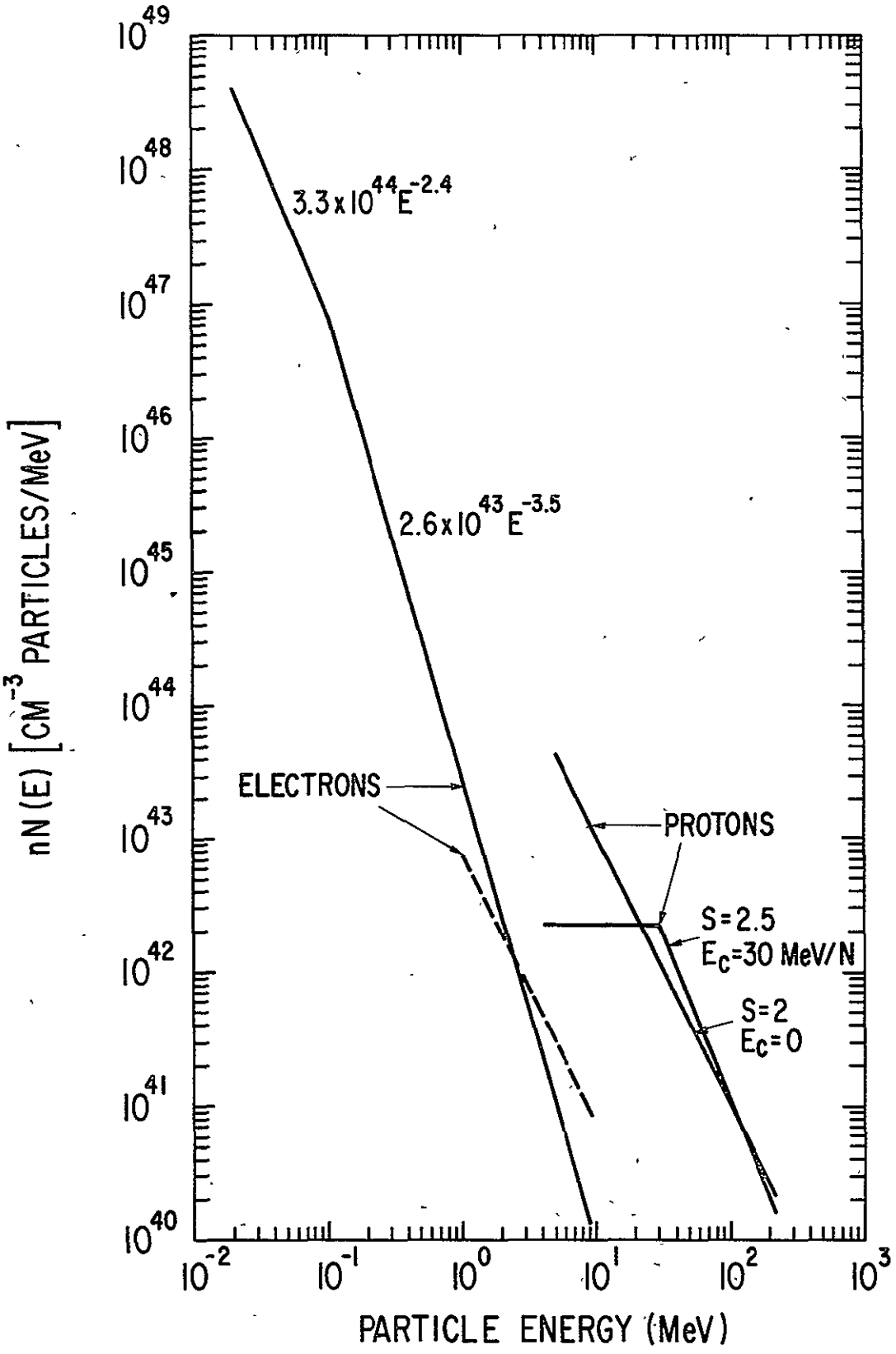
10^{49}
10^{48}
10^{47}
10^{46}
10^{45}
10^{44}
10^{43}
10^{42}
10^{41}
10^{40}
$3.3 \times 10^{44} E^{-2.4}$
$2.6 \times 10^{43} E^{-3.5}$
ELECTRONS
PROTONS
S=2.5
E_c=30 MeV/N
S=2
E_c=0
nN(E) [CM^{-3} PARTICLES/MeV]
10^{-2}
10^{-1}
10^{0}
10^{1}
10^{2}
10^{3}
PARTICLE ENERGY (MeV)

FIG. 4.8.7

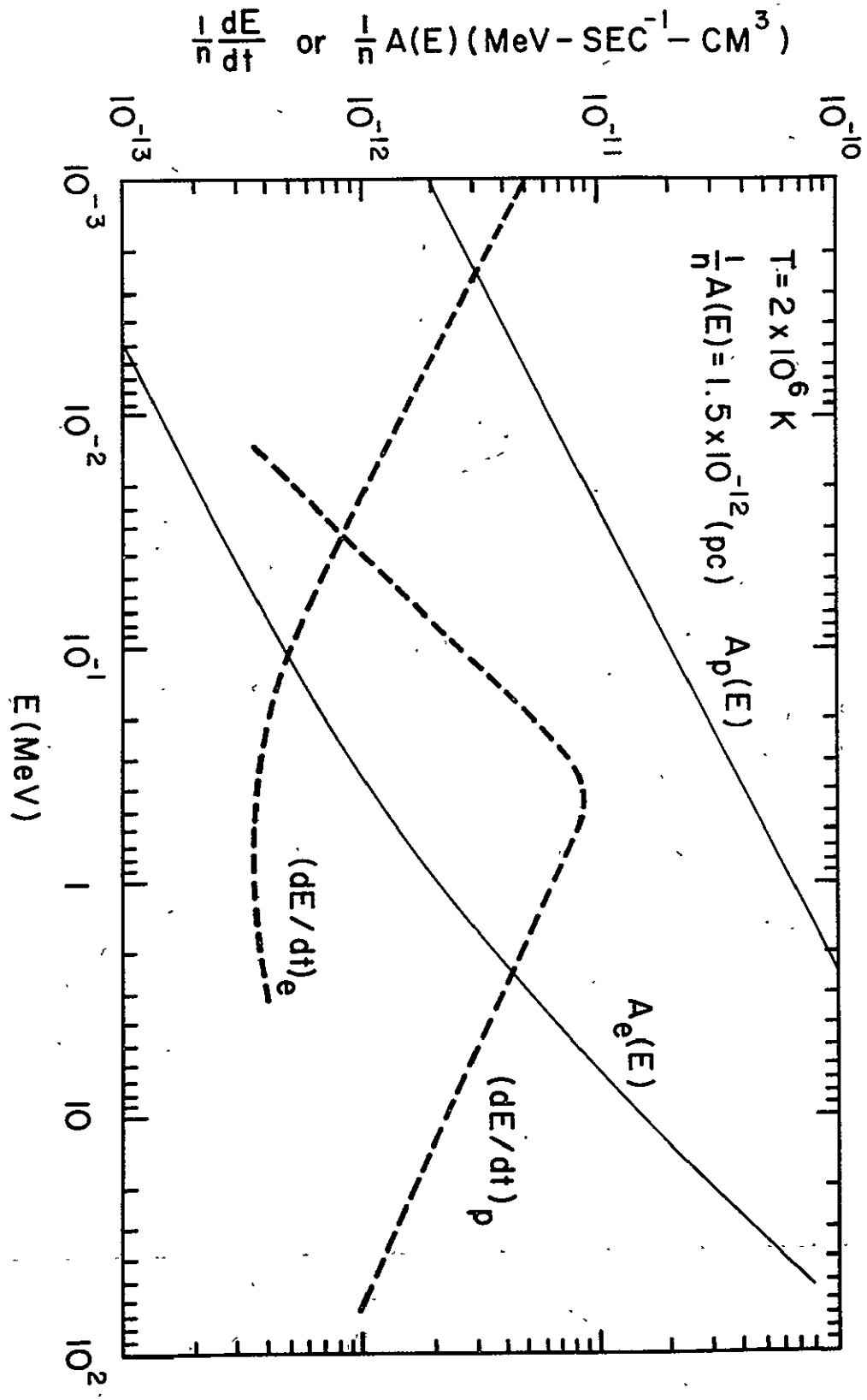

FIG. 4.10.1.

BIBLIOGRAPHIC DATA SHEET

1. Report No.	2. Government Accession No.	3. Recipient's Catalog No.
TM79660		

4. Title and Subtitle	5. Report Date
Energetic Particles in Solar Flares Chapter 4 in the Proceedings of the Second Skylab Workshop on Solar Flares	October 1978
	6. Performing Organization Code 660
7. Author(s) Ramaty et al.	8. Performing Organization Report No.
9. Performing Organization Name and Address Laboratory for High Energy Astrophyiscs Code 660	10. Work Unit No.
	11. Contract or Grant No.
	13. Type of Report and Period Covered TM
12. Sponsoring Agency Name and Address	14. Sponsoring Agency Code

15. Supplementary Notes

To be published in Proceedings of the Second Skylab Workshop on Solar Flares

16. Abstract

The recent direct observational evidence for the acceleration of particles in solar flares, i.e. radio emission, bremsstrahlung x-ray emission, gamma-ray line and continuum emission as well as direct observations of energetic electrons and ions are discussed and intercorrelated. Their study suggests that at least two distinct phases of acceleration of solar particles exist and that they can be distinguished in terms of their temporal behavior, type and energy of particles accelerated and the acceleration mechanism . Bulk energization seems the likely acceleration mechanism for the first phase while Fermi mechanism is a viable candidate for the second one.

17. Key Words (Selected by Author(s))	18. Distribution Statement
Energetic solar particles, Electromagnetic solar emission, acceleration, solar flares	

19. Security Classif. (of this report)	20. Security Classif. (of this page)	21. No. of Pages	22. Price*
UN	UN	117	

*For sale by the National Technical Information Service, Springfield, Virginia 22151.